Master's thesis

NTNU
Norwegian University of Science and Technology
Faculty of Engineering
Department of Marine Technology

Martin Steffensen

Buckling of Non-spherical Moss-LNG tanks

Master's thesis in Marine Technology
Supervisor: Jørgen Amdahl
Co-supervisor: Martin Slagstad
June 2022

NTNU
Norwegian University of
Science and Technology

Martin Steffensen

Buckling of Non-spherical Moss-LNG tanks

Master's thesis in Marine Technology
Supervisor: Jørgen Amdahl
Co-supervisor: Martin Slagstad
June 2022

Norwegian University of Science and Technology
Faculty of Engineering
Department of Marine Technology

NTNU
Norwegian University of
Science and Technology

NTNU
Norges teknisk-naturvitenskapelige universitet
Institutt for marin teknikk

MASTER THESIS 2022

for

Stud. techn. **Martin Steffensen**

Ultimate Strength of Non-spherical MOSS-LNG Carriers
Bruddstyrke av ikke-sfæriske tanker i MOSS-LNG skip

In recent years the demand for large LNG ships has increased. Ship owners are now requesting larger LNG ships with a cargo capacity up to 180 000 m^3, with ship dimensions being compliant with the limitations of the new locks of the Panama Canal. A challenge with the Moss LNG tanks is that increase in cargo capacity is most efficiently dealt with by increasing the tank diameter. Ships with spherical tanks of cargo capacity 165 000 m^3 are following the Panama Canal restrictions, but for larger capacities modification of tank shape is necessary, as discussed below.

The Moss-type LNG tank is an independent aluminium tank, supported by a cylindrical skirt, which provides the structural connection to the ship double bottom structure. The cylindrical skirt connects to the LNG tank through a central horizontal ring (the equator profile). The Moss LNG tank is very robust and is preferred by many ship owners, with more than 20 vessels in construction in early 2017.

As discussed above, increasing the cargo capacity without increasing number of tanks is challenging because the maximum ship width must remain within the Neo-panamax limitations. An option for increasing the cargo capacity is to modify the shape of the tank. An example of an altered tank shape is the apple-shaped tanks designed by Mitsubishi shown in Figure 1. The apple shape gives the tank a larger capacity than a spherical tank, while maintaining the ship width within the limitations of the Panama Canal. The center of gravity of the tank is also lower than for a vertically stretched tank, which makes it easier to meet the stability requirements. Although the tank shape is altered, the tank support system is not. Many of the important characteristics of the spherical Moss LNG tank are therefore maintained.

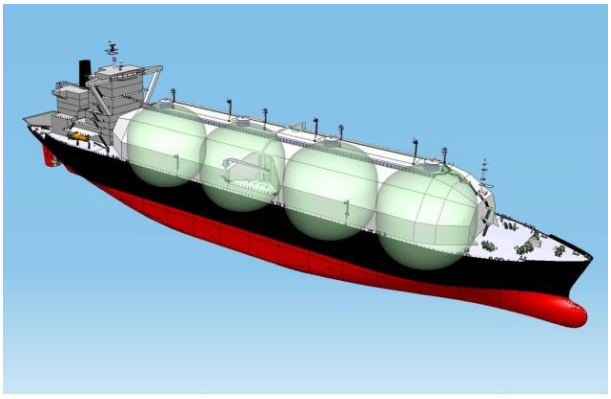

Figure 1 Illustration of apple shaped tanks on a LNG Ship.

Changing the tank shape to a non-spherical shape introduces some challenges with regard to calculating the tanks structural capacity for the Ultimate Limit State (ULS) especially.

Simplified equations for structural capacity available in Classification codes are only valid for purely spherical tanks. When the tank shape deviates from a pure sphere more complex analyses must be performed to verify the tanks ULS capacity. For the Mitsubishi design, non-linear finite element analyses (NLFEA) were performed to verify the tank's structural integrity. One should however note that non-linear finite element analyses are very time consuming both with regard to modelling and computation time, and may not be an efficient tool in the design phase.

An accurate estimate of the buckling capacity of the tank shell when the shell has a different curvature in the different directions is needed. This should also include the secondary effects of thermal contraction, as the tank shape deviate from the initial shape once it is filled. Estimates for second order geometrical loads are easily included when performing NLFEA, so the focus should first be on establishing a method for determining the buckling capacity of a non-spherical tank.

Further, the effect of thermal loads and interaction with hull girder bending modes should be investigated, where also the skirt and part of the hull girder are modelled.

NLFEA is not a very efficient method for designing structures even with the recent increases in computation capacities. Simple estimates are preferred in the design stage. The availability and validity of these simple methods is however not known.

Analysis of spherical tanks was conducted by Andreas Sanne in a master thesis in 2019 and Peder Gjestvang in 2020. The idea of this project/master thesis work is to follow up the work conducted by Sanne and Gjestvang.

The project work shall address the following topics:

1. A brief description of the design of Moss Rosenberg spherical tank and extension of this into alternative shapes, as well as the structural configuration of the skirt and cargo hold.

2. Review of the current DNL-codes for ultimate strength assessment of spherical shells. Refer e.g. to Class Note 30.1, 30.2 and 30.3, and DNV-CG-0134. A far as possible provide an explanation of the formulations adopted for ultimate strength, notably buckling requirements. Discuss the importance of shape imperfections with respect to ultimate strength and how imperfections are characterized with respect to shape and size.

3. Thermal analysis of the skirt in steady state condition. Discuss the modelling of the structure for the thermal analysis. Initially, axisymmetric - and 1-D conditions may be assumed. The temperature dependence of the thermal conductivity coefficient for aluminium, stainless steel and constructional steel shall be considered to the extent data exist. Heat loss due to convection and radiation in areas with no insulation shall be considered. Assess the temperature distribution for both LNG and liquified hydrogen (LH2).

4. Introduce the temperature distributions determined in pt. 3 to the full skirt model and calculate the thermal induced deformations and stresses. Next, calculate the influence of the thermal induced response on the resistance to buckling by linear and nonlinear analysis.

5. Analysis of skirt and hull girder interactions. Develop a structural model of the ship hull as support for the skirt. Discuss the choices made concerning the extent of the hull girder model and the adopted boundary conditions. Calculate the resistance to buckling/yielding and compare with the results in pt 4. Also compare the results with simplified formulas given in DNV-CG-0134. If the results indicate so, propose improved design formulations for assessment of skirt ultimate strength.

6. Conclusions and recommendations for further work

Literature studies of specific topics relevant to the thesis work may be included.

The work scope may prove to be larger than initially anticipated. Subject to approval from the supervisor, topics may be deleted from the list above or reduced in extent.

In the thesis the candidate shall present his personal contribution to the resolution of problems within the scope of the thesis work.

Theories and conclusions should be based on mathematical derivations and/or logic reasoning identifying the various steps in the deduction.

The candidate should utilize the existing possibilities for obtaining relevant literature.

The thesis should be organized in a rational manner to give a clear exposition of results, assessments, and conclusions. The text should be brief and to the point, with a clear language. Telegraphic language should be avoided.

The thesis shall contain the following elements: A text defining the scope, preface, list of contents, summary, main body of thesis, conclusions with recommendations for further work, list of symbols and acronyms, references and (optional) appendices. All figures, tables and equations shall be numerated.

The supervisor may require that the candidate, in an early stage of the work, presents a written plan for the completion of the work. The plan should include a budget for the use of computer and laboratory resources which will be charged to the department. Overruns shall be reported to the supervisor.

The original contribution of the candidate and material taken from other sources shall be clearly defined. Work from other sources shall be properly referenced using an acknowledged referencing system.

The report shall be submitted in two copies:

- Signed by the candidate
- The text defining the scope included
- In bound volume(s)
- Drawings and/or computer prints which cannot be bound should be organised in a separate folder.

Supervisor:
Prof. Jørgen Amdahl

Co-supervisor
PhD-student - Martin Slagstad

Deadline: June 11, 2022

Trondheim, **January 10**, 2022

Jørgen Amdahl

Abstract

In today's energy market, demand for LNG continues to increase. Both for climate and political reasons. Focus has also been directed at hydrogen as a future fuel for various engines due to its very low climate footprints. LNG vessels are already in full operation, but several opportunities have been considered to increase the capacity of transport. Among other things, to increase the capacity of the LNG tanks by stretching the tanks to non-spherical structures, both horizontally and vertically. Transport of hydrogen requires facilities to cool hydrogen to a very low temperature in order to obtain liquid form for transport in tanks. This report builds on previous work by Gjestvang and Sanne on Moss non-spherical LNG vessels, but will focus on analyzing the buckling strength of the support skirt and how the temperature affects the strength and displacement.

This report first gave an overview of Moss Rosenberg's design of spherical and non-spherical and explains the structural configuration of the tank and skirt. DNV's guidelines for the highest strength assessment of spherical shells were elaborated and explained. The focus was on two guidelines DNV-CG-0134 "Liquefied gas carriers with spherical tanks of type B" and DNV-RP-C202 "Buckling Strength of Shells" where guidelines for both LNG tanks and the skirt were explained. The importance of shape defects was discussed with regard to reduced buckling strength of the skirt.

FEM analysis of the skirt buckling was performed in Abaqus. Here, both the thermal effects of the skirt and the temperature distribution, displacement and flow were considered. A buckling analysis of the skirt was also performed as a result of the axial force applied by the tank. This analysis was combined with the temperature-displacements that occur of the cargo temperature to find the reduction in the buckling strength.

The eigenvalue analysis showed that the elastic buckling stress of the skirt was not significantly reduced due to the temperature effects. The temperature difference caused the buckling mode to change shape from buckling in the lower part of the skirt to the upper part of the steel section of the skirt as a result of the bending. In the non-linear analysis of the fragments, it was found that the elasto-plastic buckling strength was significantly reduced due to the temperature shift and the bending that occurs. This caused in the thermal brake in the structure which has lower strength than the steel section. A non-linear imperfection analysis was also performed where its influence was discussed and compared for the modes that arise from the eigenvalue analysis of the different loads. An analysis of the skirt with increased thickness was performed in parts of the structure where the margins for buckling in other parts of the structure were identified and the buckling modes discussed.

A model was made of a composite skirt and tank structure and analysed for elastic and elasto-plastic buckling was performed. It was found very similar results in the analysis between the two models and the necessity of the tank in the model was discussed. The boundary conditions used on the skirt illustrated the connection to the tank well.

Sammendrag

I dagens energimarked fortsetter etterspørselen å øke av LNG. Både av klimahensyn og politiske. Noe fokus har også blitt rettet mot hydrogen som et fremtidig drivstoff for diverse motorer på grunn av sitt svært lave klima avtrykk. LNG skip er allerede i full drift, men det er sett på flere muligheter for å øke kapasiteten av transport. Blant annet å øke kapasiteten av LNG-tankene ved å strekke tankene til ikke sfæriske strukturer, både horisontalt og vertikalt. Frakt av hydrogen krever fasiliteter for å kjøle hydrogen til en svært lav temperatur for å oppnå væskeform for transport i tanker. Denne rapporten bygger videre på tidligere arbeid av Gjestvang og Sanne om Moss ikke-sfæriske LNG skip, men vil ha som fokus å analysere knekkstyrken på støtte skjørtet og hvordan temperaturen påvirker styrken og forskyvning.

Først ble en oversikt av Moss Rosenberg design av sfæriske og ikke-sfæriske forklart og hvordan den strukturelle konfigurasjonen til tanken og skjørtet. DNV sine retningslinjer for høyeste styrkevurdering av sfæriske skall ble utdypet og forklart. Fokuset var rettet mot to retningslinjer DNV-CG-0134 '' LNG-Skip for flytende gass med sfæriske tanker av type B" og DNV-RP-C202 '' Knekkstyrke av skall" hvor retningslinjer for både LNG tanker og skjørtet ble forklart. Viktigheten av formfeil ble diskutert med hensyn på redusert knekkstyrke av skjørtet.

Det ble foretatt FEM-analyse av skjørtet i Abaqus. Her ble det sett både på de termiske påvirkningene av skjørtet og temperaturens fordeling, forskyvning og flyt. Det ble også bli utført en knekkings analyse av skjøret som et resultat av aksial kraften påført av tanken. Denne analysen ble kombinert med temperatur forskyvningene som forekommer av lasttemperaturen for å finne reduksjonen i knekkstyrken.

Egenverdi analysen viste at den elastiske knekkspenningen av skjørtet ikke ble betydelig redusert som en følge av temperatur påvirkningene. Temperaturforskjellen førte til at knekk moden endret form fra knekking i nedre del av skjørtet til den øvre delen av stål seksjonen i skjørtet som en følge av bøyingen. I den ikke lineære analysen av skjøret ble det funnet at den elasto-plastiske knekk styrken ble redusert betydelig på grunn av temperature-forskyvningen og bøyingen som oppstår. Dette forårsaket flyt i den termiske bremsen i strukturen som har lavere flyt styrke enn stålseksjonen. En ikke linear imperfeksjons analyse ble også foretatt hvor dens påvirkning ble diskutert og sammenlignet for modene som oppstår av egenverdianalysene til de forskjellige lastene. Det ble foretatt analyser av skjørtet med økt tykkelse i deler av strukturen hvor marginene for knekking i andre deler av strukturen ble identifisert og knekk-modene diskutert.

En modell ble laget av et sammensatt skjørt og tank struktur og analysene for elastisk og elasto-plastisk knekking ble utført. Det ble funnet veldig like resultat som ble diskutert hvor nødvendig det vil være å forta en modell med både skjørt og tank ved kun behov av analyse for skjørtet. Randbetingelsene som ble benyttet på skjøret illustrerte koblingen til tanken godt.

Preface

Through the Department for Marine Technology at the Norwegian University of Science and Technology, this report was written as a masters thesis to conclude five years study. The subject was chosen from one of many project works related to the specialisation of Marine Structures and to be worked at full time in the spring semester of 2022. A related project worked on the previous semester with a more general scope and was the foundation of much of the literature used in this thesis. Much of the foundation in modeling and performing analysis was developed during this project.

This report is a continuation of the thesis from Peder Gjestvang (2020) and Andreas Sanne (2019). These two thesis has been very helpful to understand elements of the topic and influenced this report.

Through this project I have personally learned quite a lot and developed myself in both theoretical knowledge, abilities using software to analyse structures, and report writing. The supervisor supporting this thesis has been Jørgen Amdahl and with co-supervisor Martin Slagstad. I would like to thank them both for their contribution, help and support through my works.

Trondheim, June 9. 2022

Martin Steffensen

Table of Contents

List of Figures

List of Tables

Nomenclature

α_c	Coefficient
δ_i	Imperfection Amplitude
η	Curvature Parameter
γ_{sum}	Safety Factor
γ	Ratio Of Stiffness Of Stiffeners
κ	Slenderness Factor
Λ_{CR}	Critical Buckling Parameter
Λ_E	Elastic Buckling
λ	Slenderness Ratio
ν	Poisson's Ratio
ψ	Plate Buckling Coefficient
ρ	Knock-Down Factor
σ_E	Elastic Buckling Stress
$\sigma_{\theta 0}$	Circumferential Design Stress
σ_{cl}	Empirical Reduction
σ_{cr}	Critical Buckling Stress
σ_{eo}	Equivalent Design Stress
σ_{x0}	Axial Design Stress
σ_{xE}	Elastic Axial Buckling Stress
σ	Normal Stress
τ	Shear Stress
$\mathbf{q}$	Heat Flow
A	Area
C_z	Buckling Coefficient
d	distances
E	Elastic Modulus
e	Eccentricity
g	Buckling Check Criterion
h	Buckling Check Criterion
h	Heat Transfer Coefficient
I_z	Second Moment of Area
I_{sef}	Stiffener Moement of Interia Including Effective Flange Length
k	Thermal Conductivity
l_{e0}	Effective Length

l	Length
m	Buckling Half Waves Circumferential Direction
N_E	Elastic Axial Buckling Load
N_x	Axial Load
N_{cr}	Critical Axial Load
n	Buckling Half Waves Length Direction
Q	Heat Transferred
R_{eH}	Yield Stress
r	Radius
s_e	Effective Shell Width
s	Stiffener Distance
T	Temperature
t	Thickness
Z	Batdorf Parameter

1 Introduction

In a growing market with increased demand for LNG, new and improved methods have been introduced for its transportation. Over long distances and across the continents, shipping is still the most practical way of transportation. As many countries are in a transition of phasing out the use of coal in power production, LNG is one of its replacements. The demand has increased in a short span of time and thus the need for more ships and ships with larger capacity. Due to the LNG carriers being quite large already, increasing their capacity poses some complications. For a design with spherical LNG tanks the traditional method to increase the tank capacities was to increase the tanks diameter. This also requires a wider ship to carry and support the tanks. By making the ships wider they may carry more LNG, but it reduces the ships utility in certain waters, ports, and channels.

The Moss-LNG carriers solution is to increasing capacity without making the ship wider by making the tank stretched and into an apple shape. This has the advantage of increasing the capacity and still maintain many of the support systems and characteristics. The center of gravity is also lowered, helping to meet stability requirements. LNG tanks are made of aluminium and are supported by a cylindrical skirt connected through the horizontal ring. It is this cylindrical skirt which will be the focus of this study and will be analysed regarding buckling strength.

1.1 Brief description of gas carriers

In this chapter a brief description of various gas carriers will be given. It will provide basic understanding of the types of LNG carries and their usage to better understand the background for further analysis.
Furthermore a description of the more specific gas tanker to Moss Rosenberg and their design will be given. These designs are of their spherical tanks and its extension into alternative shapes. The configurations to the skirt and cargo hold to fit the alternative shapes will also be described.

1.1.1 The different kinds of gas carriers

The main objective of a gas carrier is to transport natural gas from point A to point B. Today LNG is primarily transported in a liquid state. When choosing to transport the gas as a liquid there are several advantages and some posed risks. One of the main advantages the increased density of the molecules when cooled to a liquid. Thus larger amounts of the components can be transported with the tank being exposed to less pressure. This cooling and isolation will require a lot of energy to keep the liquid gas cooled (-162℃). This liquefied gas has the potential to explode should there be some source of ignition nearby. Leakages of the content could also be dangerous.

There several different designs of gas carriers. Typically these are categorised into three different categories based on the transportation properties and the carriers comes in a large variety of sizes ranging from around $19000m^3$ to $137000m^3$ (Kvearner-Moss), but some design as large as $266000m^3$ has been produced like the carrier *Mozah*, a carrier owned by Quatargas. These ships differ in how they transport the gas, either by cooling, by size, or both. These are categorized as:

- Fully pressurised gas carriers
- Semi-pressurised gas carriers
- Fully refrigerated gas carriers

A fully pressurised gas carrier transports the natural gas in gas state. This requires strong tanks as the pressure from the gas is quite large and will reduce the amount of gas that can be transported. These ships are typically of the smaller sizes, ranging from $500m^3$ to $6'000m^3$. Their use is advantageous when transporting smaller amounts of gas in not to far distances. Pressurised ships typically transport alkanes such as propane and chemical gasses.

The Semi-pressurised gas carriers used a combined solution of pressured gas and refrigerated gas into liquid state. This combined solution is very flexible due to the ability to carry different categories of cargo, both refrigerated and atmospheric. A typical semi-pressurised ships carries has the carrying capacity of $3'000 - 15'000m^3$. Tough larger ships has been delivered in later years.

A fully refrigerated gas carrier is designed to only transport liquefied gas. They are large and their purpose is to deliver large quantities of gas over longer distances. Their carrying capacity are usually $20'000 - 100'000m^3$. Their tanks has to be outfitted with refrigeration systems and isolation. This equipment's and systems are costly and requires a lot of energy to operate. Thus it makes most economic sense to use these kinds of ship to transport large quanta of gas.

The Liquefied natural gas carriers (LNG) are a type of refrigerated carrier. As the gas occupies substantially less space when cooled down to a liquefied state the ship can carry larger quanta in the tanks rather than in a atmospheric pressure. Thus the challenge is to keep the gas below its low boiling point (Methane $-182C^o$) and the greater weight of the liquid which needs to be assessed in terms of stability of the ship. A modern LNG carrier is typically of the size $125'000 - 135'000m^3$ [17].

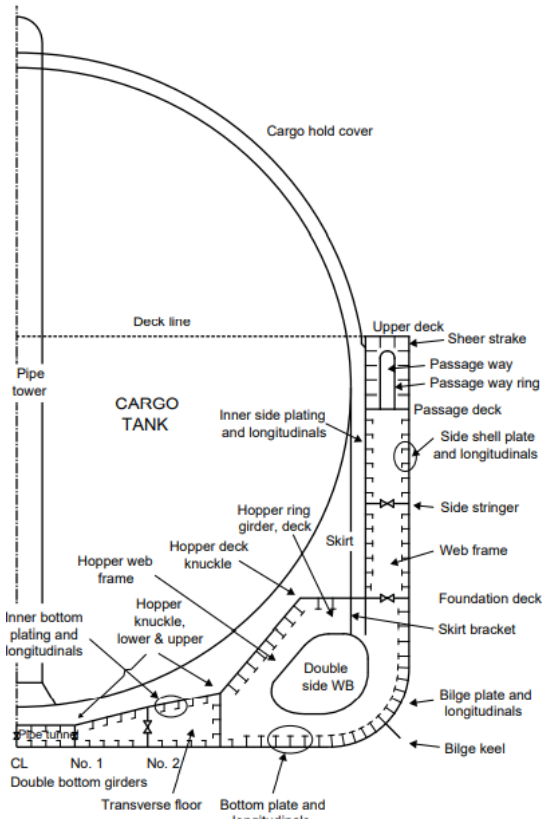

Figure 1: Illustration of Type B LNG tank [12]

Other kinds of ships include carriers of Ethylene and other chemical carriers. Some of these also requires or is practical to have refrigerated tanks. Tough such chemicals usually is not demanded in the same quantity as natural gases these ships is typically not as large as the LNG carriers.

1.1.2 Moss-Rosenberg spherical tank design

The Moss-Rosenberg spherical tank is a self-supporting 'B' type spherical tank. This is a tank design developed by Kvaerner Moss. Its has some enhanced design factors and requires only a partial secondary barrier in which a drip tray is used beneath the tank. A type B tank does not have to be spherical and some alternative designs are used.

The prismatic 'B' tank designs are supported along the hull and internally for each layer. On the other hand, spherical 'B' tank designs are supported along the equator ring section. Using a support *skirt* which is a cylindrical support connected on the tank equator to the bottom foundation of the ship, supporting the tank by distributing forces towards the keel. As the skirt forces are quite strong there is need for a sufficient supports in the ship beam to carry these. This requires a foundation designed to withstand these forces.

For a refrigerated ship its important to keep the content refrigerated with minimal loss of energy. The more the contents temperature can be hindered from rising the less energy has to be spent to keep the content refrigerated. Thermal insulation is mainly used to minimize the heat flow into the tanks them self and hinder boil-off. As the tanks have content with very low temperatures it is also important to keep the ship from cooling down from the content. This is to protect the structure and materials as their properties can change with lower temperatures.
A typical LNG content has to be refrigerated at about -163℃ and quite advances insulation technology is required. A modern LNG tank insulation is outfitted with a nickel-alloyed steel insulation. The material is chosen because of its low thermal conductivity, ability to bear loads, material strength, light weight, and ability to withstand cargo liquid. For type 'B' tanks the insulation's is applied to the outer surfaces of the tanks. The cylindrical skirt is also outfitted with a thermal break to hinder temperature loss through the skirt.

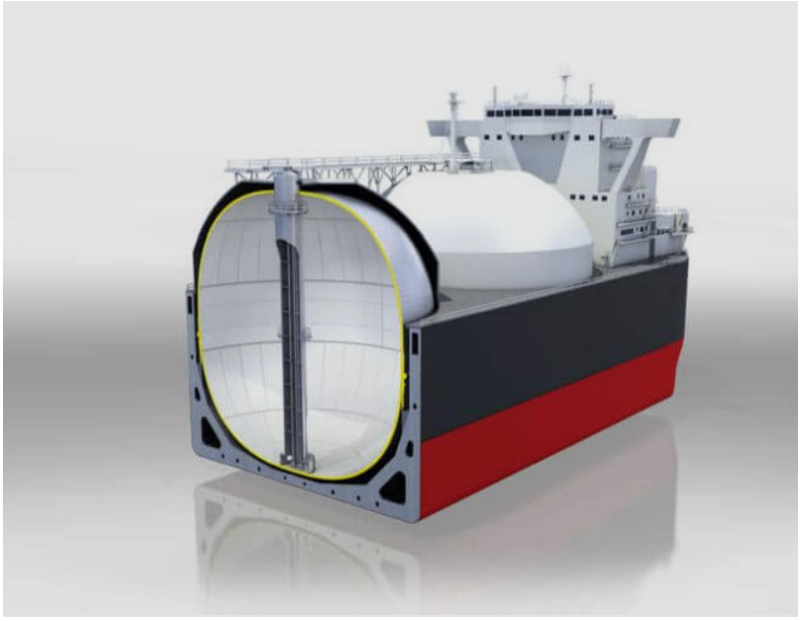

Figure 2: Moss non-spherical LNG tank [15]

1.1.3 Extension of tank into alternative shapes

As the demand for for natural gas has increased both due to the need for alternative source of electricity production from coal and need for gas in household, the need for transportation of LNG increased. This has created a demand both for more and larger LNG ships. One of the major transport lines is between Asia and North-America. To quicker route to the east coast of North-America is thought the Panama canal. The LNG ships going through channel has already

reached the largest size that can fit through the canal. Using a type 'B' spherical tank, increasing the tank size will also increase the ship width making the ship to large to fit the canal. One way to overcome this is to extend the tank vertically rather than increasing the diameter. This poses other problems as higher center of mass of the cargo, making the ship more unstable.
The Moss Rosenberg spherical tanks design seeks to increase the tank volume with out increasing the diameter. This solution designs the spherical tanks into a cylindrical shape, but keeping the round edges. Thus the tank takes form more like a apple shape. Such a tank will have higher capacity but at the expense of the need for more support and strength to the more load exposed sections of the tank. Thus a analysis will have to be conducted to see how much the tanks realistically can be increased without too significant cost.

1.1.4 Support Skirt

To support the tank weight and distribute forces rotations of the tank a cylindrical skirt is place around the tank. More specifically the skirt is connected around the tanks equator line and stretches to the foundation of the skip. Depending on the placement of the tank on the ship, the skirt can have different lengths and designs. Typically the support skirt mounted to the foundation of the ship through the hopper ring girder deck, seen in figure 1. It consists of three section composed of different materials. The longest section at the bottom is mild steel and is usually vertically stiffened. In the middle a thermal break is installed to insulate the cargo from external temperatures through the structure and is composed of stainless steel. Above the thermal break is the transition section to the tank which is made of aluminium.

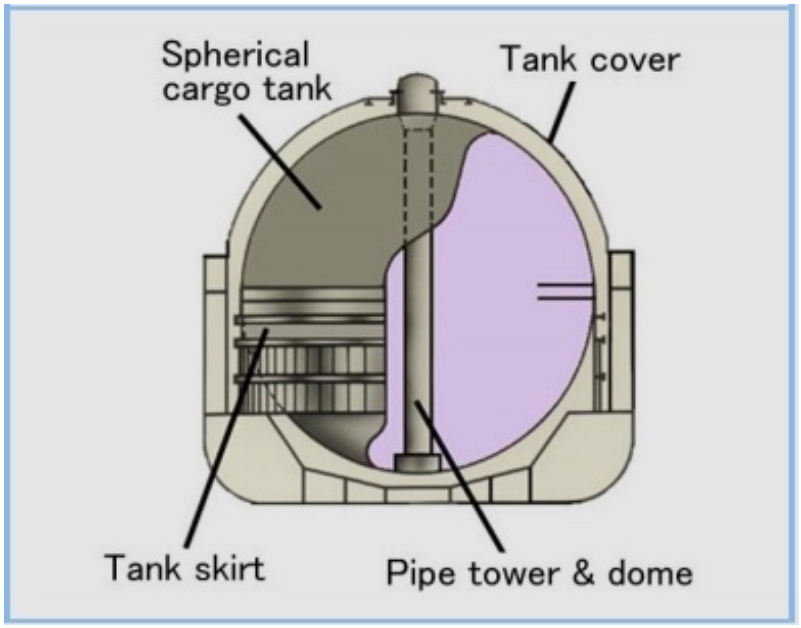

Figure 3: Moss spherical tank with skirt structure [13]

1.1.5 Cargo Hold

The cargo hold is composed of a aluminium shell with different thicknesses throughout the height. For a both a spherical and non-spherical tank the thickest shell is at the bottom half and its greatest around the equator line where the tanks are supported. For a non-spherical tank the thickest section would be the extended cylindrical section.

Insulation is placed around the tanks to prevent heat flow to the cargo and reduce the energy needed to cool the cargo. It is composed of fiber glass and covers around the tank and over the thermal break in the support skirt. A pipe tower is fitted in the middle of the tank to be able to pump out the cargo and provide some support.

1.2 Cargo

LNG carriers transport natural gasses by cooling down the cargo til liquefied to be able to transport higher quantities at a lower pressure. Cargoes transported in a liquefied state are typically LNG, ammonia, and hydrogen.

1.2.1 Natural gas

Liquefied natural gas (LNG) is widely used world wide for different purposes that required energy. Its a composition of hydrocarbons with mainly methane and a mixture of ethane. LNG is used both in gas plants to create electricity and in engines. In recent years it been promoted for its lower carbon footprint compared to coal and heavy fuels. Thus the demand for LNG has been increasing in the later years which gives cause for innovation in transportation and use of the gas.

Transporting LNG required the ability to cool down the natural gas til liquefied at a temperature of -163℃ or $165K$. Gas processing plants are required to cool down the gas and systems installed in the gas carrier to keep the gas at the right temperature and insulated to prevent heat flow to the LNG. When the gas is liquefied it has a density of $0.5kg/L$ roughly half that of water. Compared to other raw materials transported such as iron, this gives the carrier the ability to carry large volumes of LNG with tanks panning above the carrier deck. This needs to be balanced with the center of gravity of the carrier.

1.2.2 Liquid Hydrogen

Liquid hydrogen (LH2) has also seen new potentials and markets. With focus on developing new solutions and alternatives to fossil fuels hydrogen been examined for its uses as fuel for cars, ships, and aircrafts. This has increased the demand for both liquid hydrogen and investments into productions of it for the expected demands to come. In June 2020 the Norwegian Minister of Petroleum and Climate and Environment outlined their focus and strategy for hydrogen in their mission to reduce the use of fossil fuels. The areas of focus were in particular scheduled routes operated by vessels such as ferries, high-speed vessels and other short sea ships [24]. There is high potential for usage of hydrogen in Norway, and as the production is developed there will be need need for transportation of the hydrogen both in and out of Norway. Over time when hydrogen production and usage increases there will be a need for transportation of liquid hydrogen in larger quanta. One way to transports the hydrogen cross continental would be by in carrier ships. LNG is already transported in carriers with tanks where the cargo is cooled to a liquefied state and transported. The same method could be implemented for liquid hydrogen by liquefying it and transported in similar tanks. One of the main differences between LNG and LH2 is the boiling temperatures and density when liquefied.

When hydrogen is liquefied and stored its temperature is -253℃ or $20K$. It has to be stored with great care and kept in pressure and thermally cooled and insulated to keep it liquefied which requires high amount energy. When liquefied, hydrogen has a density of only $0.07kg/L$ which is quite light compares to LNG of $0.5kg/L$.

1.3 Scope of work

In this report the objective is a thermal and structural study of the support skirt of LNG carriers. The effect of the temperature due to a cold cargo will be studied and its effect on the buckling strength of the skirt for both LNG and LH2. FEM-analysis of the skirt will be performed using the software Abaqus and the model will be created in DNV Genie. The model used for the skirt and tank is from a Moss Rosenberg spherical LNG carrier and dimensions and materials used follows the drawings provided from Moss Maritime. This report will not emphasise non-spherical tanks as the focus in on the support skirt which will be studied cylindrical.

1. Description of Moss Rosenberg spherical design with spherical tanks and with extension of alternative shapes and the structural configurations of the skirt and cargo hold
2. Review of the current DNV class notes: DNV-RP-C202 and DNV-CG-0134 and the relevant formulas for the scope of the report. The importance of imperfections will be discussed in respect to shape and size.
3. A temperature analysis of the support skirt in steady state condition will be performed. The model will be discussed and a 3D- analysis of the temperature distribution and displacement will be presented both for LNG and LH2. Application of temperature through convection and conduction will be discussed. Heat loss through the thermal break will be analysed.
4. Perform a buckling analysis of the skirt model with temperature-displacements and stresses found. A linear eigenvalue analysis and a non-linear analysis with and without imperfections will be performed.
5. Imperfection non-linear analysis on the skirt for buckling modes of the load cases. Comparison of buckling modes and strength for different parts of the skirt and thicknesses will be studied.
6. A full model with both a spherical tank and the skirt will be modeled and analysed regarding temperature effect and buckling. It will be compared to the results of only modelling a skirt. The requirement for a full model for a skirt analysis will be discussed as well as the computing time this implies.
7. Conclusion and recommendations for further works

1.3.1 Changes to Project Work

It was decided to focus the review of the DNV class note to the most relevant for buckling of the support skirt and design rules for LNG carriers. Thus the class notes *DNV-RP-C202, Buckling Strength of Shells* and *DNV-CG-0134* will be reviewed. The DNV notes 30.1,30.2,30.3 contains more general buckling notes which will be addressed partially, but much of the content overlap.

After discussion with the supervisor and co-supervisor it was decided to change point 6. of the scope due to lack of data and drawings of the hull girder. The scope was then changed to focus on the skirt interaction with a tank and study if the boundary conditions used on the top of the skirt was applicable compared to modeling a full structure with tank and skirt. A buckling analysis would also be performed on the full size model and compared to the skirt model.

2 Theoretical Background

In this chapter the theoretical background for in this report will be presented. This revolves the theory regarding the thermal effects on the structure and heat flow through the thermal break. Buckling of cylindrical shell and curves panels will also be presented.

2.1 Thermal Effects on the Skirt

The thermal effects on the skirt structure occurs through the effects of conduction through materials and convection of fluids. Conduction is the physical transfer of heat is due to conduction of the temperature between the cargo and the hull through the thermal break. The interaction between the hull and skirt with the air fluid is relayed through convection.

2.1.1 Conductivity

Thermal conductivity is the ability to conduct heat through a material. A material is typically exposed to a temperature on opposite positions of the material and the material body will be the conduction solid which the heat will flow. Materials will conduct the heat with different intensity depending on their thermal conductivity denoted k. The rate at which the heat flow is called heat flow q and is given by using the two different surface temperatures over the length with the thermal conductivity of the material. The second law of thermodynamics states that heat will flow from the hotter surface towards the colder surface. Heat transfer per area is called the heat flux and is given by $\mathbf{q}$ and is a vector quantity of the flow direction

$$\mathbf{q} = -k\Delta T \tag{1}$$

The heat flow through a material over e given length is given by q. Its directly proportional with the difference in temperature and inversely so for the length between the two temperatures. Over a length L the heat flow q through the material is given by

$$q = -k\frac{T_2 - T_1}{L} \tag{2}$$

The heat flow is also proportional to the materials conductive ability given by its thermal conductivity. Thus a material with low thermal conductivity can be used as insulation without depending on the temperature of the length between them.

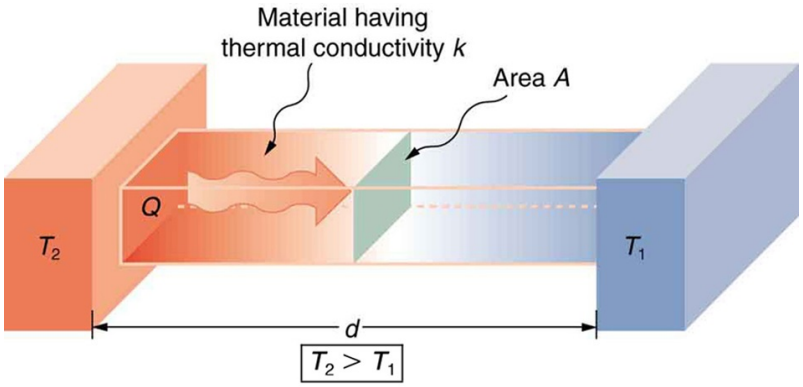

Figure 4: Heat flow through a material with area A and length d [1]

The thermal conductivity is given by

$$k = \frac{Qd}{A\Delta T} \tag{3}$$

where Q is the heat transferred, d is the distance between the two temperature surfaces, A is the area of the surface which the heat transfers, and ΔT is the difference in the temperatures.

Thermal conductivity is described as a materials ability to transfer energy per Kelvin meter. It has the notation W/mK. Solid materials typically has a higher ability to conduct heat compared to liquids and in particular gasses. An example is copper, which has an 10'000 amplified heat conducting effect compared to that of air [6].

Solids are particularly good at conduction heat. When one end of a metal is exposed to higher heat and energy the molecules close to the heat source will start vibrating with higher energy. These vibrating molecules will effect those molecules next to them which might not be as exposed to the energy source. Some of the energy is given to these molecules as well and this process extends itself through the molecules along the material away from the source, causing heat through parts of the material. What makes metals in particular great heat conductors among the solids is their free de-localised electrons around the molecules which also will transfer heat and move even more freely then the molecules. In an isometric material with two different temperatures opposite each other the heat will distribute itself proportionally.

2.1.2 Convection

Convection is a heat transfer through a fluids which is caused by movement in the fluid. This can occur due to pressure differences when gravitational effect due to lower densities occurs.

When a heat source is present next to a fluid, some of the fluid molecules will be heated up by this source gaining energy. These molecules will then be less dense causing them to transfer placement with higher density molecules. This will cause a movement in the overall fluid and the process will repeat as other molecules will heat.

Its relevance to the ships hull and support skirt is the air fluid temperature which will heat the ship and the skirt. As the cargo will have a low temperature relative to the air temperature a heat flow will be present as its impossible to fully insulate. Air heats the skirt through convection which is cooled by the cargo.

The rate at which the heat transfers from the fluid to the metallic surface is determined by the relationship of convection given as

$$Q = hA(T - T_f) \tag{4}$$

Q is the rate at which heat transfers over time. As in conduction A is the area of the transition surface and T is the material temperature and T_f the fluid temperature. A heat transfer coefficient h is the individual fluid ability to transfer heat and has the unit $W/(m^2K)$.

The heat transfer from a fluid to a solid material typically has a relatively low heat transfer coefficient depending on the material.

2.2 Buckling of cylindrical shells

This section will cover the buckling theory relevant for the support skirt. As the skirt is has a cylindrical geometry the buckling theory is based on buckling of cylindrical shells. The support skirt is stiffened with vertical stiffeners and ring stiffeners and thus local buckling between these stiffeners will have to be studied with theory concerning buckling of curves panels.

2.2.1 Buckling and Stability

In plate buckling there are two different ways a plate may buckle and lose its stability.

- Buckling by load past load limit
- Buckling past bifurcation point

Buckling by load past load limit happens when there load asserted to the plate is too great such that the plate yields and plastic deformation occurs. This is known as *snap-through* buckling and the plate snaps due to the excessive load. Figure 5 illustrates a perfect and imperfect plates deflection when loaded.

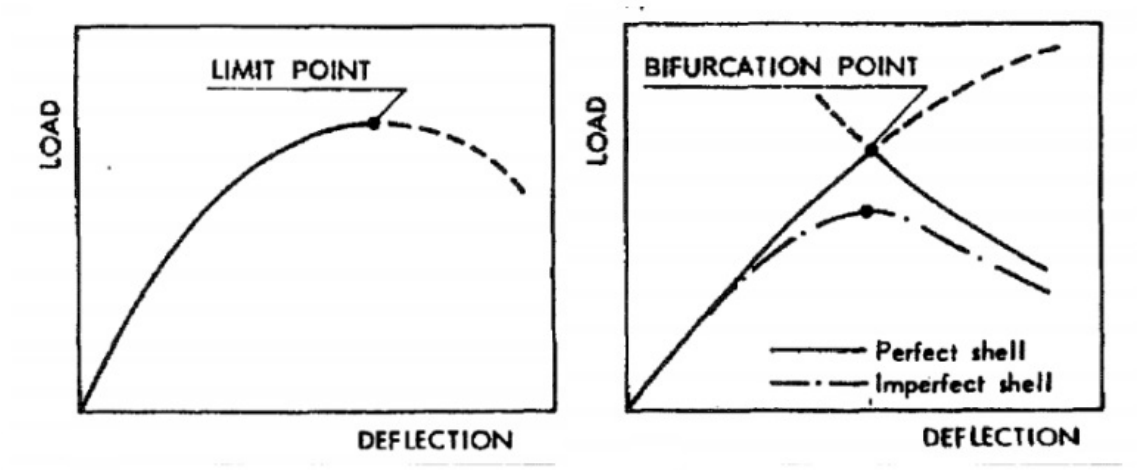

(a) Load Past Load Limit

(b) Past Bifurcation Point

Figure 5: Deflection of a loaded shell, perfect and imperfect [9]

For thin cylinders the impact of imperfections are very important. Even small imperfections can reduce the buckling strength for cylinders with large diameters if its relation to the thickness is small. For non-linear analysis of such structures its important to include non-linear effects and imperfections for a proper result of the analysis.

In buckling one unique solution is not always the case for a given load. Several equilibrium points can occur depending on the structure for a load. The load-displacement curve can thus not be faithfully followed through increasing the load. Figure 6 illustrates the *snap-through* effect which occurs when the load reaches the limit point. The plate will then jump to the next stability point which is able to withstand the load.

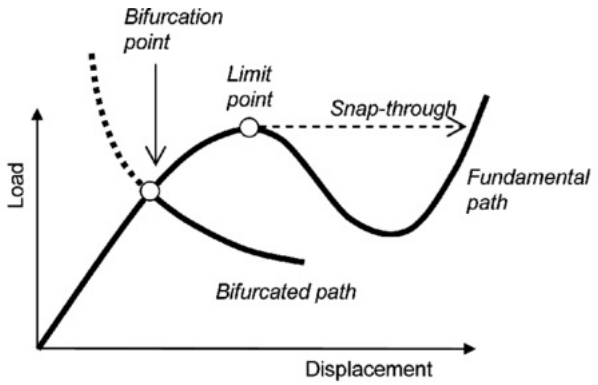

Figure 6: Snap-through from Limit Point to Stability Point for a given load [2]

Buckling past bifurcation point is buckling where due to imperfections the plate will find an equilibrium state called *prebuckling state*. Increasing the load will cause the plate to reach the bifurcation point and a new equilibrium will be established. This creates a path which the plate can buckle due to the imperfection and the plate becomes unstable.

The buckling strength analysis should be based on the most unfavorable mode, which means studying the buckling mode the lowest loads..

The stresses are categorised different to when performing buckling strength analysis. *Reference stress* , σ is a state of stress category in the structure also called equivalent stress. When analysing buckling, the critical stress σ_{cr} is of importance. This is the critical reference stress for structures buckling strength. Relative to critical stress, the yield stress σ_F together with the buckling strength gives the slenderness ratio σ_{cr}/σ_E. The structural slenderness is defined using the reduced slenderness, using the elastic buckling stress σ_E:

$$\lambda = \sqrt{\frac{\sigma_{cr}}{\sigma_E}} \tag{5}$$

σ_E is derived using classical buckling theory. Structures with imperfections will have to modify σ_E to account for the reduction.
A "usage factor" η is introduced which is the ratio between the reference value and the critical value and is used in the buckling stress analysis.

$$\eta = \frac{\sigma}{\sigma_{cr}} \tag{6}$$

The usage factor has its maximum allowed value based on loading condition, structure, and slenderness.

The reduction of buckling strength between a realistic buckling and an ideal buckling is called "knock-down" factor ρ. It is an empirical reduction (σ_{cl}) in the elastic buckling strength (σ_E) due imperfections and non-linear behaviors of material and geometry.

$$\sigma_E = \rho\sigma_{cl} \tag{7}$$

The impact of imperfections on buckling depends on the geometry of the structure. For an cylindrical shell this depends on the relation between the radius and thickness of the structure. Even smaller imperfections can cause large reductions in buckling strengths when compressed axially. When designing a cylindrical shell structure requirements are set on the upper limit of geometric imperfections in production. A knock-down parameter is introduced to calculate the reduction of the buckling strength due the expected imperfections which the cylindrical shell will have to be designed for. This will be further discussed in chapter 4.

2.2.2 Cylinder Structure

Cylindrical structures comes in various different shapes. They can be vertically stiffened, ring stiffened or both. By vertically stiffening a cylindrical structure it is strengthened against bending. Ring stiffening reduced the buckling length of the cylinder and effectively separated a longer cylinder into smaller cylinders. Figure 7 shows how a vertically and ring stiffened cylinder is separated into curved panels.

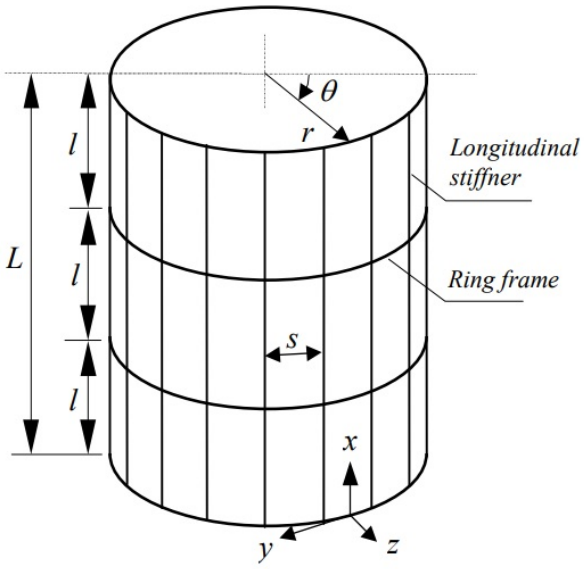

Figure 7: Longitudinal and ring stiffened skirt with described parameters used in theoretical description [2]

A requirement for the applied theory is short cylinders relative to its diameter. Stiffened cylinders have different failure modes, which are linked to how the shell is stiffened.
When assessing buckling of a cylindrical shell the modes associated longitudinal stiffened are expected to follow a pattern based upon the relationship between the height of the cylinder and the distance between the stiffeners.

The support skirt of a LNG tank is both ring and longitudinally stiffened. Two unstiffened short cylinders is separated by a ring stiffener and is composed of different materials. The longest section of the skirt is a vertically stiffened cylinder separated with one ring stiffener. In this part the curved panels between the vertical stiffeners will be studied for buckling. In figure 8 the buckling modes expected for stiffened and unstiffened cylindrical structures is illustrated.

Buckling mode	*Type of structure geometry*		
	Ring stiffened (unstiffened circular)	*Longitudinal stiffened*	*Orthogonally stiffened*
Shell buckling			
Panel stiffener buckling			
Panel ring buckling	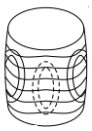		

Figure 8: Buckling modes for different types of cylinders [2]

A stiffened cylindrical shell is divided into curved panels between the vertical and ring stiffeners. Buckling in these panels are analysed locally. For closely spaced stiffeners a *effective length* l_{e0} is used which is the length of the curved plate in between the ring stiffeners and thus their distance from each other. The relation between the effective length and the β parameter is illustrated in figure 7.

As only the longitudinal stiffened shell using the same full length of the cylinder the critical buckling stress will become lower than is if ring stiffeners was used and the curved plates divided into smaller plate sections.

The approximation of the effective length is given by $l_{e0} = l$ or $l_{e0} = 1.56\sqrt{rt}$ and the smallest of these should be used.

$$l_{e0} = min\{l, 1.56\sqrt{rt}\} \tag{8}$$

The relation between the length and the efficient length is given by

$$\beta = \frac{l}{1.56\sqrt{rt}} \tag{9}$$

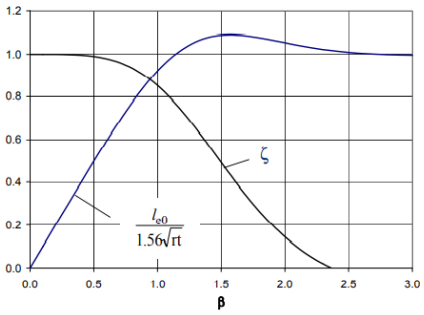

Figure 9: Effective length [2]

2.2.3 Buckling of Cylinders

The support skirt is composed of three different sections. These have different materials, thicknesses, and serve different functions in the structure. It's the two upmost sections closet to the tank which are unstiffened cylinders and will be relevant using the theory for buckling of cylindrical shells. The theory in this chapter covers the formulas to calculate the critical elastic buckling strengths and how the wave patterns impacts the strength.

A cylinder exposed to an axial force in compression given by:

$$N_x = \frac{P}{2\pi r}, N_{x\theta} = N_\theta = 0 \tag{10}$$

based upon the differential equation of the deflection of the cylinder

$$D\Delta^8 + \frac{Et\delta^4 w}{r^2 \delta x^4} + \frac{P}{2\pi r}\Delta^4(\frac{\delta^2 w}{\delta x^2}) = 0 \tag{11}$$

Solved this give the deflection

$$w = \delta(sin\frac{m\pi x}{l})sin(n\theta)(\frac{\delta^2 w}{\delta x^2}) = 0 \tag{12}$$

As buckling occurs the number of half waves expected in the buckling is given by the parameters m and n. In longitudinal direction m is the number of half waves and n is for the entire circumferential waves.

These are given as

$$m = \frac{l}{s} \tag{13}$$

and

$$n = \frac{\pi r k}{s} \tag{14}$$

The critical axial stress for a cylinder is given by

$$\sigma_{xE} = \frac{\pi^2 E}{12(1-\nu^2)}\left(\frac{t}{l}\right)^2\left[\frac{(m^2+\bar{n}^2)^2}{m^2} + \frac{12Z^2}{\pi^4} + \frac{m^2}{(m^2+\bar{n}^2)^2}\right] \tag{15}$$

Z is the Batdorf parameter. For a unstiffened cylindrical skirt the Batdorf parameter uses the length of the cylinder and is expressed as:

$$Z = \frac{l^2}{rt}\sqrt{(1-\nu^2)} \tag{16}$$

$\bar{n}$ is given by

$$\bar{n} = \frac{nl}{\pi r} \tag{17}$$

A estimate of the smallest critical load can be found by using the minimization of equation 2.2.3.

$$\left(\frac{m^2+\bar{n}^2}{m}\right)^2 = \frac{2\sqrt{3}}{\pi^2}Z \tag{18}$$

This will give the critical axial load

$$\sigma_{xE} = \frac{\pi^2 E}{12(1-\nu^2)}\left(\frac{t}{l}\right)^2 \cdot \frac{4\sqrt{3}}{\pi^2}Z = 0.605\frac{Et}{r} = \sigma_{cl} \tag{19}$$

Equation 19 is the estimated lowest elastic buckling stress which the cylinder will buckle. Using a conservative approach to the impact of the waves around the cylinder and longitudinally over the length.

The buckling coefficient of a axially compressed cylinder is given by

$$C_z = \frac{4\sqrt{3}}{\pi^2}Z \tag{20}$$

2.2.4 Buckling of Curved Panels

The longest and thinnest section of the skirt is the steel section at the bottom. It is the only section which is vertically stiffened to strengthen the structure, while the two upper section of the thermal break and the aluminium section mounted to the tank are unstiffened cylinders and is shorter and thicker.

To find the local buckling the the stiffened part of the support skirt the shell between the stiffeners has to be treated as curves panels. The width of the panel is the stiffeners spacing distance s and the length is the distance between the ring stiffeners.

The number of buckling waves expected in the panels n is found by using the term

$$n = \frac{\pi r k}{s} \tag{21}$$

where the number of half waves expected is k and r is the radius of the cylinder. For cylinders with lower stiffener spacing the number of half waves is set to $k = 1$ where the panels are narrow.

The Batdorf parameter Z is used to calculate the buckling coefficient and is scaled by using the relation between the length of the panel in the cylinder and the radius thickness. It is a relation of slenderness of the cylinder and its effect on the buckling coefficient. In figure 10 the relation between the buckling coefficient and the Batdorf parameter is plotted in relation to the half waves.

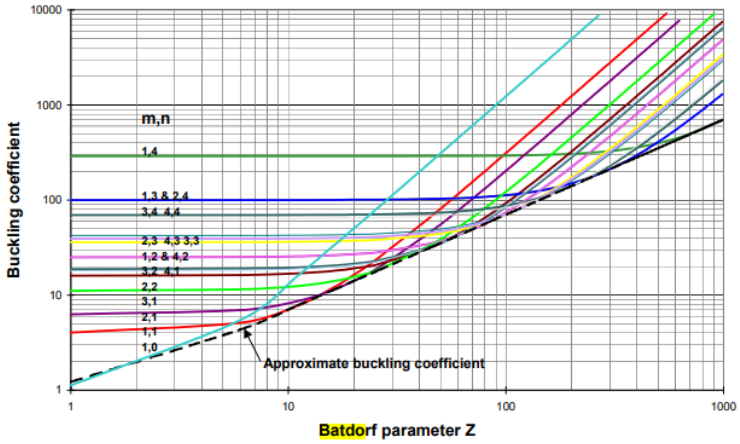

Figure 10: Buckling Coefficient with increasing Batdorf parameter [2]

For curved panels the length is equal to the stiffener spacing and the Batdorf parameter used is

$$Z_s = \frac{s^2}{rt}\sqrt{(1-\nu^2)} \tag{22}$$

Both Batdorf parameter are used in the analysis of the support skirt. For local panel buckling Z_s is used and buckling in a unstiffened cylinder Z_l is used.

With reduced stiffener spacing the elastic buckling for narrow panels can be calculated using Equation 23.

$$\sigma_E = \frac{\pi^2 E}{12(1-\nu^2}\left(\frac{t}{s}\right)^2\left(4 + \frac{3Z_s^2}{\pi^4}\right) \tag{23}$$

It calculates a lower bound of the elastic buckling stress using the formula for buckling of a plane plate (the first term) together with the curvature adjustment for the panel (second term) using the Batdorf parameter.

The approximation of the buckling coefficient for the curved shell is the second term

$$\bar{C_z} = 4\sqrt{1 + \frac{3Z_s^2}{\pi^4}} \tag{24}$$

2.2.5 Buckling of Longitudinally Stiffened Shells

The stiffened cylindrical shells are categories differently into categorised of A, B, and C. The different categories considers to what degree the shells are stiffened and which stiffeners are used.

The category A is a lightly stiffened shell with few or no stiffeners. The category B is a closely longitudinal stiffened cylinder with narrow stiffener spacing. Category C cylinder is a orthotropic stiffened cylindrical shell.

The skirt assessed in this paper is a longitudinal stiffened orthotropic shell with L-stiffeners.

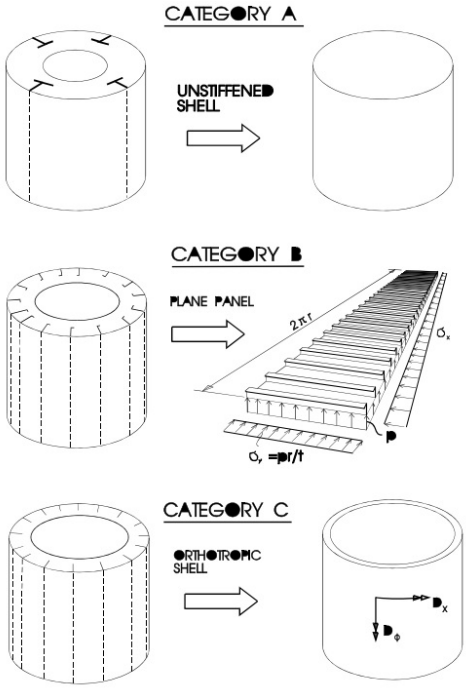

Figure 11: Categories of longitudinally stiffened cylindrical shells [2]

For these stiffened shells the new Batdorf parameters are:

$Z_s < 9$ i.e $\frac{s}{t} < 3\sqrt{\frac{r}{t}}$

For curved panels of width the length of the stiffener distance s and length l the number of half waves for each panel is given by

$$n = \frac{\pi r k}{s} \tag{25}$$

where k is the number of half waves between each stiffener. With lower stiffener distance s each width becomes very low and don't allow many half waves and $k = 1$. The Batdrof parameter for the curved panels in between the stiffeners becomes:

$$Z_s = \frac{s^2}{rt}\sqrt{1-\nu^2} \tag{26}$$

For the curved panels the buckling stress becomes

$$\sigma_E = \frac{\pi^2 E}{12(1-v^2)}\left(\frac{t}{l}\right)^2\left(4 + \frac{3Z_s^2}{\pi^2}\right) \tag{27}$$

For the stiffened cylindrical shell the critical axial compression is derived from the same equation as an unstiffened one, but has to account for the stiffeners and their resistance to bending through their moment of inertia. The stiffener ratio A using the effective plate flange and a ratio between stiffness of stiffeners γ and shell plating is given by:

$$\gamma = \frac{12(1-\nu^2)I_{lef}}{st^3} \tag{28}$$

Where I_{lef} is the moment of inertia of the stiffeners where the effective stiffener flange is accounted for. The choice of effective flange determined to be the effective stiffener length between the stiffeners. As the stiffeners are numerous and their spacing quite narrow the effective flange range is given by equation 8.

Thus the axial compression for a stiffened shell is given by

$$\sigma_{xE} = \frac{\pi^2 E}{12(1-v^2)}\left(\frac{t}{l}\right)^2\left[\frac{1}{1+\left(\frac{A}{s_e t}\right)}\left(m^2\gamma + \frac{(m^2+\bar{n}^2)^2}{m^2} + \frac{12Z^2}{\pi^4}\frac{m^2}{(m^2+\bar{n}^2}\right)^2\right)\right] \tag{29}$$

Since most shells buckle with one wave at the ends the longitudinal half wave $m = 1$.
The buckling coefficient for stiffened cylindrical shell can be given by:

$$C_x = \frac{1}{1+\frac{A}{s_e t}}\left(\gamma + \frac{4\sqrt{3}}{\pi^2}Z\right) \tag{30}$$

The buckling coefficient can be use with the buckling stress for a cylinder:

$$\sigma_E = \frac{\pi^2 E}{12(1-\nu^2)}\left(\frac{t}{l}\right)^2 C_x \tag{31}$$

2.2.6 Critical Buckling Load

The equations to calculate critical buckling stresses has been established for both a stiffened and unstiffened cylindrical shell and curved panels. Using these equation the corresponding critical buckling load applied axially to a cylindrical shell is found based on the formula for stress $\sigma = \frac{F}{A}$. The stress for a unstiffened axially loaded cylinder is given by:

$$\sigma_E = \frac{N_x}{A} = \frac{N_x}{2\pi r t} \tag{32}$$

For a stiffened cylinder the contribution from the stiffeners have to be included which gives an increased area and will help reduce the stresses when axially loaded.

$$\sigma_E = \frac{N_E}{2\pi r t(1+\frac{A}{st})} \tag{33}$$

where s is the distance between the stiffeners and A is the cross section area of the stiffener.

3 Method

In this chapter the method used to conduct the study will be described. It will cover the method used to perform the thermal analysis and temperature displacements and how the buckling analysis was performed. This includes both a description of how the analytical results were calculated and the analysis conducted in Abaqus. The assumptions and negligible factors will also be described.

3.1 Model

The model used for the support skirt is a MOSS Maritime design of a spherical LNG ship. An excerpt of the drawing of the support skirt is is presented in Appendix A. It is designed for the cargo temperature of LNG with $-163C^{\circ}$. As the study will be performed for a cargo of liquid hydrogen with a lower temperature of $-253C^{\circ}$ the model cant be expected to perform as well for this cargo. The weaknesses in this model with a lower temperature cargo will be studied and be discussed on how to be improved on.

As the report is focuses around the thermal effect on the support skirt and its effect on buckling the model was limited to a spherical design rather than a non-spherical. If the tank were to be designed non-spherically by extending it vertically it would still use a cylindrical skirt as will be studied here, but with some modification to account for a higher center of gravity and weight from cargo and the tank.

3.2 Analysis using Finite Element Method

The focus of this report will be on using Abaqus to perform the analysis both of the thermal effects on the support skirt and its buckling strength. At first both will be studied separately to find their insulated effects and then combined to see the combines effect of the temperature on the buckling strength of the support skirt. The buckling strength will first will estimated analytically using the DNV guidelines for calculations and then studies linearly and non-linearly using Abaqus. The results will then be compared and discussed.

3.2.1 Thermal Analysis of the Support Skirt

The linear thermal analysis calculates the thermal distribution and displacement as a result of the thermal loads and boundary conditions. A coupled thermal-stress analysis is used to find the solutions of the stresses as a result of the temperature. The material properties of conductivity and thermal expansion coefficients are used to determine how the temperature will change based on its distance from the thermal loads. There are two thermal contributors in the support skirt model. This is the temperature from the tank which is a line load around the upper edge and an thermal interaction between the air around the non-insulated part of the support skirt. The interaction between the air temperature and the skirt transfers heat trough convection. This creates a section in the skirt which there are no directly applied thermal loads and only whats gets distributed through the material. A linear calculation of the temperature is performed for each element using the material conductivity and the distance between the sources. The local temperatures in the nodes is then used together with the thermal expansion coefficient to calculate the temperature-displacements.

3.2.2 Linear Eigenvalue Analysis

The theoretical buckling loads is found using a linear eigenvalue analysis which solves the eigenvalue problem and finds the lowest buckling modes which will occur in a structure for a given load. In the linear analysis small perturbations are assume per element and solves the problem til an elements stiffness matrix becomes zero for a given axial load.

The boundary conditions is set to fixed both in the top and bottom of the skirt, but allowed to translate in the top of the skirt in z-direction to buckle. A shell edge force, which is a line load is placed on the top of the cylindrical shell and exerts axial compression. The analysis is then conducted using the linear perturbation buckling analysis. A requested number of eigenmodes is returned with their respective eigenvalues. The eigenvalues returned is thus the factor which the load has to be amplified to cause the buckling of the eigenmode.

3.2.3 Non-Linear Buckling Analysis

A non-linear analysis in an incremental analysis that combines of several linear analysis which together gives a more accurate calculation. It accounts for non-linear material and geometric behaviors which changes as the buckling occurs. Both the geometry is changed due to elastic material and the materials properties change due to large strains. All over a non-linear analysis gives a more realistic result of the buckling behaviour and calculations. The downside is the increased computing time required to run all the increments that forms the analysis.

The non-linear analysis is conducted in two ways in this study. The first analysis will perform a non-linear elasto-plastic buckling analysis of the skirt with axial force and no imperfection. Then a analysis which imperfections are added together with the same eigenmodes obtained in the linear eigenvalue analysis to study these modes non-linearly.

Different imperfections will be analysed and compared to the minimum requirements of the DNV regulations. The non-linear static riks methods in Abaqus uses the Arc-length method for the analysis. It is a method with high accuracy and able to solve the problem for local yield in parts of the structure. Arc-length method efficiently solves the systems of equations for systems with assigned loads and boundary conditions. The path converges towards the solutions as the increments are added up. It gives a good solution in which both ductile and brittle collapse are accounted for in a manner which represent buckling well.

3.2.4 Buckling Analysis with Temperature-Displacements

To analyse the effect of the temperature-displacement on the buckling strength due to the cargo temperature both studies will be combines to one analysis with both steps. First a step witch calculate the temperature-displacements due to the thermal load will be analysed. Then the results from the thermal step will be applied in a buckling analysis. The axial load will then be placed in the displaced upper edge of the support skirt causing bending. When these effects are combines the analysis is run. First a linear analysis will be conducted, then a non-linear analysis.

3.3 Software

The software use in this report to study the support skirts buckling capacity are DNV Genie for modelling and Abaqus for assigning all properties, meshing, and performing the analysis. In DNV Genie the geometry of the support skirt was modelled and assigned its dimensions. The model is then exported from Genie as an XML file which can be imported in Abaqus. In Abaqus the model is assigned its correct material properties as well as the shell thicknesses. The model is then assembles and the relevant steps created for analysing. This would be the temperature analysis and the buckling analysis step. The model is then meshed with a proper fine mesh to get a accurate solution. Loads and boundary conditions are applied to represent the realistic conditions in which the support skirt is fixed to the tank and loaded through the equator line. A analysis is created which uses all the current setting described and conducts a analysis based on the one requested in the steps. The results can be visualized for the parameters requested.

4 DNVGL Class Guidelines

In this chapter the guidelines DNVGL-GG-0134 and DNV-RP-C202 will be reviewed and the design rules for LNG carriers and buckling theory for cylindrical shells.

The DNVGL-CG-0134 is the class guideline which is used in the design of type B spherical LNG-tanks. It is the main guide lines for these designs and uses defined parameters and formulas to calculate the necessary requirements to support the loads. The guidelines are given for different aspects and components of the spherical tanks such as the hull of the tank, the supporting components such as the skirt and tower, and the insulation system.

4.1 Forces in a Spherical Tank

There are several forces acting on the tank. Both internal and external. Some of these include the external pressure on the tank, the weight of the tank and the cargo, forces due to the temperature differing, and forces exposed to the ship from the sea relayed to the tank.

A spherical tank supports its weight on the bottom of the tank to the bottom hull. The tank is also supported with a cylindrical skirt around the tanks equator line. This skirt supports the tanks weight and moments.

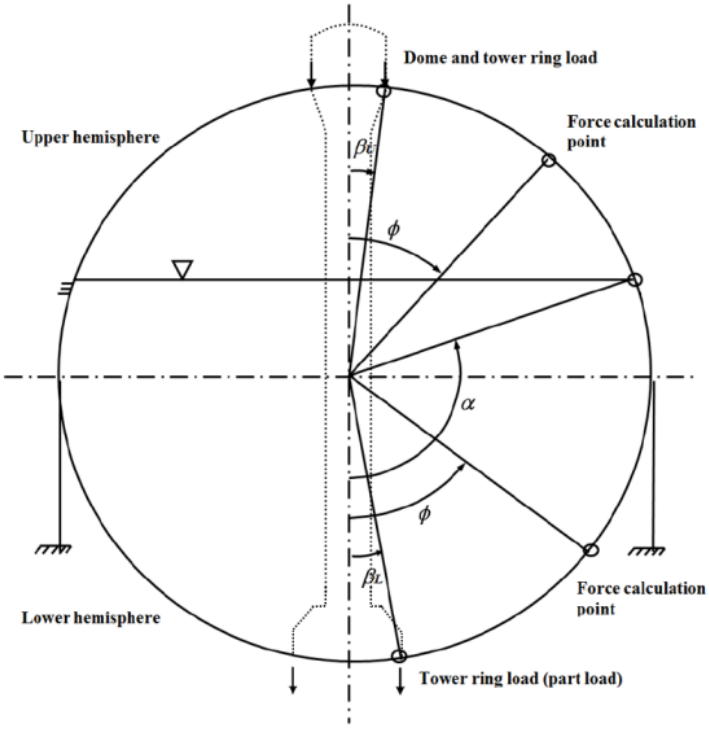

Figure 12: Illustration of LNG tanks forces and supports [12]

4.2 Thermal Loads

Structures dealing with high temperatures differences has to be analysed for thermal loads and stresses. For a LNG tank the impact of thermal loads impact shrinking of certain components and the spherical tank. Steady state analysis of the pump tower cargo hold, and skirt will have to be performed. The structure has to be analysed for temperature distributions and stresses and how this impacts the buckling and yield with load conditions both partially and fully loaded. This is

to be performed for all structures which deal with cargoes and temperatures below −55℃.

For a support skirt the thermal loads analysis also has to be performed. The skirt has a uneven temperature distribution compared to the spherical tank which have relatively low temperature differences while carrying cargo. At the top the skirt is mounted to the tank and is cooled to the cargo temperature. While at the lower section of the skirt fixed in the ship foundation is effected by the sea and air temperatures. Warm weather conditions should be assumed when performing a thermal analysis of the skirt and DNV recommends temperatures of:

- air temperature: 45℃
- sea temperature: 32℃
- cargo temperature (LNG): −163℃

The heat flow is analysed in full load condition and the temperature distribution. A thermal break consisting of an insulating low conductive material is usually installed between the aluminium and mild steel section which is composed of stainless steel. In figure 13 a DNV example of the temperature distribution is illustrated.

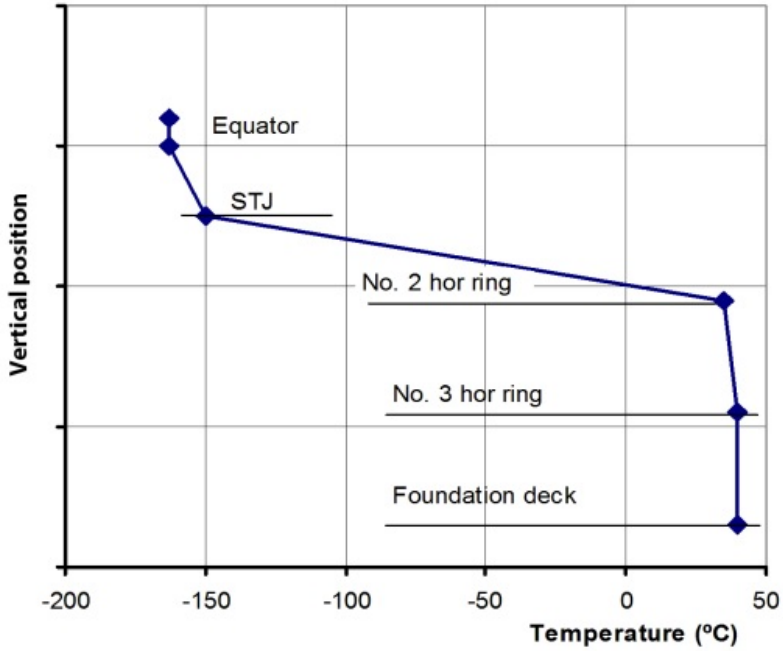

Figure 13: Temperature distribution example of a skirt [12]

4.3 Buckling Criteria of LNG Spherical Cargo Tank Skirt

Design criteria for buckling of the cargo tank skirt are derived using the direct calculations using linear FEM analysis. The critical design stresses ($\sigma_{10}, \sigma_{20}, \tau_0$) should be found related to buckling and their placement in the structure.

4.3.1 DNV Description of a Support Skirt

The skirt is composed of different parts of which some are made of different materials. These are traditionally separated into three different section, each with their unique functions as well as their structural support.

- Aluminium section, ring- stiffened/unstiffened
- Stainless section (Thermal break), ring stiffened
- Steel section, orthogonality and usually ring stiffened

The support skirt supports the cargo tank through transferring the loads to the ship foundation via the equator profile. It also insulated the ship from the lower temperatures from the cargo.

A transition joint is fitted between the aluminium section and thermal break to ensure proper weld transitions between the section.

Figure 14 shows a traditional skirt with its geometry and structural items outlined by the DNV guideline [12].

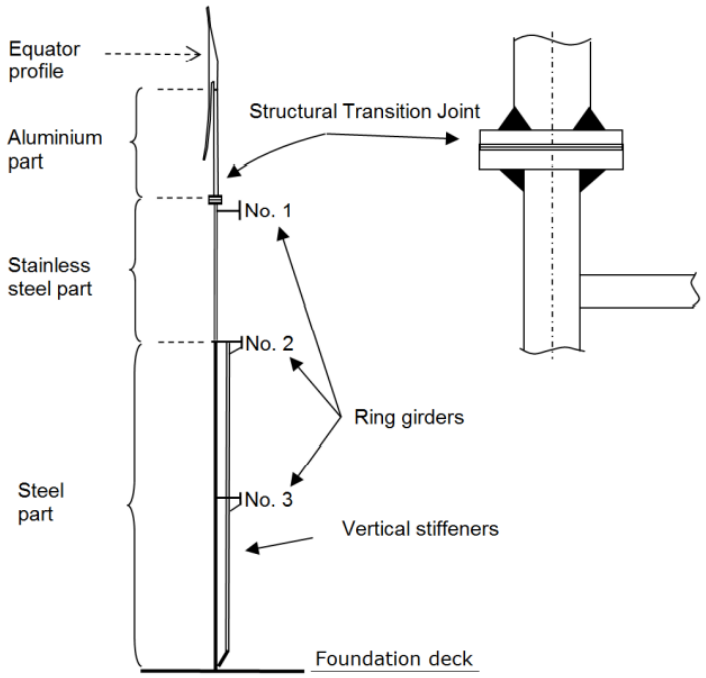

Figure 14: DNV, drawing of main geometry of tank skirt [12]

4.3.2 Load Cases for ULS Buckling Assessment of Spherical Tanks

To check for buckling capacity the load cases for the tank has to be analysed. The different load cases and load conditions are addressed for all loads which the tank is exposed to, both externally and thought the cargo and ship. Identifying the components which are exposed to high stresses is critical for the design and lifetime of the structure. Figure 15 shows the load cases for ULS buckling of the spherical tank addressed in DNV-CG-0134 [12]

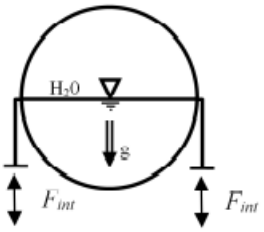

('H_2O' = 'fresh water')
Note: Pure static condition.

(a) Pure static condition with fresh water as content

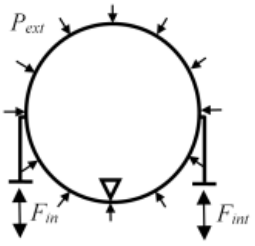

Note: Governing LC for buckling of upper hemisphere.

(b) Load condition for buckling of the upper hemisphere

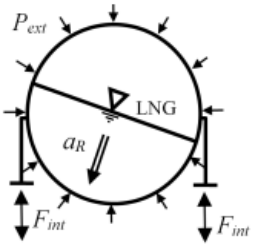

Note: Governing LC for buckling of lower hemisphere.

(c) Load condition for buckling of lower hemisphere

Figure 15: Load Cases for ULS Buckling Assessment of the Spherical Tank [12]

In DNVGL-CG-0134 Chapter 5.6 Table 6 the load cases for ULS buckling assessment of spherical tanks is presented in the class guideline [12].

The first load case is a test condition in which the tank is partially filled with fresh water. The loads the tank is exposed to is the gravitational forces from the weight of the fluid content and the tank self-weight.

Static and dynamic loads for LC1:

- Tank self-weight (tank material, insulation, piping)
- Partial filling of fresh water
- Static interaction due to still water bending and external static pressure.

The second load case depicts a sea going ship, but with no content in the tank. Thus this load case does not consider the weight contribution from a fluid content, only the tank self-weight. This case also has an external pressure difference which causes stress inwards. As the ship is sea going the case also regards dynamic forces.

Static and dynamic loads for LC2:

- Tank self-weight (tank material, insulation, piping)
- Static interaction due to still water bending and external static
- External pressure of $0.005MPa$
- Dynamic interaction force due to wave bending moment and external wave pressures

The third load case is a sea going ship with a partial filled tank. It is a combination of load case 1 and 2. A sea going tank with fluid content i the tank will also have to account for sloshing and movement of the fluid in the tank.

Static and dynamic loads for LC3:

- Tank self-weight (tank material, insulation, piping)
- Static interaction due to still water bending and external static
- External pressure of $0.005MPa$
- Dynamic interaction force due to wave bending moment and external wave pressures
- Partial filling of cargo; static and dynamic part combines based on resulting skewed acceleration a_R from the accelerated ellipse see figure 15c

In turn the forces form the load cases will be transferred to the foundations through the skirt. The skirt will thus be prone to buckling form these loads and a analysis will have to be carried out to make sure the skirt can withstand these loads both static and dynamic.

4.4 Appendix D Buckling Criteria of LNG Spherical Cargo Tank and Skirt

In the Appendix D the methods of calculation for the skirts acceptable buckling strength is described.The skirt is a cylindrical structures that supports the spherical LNG tank and transfers the axial forces towards the foundation deck. To strengthen the skirt against buckling the skirt may be stiffened both with ring and vertical stiffeners inside or outside of the structure.
In summary the skirt is checked for the buckling modes listed below:

- Shell buckling: Buckling that can occur between the rings/stiffeners
- Panel stiffener buckling: Overall buckling of vertical stiffeners
- Panel ring buckling: Overall buckling of rings including shell
- General buckling: Overall buckling of rings and vertical stiffeners
- Local buckling of vertical stiffeners/rings

A simplified eigenvalue analysis is carried out accounting for non-linear pre-buckling effects and elastic knock-down factor. For this analysis a computer is used to perform the buckling analysis of this magnitude. The buckling modes are found using the eigenvalue analysis and a non-linear analysis is performed for refined results which also can include imperfections [12].

4.5 Limit states - Design criteria

There are two limit states for each buckling type that have to be checked ensure safety. Each buckling mode will have to be to be checked with these criteria.

1. Elastic buckling
2. Elasto-platic buckling

Elastic buckling is the when the buckling occurs prior to any part of the shell reaching the yield stress. Thus a cylindrical shell may collapse due to great bending, causing instability. It is of vital consideration as once can not rely only on the yield strength itself.
Elasto-plastic buckling on the other hand is when the buckling occurs such that the collapse happens after the initiation of material yielding. The most severely loaded part of the cylindrical shell with highest stresses in relation to its yield strength is exposed to elastic-plastic buckling.

4.5.1 Buckling Criterion

The buckling strength criteria that has to be satisfied is a combined elastic and elasto-platic criteria. The two criteria are defined as

$$g > 0 \text{ or } h > 1.0 \tag{34}$$

where g and h is given by:

$$g = \Lambda_{CR} - \gamma_{sum} \text{ and } h = \frac{\Lambda_{CR}}{\gamma_{sum}}$$

Λ_{CR} is the critical buckling parameter. It uses the yield stresses from the *von Mises* formula and the reduced slenderness parameter Λ_E.

$$\Lambda_{CR} = \frac{1}{\sqrt{1 + \Lambda_E^4}} \frac{\sigma_F}{\sigma_{e0}} \tag{35}$$

Where the reduced slenderness parameter is given as:

$$\Lambda_E = \sqrt{F_E \frac{\sigma_F}{\sigma_{e0}}} \tag{36}$$

Using the *von Mises* two dimensional equation:

$$\sigma_{e0} = \sqrt{\sigma_{xo}^2 + \sigma_{\theta 0}^2 - \sigma_{x0}\sigma_{\theta 0} + 3\tau_0^2} \tag{37}$$

and the safety factor γ_{sum} is derived using the partial safety factors γ_m and κ.

$$\gamma_{sum} = \kappa \gamma_m \tag{38}$$

4.5.2 Partial Safety Factors

The partial safety factors γ_m is the material factor and κ is the slenderness factor.
The material factor is taken as:

$$\gamma_m = 1.15 \tag{39}$$

The slenderness factor:

$$\kappa = 1.0 \quad if \quad \lambda_E < 0.2 \tag{40}$$

$$\kappa = 0.925 + 0.375\lambda_E \quad if \quad 0.2 < \lambda_E < 1.0 \tag{41}$$

$$\kappa = 1.3 \quad if \quad \lambda_E > 1.0 \tag{42}$$

the dependent mode λ_E is:

$$\lambda_E = \sqrt{F_E \frac{R_{eH}}{\sigma_{e0}}} \tag{43}$$

where R_{eH} is the minimum specified yield stress at room temperature and and σ_{e0} the two dimensional von Mises stresses. F_E is given as:

$$F_E = \frac{1}{\Lambda_E} \tag{44}$$

where Λ_E is the elastic buckling parameter for cylindrical shells exposed to axial compression, shear stress and circumferential compression.

$$\Lambda_E = \frac{1}{2a}[b \pm \sqrt{b^2 - 4ac}] \tag{45}$$

4.5.3 Imperfection Amplitude

In geometrical design there is always expected some imperfections in the structure compare to the designed model. The model studied is a cylindrical shell structure and one important imperfections is due to the curvature of the plates and the iterations steps. The imperfections is closely related to the mesh applied. An imperfection amplitude is used to compare the relation between the ideal spherical shell and the imperfect spherical shell. This amplitude δ_i in the DNV regulations is defined as:

$$\delta_i = \frac{0.01g}{1 + \frac{g}{R}} \tag{46}$$

where there parameters $g = g_1$ or g_2 depending of the shell studied. For unstiffened cylindrical shells between the ring stiffeners g_1 is used.

$$g_1 = min[l, 4\sqrt{Rt}] \tag{47}$$

where l is the length between the ring stiffeners
For stiffened cylinders, the curved panels have imperfection limit. g_2 is given as

$$g_2 = min[s, 1.15(l\sqrt{rt})^{1/2}, \pi R/2] \tag{48}$$

where s is the distance between the stiffeners and l is the length between the ring stiffeners.

The imperfection amplitude for the vertical stiffeners is simply takes and

$$0.0015l \tag{49}$$

where l is the length of the vertical stiffeners between the ring stiffener.

These imperfections are further used in a non-linear FEM analysis to calculate the buckling strength. Both material and geometric non-linearity are included with the imperfection so give a realistic analysis. The non-linear analysis uses the eigenmode obtained from linear eigenvalue analysis with added imperfection.

4.6 DNV-RP-C202, Buckling Strength of Shells

DNV-RP-C202 give detailed guideline of buckling of curved panels and cylindrical shells in general. The theory outline in DNV-RP-C202 are based on the same general theory as refereed to in chapter 2 for buckling of cylindrical shells, but with some recommended practice and requirements for production [11].

4.6.1 Stability Requirements

DNV-RP-C202 also provides guideline for stability of shells subjected to axial compression and tension, bending, circumferential compression and tension, torsion, and shear forces.

The design shell buckling strength is designed as

$$f_{ksd} = \frac{f_{ks}}{\gamma_M} \tag{50}$$

and should be less or equal to the design equivalent von Mises' stress $\sigma_{j,Sd}$

$$\sigma_{j,Sd} \leq f_{ksd} \tag{51}$$

γ_M is the material factor and is given by:

- $\gamma_M = 1.15$ for $\bar{\lambda_s} < 0.5$
- $\gamma_M = 0.85 + 0.60\bar{\lambda_s}$ $0.5 \leq \bar{\lambda_s} \leq 1.0$
- γ_M 1.45 for $\bar{\lambda_s} > 1.0$

4.6.2 Characteristic Buckling Strength of Shells

The definition of characteristic buckling strength of shells is given by:

$$\bar{\lambda_s}^2 = \frac{f_y}{\sigma_{j,Sd}}\left[\frac{\sigma_{a0,Sd}}{f_{Ea}} + \frac{\sigma_{m0,Sd}}{f_{Em}} + \frac{\sigma_{h0,Sd}}{f_{Eh}} + \frac{\tau_{Sd}}{f_{E\tau}}\right] \tag{52}$$

where

- $\sigma_{a0,Sd}$ is the design membrane stress in the longitudinal direction due to uniform axial force
- $\sigma_{m0,Sd}$ is the design membrane stress in the longitudinal direction due to global bending
- $\sigma_{h0,Sd}$ is the design membrane stress in the circumferential direction
- τ_{Sd} is the design shear stress in the shell due to torsional moments and shear force

and the elastic buckling strengths :

- f_{Ea} = elastic buckling strength for axial force
- f_{Em} = elastic buckling strength for bending moment
- f_{Eh} = elastic buckling strength for hydrostatic pressure, lateral pressure and circumferential compression
- $f_{E\tau}$ = elastic buckling strength for torsion and shear force

Further the elastic buckling strength of curved panels is based the same equations as given in chapter 2.2.4 and chapter 2.2.3 for cylindrical shells.

4.6.3 Elastic Buckling Strength of Shells

In chapter 2 the theory of buckling cylindrical shells and curves panels was presented. This is the basis for the DNV class notes for buckling cylindrical shells and panels, but introducing parameters to account for imperfections relative to the structure dimensions. This are the plate buckling coefficient ψ, the curvature contribution ζ, and the knock-down factor ρ which accounts for the acceptable imperfections limit in production.

The elastic buckling strength equation for buckling of cylindrical shells is given as

$$\sigma_E = \frac{\pi^2 E}{12(1-\nu^2)}\left(\frac{t}{l}\right)^2 C \tag{53}$$

Where C is the reduced buckling coefficient that adjusts the buckling strength as the imperfections and curvature is accounted for. It is given by

$$C = \psi\sqrt{1+\left(\frac{\rho\xi}{\psi}\right)^2} \tag{54}$$

Using the Batdorf parameter Z_l from equation 16 for cylindrical shells and Z_s from equation 26 for curved panels.

When calculating the elastic buckling strength for curved panels the length is takes as the distance between the stiffeners and thus becomes

$$\sigma_E = \frac{\pi^2 E}{12(1-\nu^2)}\left(\frac{t}{s}\right)^2 C \tag{55}$$

The parameters used to calculate the buckling coefficients depends on the load case. In table 1

	Buckling of Curved Panels	Buckling of Unstiffened Cylindical Shells	Buckling of Stiffened shells
ψ	4	1	$\frac{1+\alpha_c}{1+A/(s_e t)}$
ξ	0.702 Z_s	0.702 Z_l	0.702 Z_l
ρ	$0.5(1+\frac{r}{150t})^{-0.5}$	$0.5(1+\frac{r}{150t})^{-0.5}$	0.5

Table 1: Buckling parameters for calculation of the Buckling Coefficient for axial stress [11]

where

$$\alpha_c = \frac{12(1-\nu^2)I_{sef}}{st^3} \tag{56}$$

A = Stiffener cross section area, without shell plate

I_{sef} Stiffener moment of inertia with effective shell width s_e
Z_l and Z_s is the Batdorf parameters which was given in equation 16 and 26 in chapter 2.

5 Description of Model

This chapter will briefly describe the model chosen for the analysis with its respective dimensions and materials. The model is based drawing provided by Moss Maritime of a spherical LNG carrier which was created in 2008. Due to copyright restrictions the full drawings will not be posted in this report directly as the drawings is owned by Hyundai Heavy Industries. Only a excerpt is listed in Appendix A

5.1 Model and Parameters

The parameters used for the skirt in this study are based upon the drawing, but fully identical. Reasonable parameters have been determined together with supervisor and co-supervisor for use in the study. All parameters used in this study will be given in table 2. In later chapters, some of the analysis will be performed for different parameters and the updated parameters will be provided in the current chapter. The model is based on a traditional skirt design outlined by DNV in chapter 4.3.1.

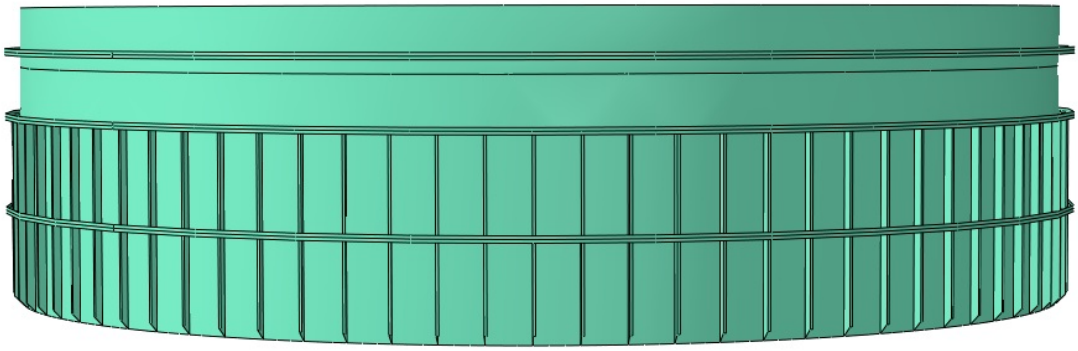

Figure 16: Model of the Skirt

These parameters are used in the model created in DNV Genie and then exported to Abaqus to perform the analysis. Figure 16 shows the modelled skirt with the parameters in table 2. All relevant material properties are described in the current chapters where they are used. The three materials use are Aluminium Grade-5083, Stainless Steel (SUS) Grade 304, Higher Tensile Steel LR Grade "EH36".

Skirt Module	**Length [mm]**	**Thickness [mm]**
Aluminium Secton	2330	62
NO.1 Ring Stiff. Step, Aluminium	600	32
NO.1 Ring Stiff. Flange, Aluminium	250	32
Thermal Break Section	1913	45
NO.2 Ring Stiff. Step, SUS	600	20
NO.2 Ring Stiff. Flange, SUS	250	31
Steel Section	7305	28
NO.3 Ring Stiff. Step, Mild Steel	600	20
NO.3 Ring Stiff. Flange, Mild Steel	250	31
Vertical Stiffener Step, Mild Steel	350	12
Vertical Stiffener Flange, Mild Steel	1000	17

Table 2: Dimensions used in the skirt model

The skirt is stiffened with three ring stiffeners, one with each of the three materials. They use the shape of T-stiffeners. Vertical stiffeners are placed along the circumference of the steel section. They number 80 stiffeners and take the shape of L-stiffeners.

5.2 Boundary Conditions

A support skirt is in reality constrained in the bottom of the structure to the ship foundation and at the top with the tank. It was then reasonable to set the boundary conditions to be fixed in bottom and top of the skirt. To be able to analyse for buckling, the skirt was allowed to translate in z-direction at the top of the structure.

The thermal analysis in chapter 6 constraints are not added to the structure. This is to let the skirt top displace together with the tank in radial direction towards the centre due to the temperature difference.

In the buckling analysis chapters, both linear and non-linear the skirt is constrained in both ends. When performing the buckling analysis on the temperature-displaced skirt, the constraints are applied at the current position of the displaced nodes.

The later chapters will briefly mention the boundary condition used. Loads conditions will also be described in their relevant chapters.

5.3 Choice of Mesh

For this report a lot analysis are conducted, both get the necessary results and to try out the inputs for errors and compatibility. Its important to have a suitable mesh to get accurate results, but also have to computing capability to perform the analysis in a reasonable time. This is particularly important for the non-linear analysis. The mesh was determined with these factors in mind and to use the same mesh for the analysis.

The mesh chosen for the analysis is a size of $0.3m$ per element and was discussed with co-supervisor. This is a reasonable choice which should give sufficient accuracy of the results and computing times suitable for the time given. With a size of $0.3m$ per element, about 5 elements will be placed between the vertical stiffeners and 2 on the ring stiffener flange. With this mesh size a total of 25523 elements are created for the model.

6 Thermal Analysis of the Skirt

In this chapter the thermal effects and the temperature difference along the support skirt is described for steady state conditions. The analysis will find the expected thermal loads from the cargo through conduction in the material and the airs heat transfer through convection. Warm weather conditions is assumed. The temperature distribution along the skirt will be found and described, displacements which occurs due to the temperature, and the heat flow through the thermal break. Both a linearly and non-linearly temperature-displacement analysis will be studied. The thermal analysis will be conducted both with cargo of LNG and LH2 and compared.

6.1 Description of the Skirt

The skirt is composed of three sections which consists of different metals. All these have different properties both thermal and structurally. Connected directly to the tank with cold cargo is upper section of the skirt which consists of aluminium. It has a high ability to lead heat and lower structural properties compared to steel. Below the aluminium section is the thermal break. The skirt is composed of stainless steel with a low thermal conductivity and its role is to reduce the heat flow to separate the temperature of the other two section. The lower section is the longest and consist of mild steel with a much lower thermal conductivity than aluminium. This section is not insulated with fiber glass and exposed to the air temperature. Its role is to act as the structural backbone of the skirt and is fitted with vertical stiffeners. In figure 17 a 2D illustration of the three sections of the support skirt can be seen. The thermal properties of the material is listed in table 3

Figure 17: 2D Illustration of a support skirt [16]

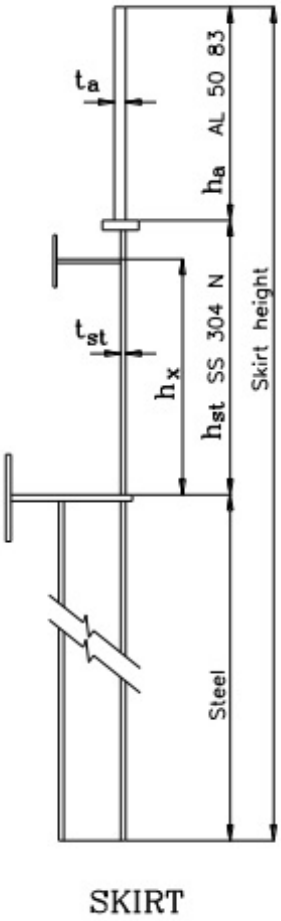

Cargos transported in the tanks has a low temperature due to them being transported as liquids which has a low boiling point. As its important to keep the content cold the tanks are insulated from its surroundings to mitigate the heat flow of the air temperature. Around the tanks and the upper sections of the support skirt there is installed insulation composed of fiber glass.

The tanks are insulated to prevent heat flow due to the air interacting with the tank, but there is still an physical interaction between the tanks and the foundation of the ship through the support skirt of the tank. It cant be insulated in the same way as the tank as the skirt served a structural supporting role.

The insulation stretches around the tank and over the two first section of the support skirt, covering the aluminium and the thermal break. By covering both the stainless and aluminium section, optimal heat loss prevention is achieved.

For this study the following parameters in table 3 are used in the calculations and analysis of the temperature effects.

Material	Thermal Conductivity $[W/mK]$	Expansion Coefficient [1/℃]
Aluminium	116	2.2 E-5
Stainless Steel	14	1.35 E-5
Mild Steel	35	1.2 E-5

Table 3: Thermal properties of the three materials in the support skirt [6][8]

6.2 Thermal Break

The tank and upper section of the skirt is insulated with
fiber glass to mitigate heat flow to reach the cargo. To insulate the cargo and the tank from its physical connection to the foundation a thermal break is used. It low conductivity reduces the heat flow through the material due to convection. There are several low conducting materials to use, but the material chosen has to have both low conductive ability, suitable structural properties, and be affordable as well. The material chosen for the support skirt is the stainless utility steel (*SUS 304*) which have similar material properties to mild steel, but with much lower thermal conductivity.

It is an expensive material and mild steel still serves the best structural function with its higher yield strength and limiting the use of stainless steel is advantageous for structural integrity. Thus the thermal break is designed to be a smaller part of the skirt between the two section of aluminium by the tank and the mild steel stretching to the foundation.

The effect of the thermal break is dependent of the length between the two temperature sources through a material as well as the conductivity. A optimal length has to be chosen based on the materials properties, both thermal and structural. Cost is a factor both in production and cost of the material, but as well as the heat loss which could be prevented and thus save energy. The heat flow is described further in chapter 6.6

6.3 Temperature-Distribution of the Support Skirt

All dimensions used in for the skirt model are given in table 2. Using the full 3D model will give the best thermal analysis of the skirt and how it effects the structure. The support skirt model studied includes the structure from its bottom foundation to the ship all the way to the connector section to the cargo tank.

Boundary conditions used for model in the temperature analysis are free from all constraints and allowed deformations only due to the thermal loads. The top of the skirt and the tank sphere is assumed to have roughly the same deformations as they both have the same temperature and radius. In the bottom connection to the ship foundation there will be little or no thermal deformations as the cargo temperature is isolated and the bottom skirt section will be affected by the air temperature. The sea temperature was neglected in the thermal analysis as the main contribution to the temperature of the skirt would be the surrounding air temperature.

The thermal loads are applied in two different ways. The cold temperature from the tanks cargo is applied as a boundary condition at the upper edge of the skirt model to represent the temperature from the tank. No temperature loss from the cargo to the top of the skirt is assumed in this analysis. Where the aluminium and stainless steel sections is insulated from the air, the steel section is exposed to it. The air is set to a higher temperature of $40C^{\circ}$ as it could realistically be exposed to such a temperatures at some places or even higher. Surrounding air transfers its heat to the skirt material through convection. An interaction is placed at the steel section between the material and the air with a constant film coefficient of $13W/m^2K$ [4]. This coefficient is chosen for low-medium free air convection. Due to the interactions effect over such a large area the steel section will have the same temperature as the air. This can be seen in figures 18 where the lower section approaches constant temperature.

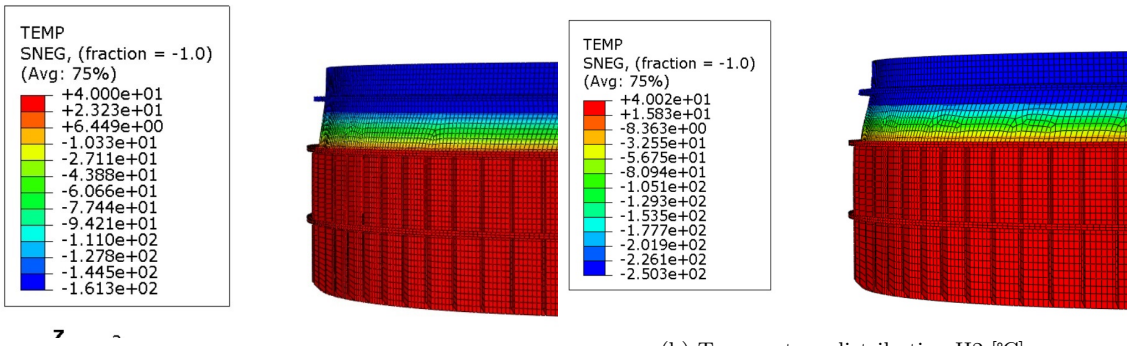

(a) Temperature distribution LNG [℃]

(b) Temperature distribution H2 [℃]

Figure 18: Temperature-distribution

In figure 18 the temperature distributions for both LNG and LH2 is presented. Due to its low thermal conductivity the thermal break reduces the heat flow between the ship and the tank. It manages to reduce the heat flow sufficiently enough such that most of the temperature change occurs in the thermal break. Both cargo loads has the majority of the temperature insulated through the thermal break, but the LH2 has a greater temperature difference per length. For LH2 the heat flow would be higher through the thermal break than for LNG, which will be presented in chapter 6.6.

The temperature distribution is plotted along the vertical height of the support skirt for both cargoes in figure 19.

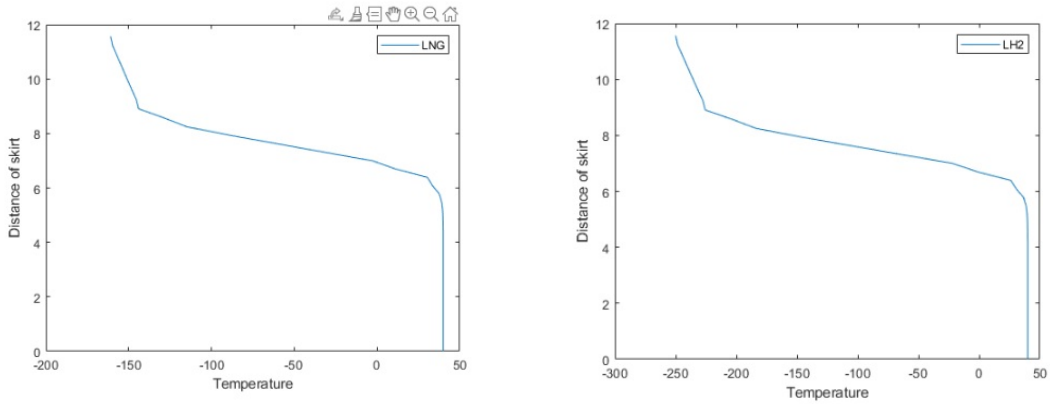

(a) LNG cargo

(b) LH2 cargo

Figure 19: Temperature-distributions of the support skirt

6.4 Comparison of Results

DNV class guideline CG-0134 outlines the requirements for calculations of the thermal stresses based on the temperature distribution along the support skirt. The regulations express that any tank system where thermal stresses is caused by the cargo should be analysed for yield and buckling based on the current temperatures [12]. It states that warm weather conditions should be assumed as a conservative analysis depending on the intended trading area. In this study the temperature of 40℃ was assumed. Warm sea temperature is usually set around 32℃, but was neglected in this study as its impact is negligible when compared to the air temperature contribution.

An example of the temperature distribution of the support skirt with a tank cargo of LNG is shown in figure 20.

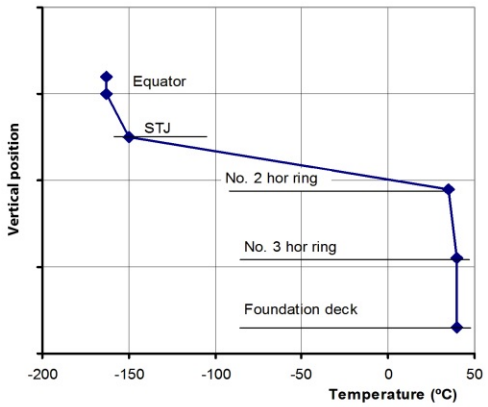

Figure 20: Example of temperature distribution of skirt by DNV [12]

The temperature-distribution found in this study of the support skirt shown in figure 19 follows the typical temperature distribution proposed by DNV shown in figure 20. More reference points along the vertical position is used in the analysis. In the distribution plots, the conductivity of the materials can clearly be seen for each section by the gradient of the temperature change. The lower gradient seen in both plots are due to the thermal break with high temperature change per length. Use of stainless steel with a conductivity of $14W/(Km)$ was able to insulate the lower temperature of LH2 sufficiently through the thermal break.

Without the thermal break in the skirt the heat flow to the cargo would be higher. The temperatures would distribute more evenly through the skirt depending on the material. It would also cause temperature-displacements evenly along the skirt and might even be reduced at the top of the skirt. Figure 21 show the temperature-distributions compared for both cargoes.

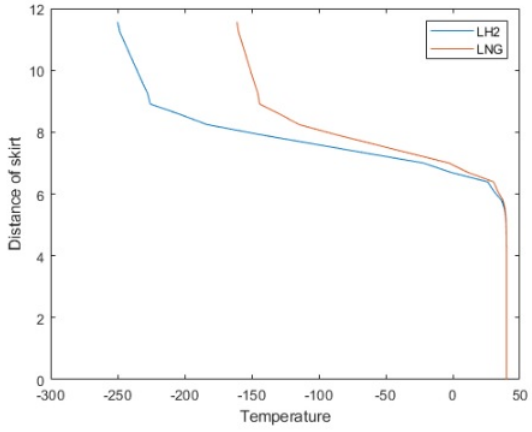

Figure 21: Comparison of temperature distribution of both cargo's along the skirt

In the thermal analysis of the support skirt it was found that the thermal break was able to isolate temperature between the sections quite extensively, both for LNG and liquid hydrogen. The low thermal conductivity of stainless steel make it possible to reduce the heat exchange for both cargoes substantially.

The plot in figure 21 shows that at the upper end of the thermal break there is still a some degrees left until reaching the cargo temperatures. With LH2 cargo the gradient in the aluminium section was less steeper than for LNG. When temperature is braked over a material with a higher conductivity, in this case aluminium the result is a higher heat flow through the support skirt. The

heat flow can be reduced by increasing the length of the thermal break or by using a even lower conductivity material.

6.5 Temperature-Displacement

The difference in temperature between the air and cargo causes temperature-displacements and shrinking in the upper part of the skirt. As warm conditions are assumed and a potential manufacturing temperature of 40℃, this is set as the reference point in which the displacement is measured. With the reference point set at a straight vertical cylinder at the air temperature the cold cargo temperature causes the metals to retract in the radial direction towards the cylinder center. The analysis of the temperature-displacements uses the same model and properties used earlier in this chapter.

6.5.1 Linear Analysis of the Temperature-Displacement

A linear analysis is carried out in Abaqus linearly using a coupled temperature-displacement step which find mechanical and thermal solutions allowing elements with both temperature and displacements. It find the steady-state displacements for all the elements and calculates the stresses which occurs due to the temperatures. In this analysis the skirt uses the same boundary condition and loads as in the temperature distribution where its allowed to displace freely in the top of the skirt.

The temperature-displacement is directly related to the at the temperature as seen in figure 22 and the displacements become larger for colder temperatures. Due to different expansion coefficients of the materials the sections will displace differently for the same temperatures. As aluminium has the highest expansion coefficient it will have the largest displacement for each degree ℃ its reduced. At the top of the skirt the largest radial displacements occurs as it has the coldest temperatures. In table 4 the temperature-displacements at the top of the skirt and the highest stresses as a result of the displacements.

Cargo	Temperature Difference [℃]	Temperature - Displacement $[mm]$	Stresses $[MPa]$
LNG (-163℃)	203	97.3	158.9
LH2 (-253℃)	293	140.4	229.4

Table 4: The temperature-displacement that occurs on the top of the support skirt and its resulting stresses, linear-analysis

It is the radial displacement which is of interest regarding its effect on the buckling of the skirt. The displacement caused by the temperature gives an eccentricity between the upper end lower ends of the skirt which gives bending when loaded axially. This will reduce the buckling strength of the cylinder which will be studied in later chapters.

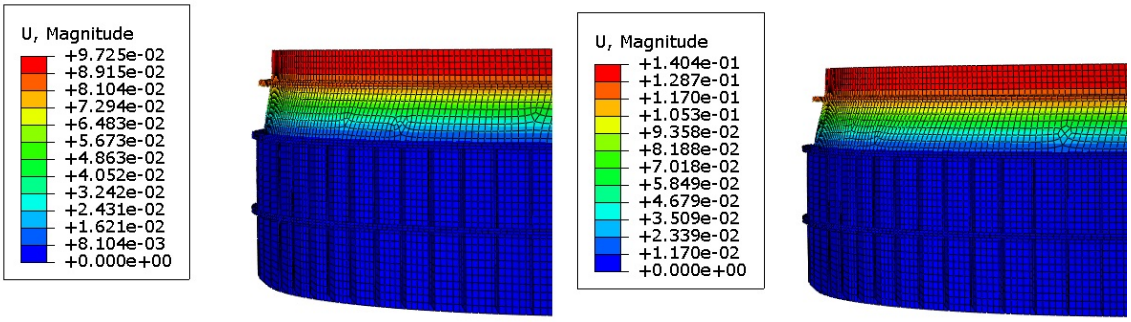

(a) Temperature-Displacement LNG $[m]$

(b) Temperature-Displacement LH2 $[m]$

Figure 22: Temperature-displacements for the two cargo's with the displacements in the visualisation scaled with a factor of 5

Stresses occurs in the support skirt as a result of the temperature differences. This is due to the bending between the displaced elements and some reaction forces which occurs as a result of the thermal retraction. The greatest stresses occurs in the upper section of the vertical stiffeners and in their connection to the steel shell of the curved plates. This can be seen in 23 and their respective highest stresses in table 4.

The yield strength of the steel used in the shell and the stiffeners are set to $350MPa$ which is higher than what occurs in the skirt due to the temperature-displacements. Yield caused by the temperature difference alone on the skirt will not occur. These stresses will be present when the skirt is analysed for buckling and their impact in reduction of buckling strength of the skirt studied in the non-linear buckling analysis in chapter 7.4.

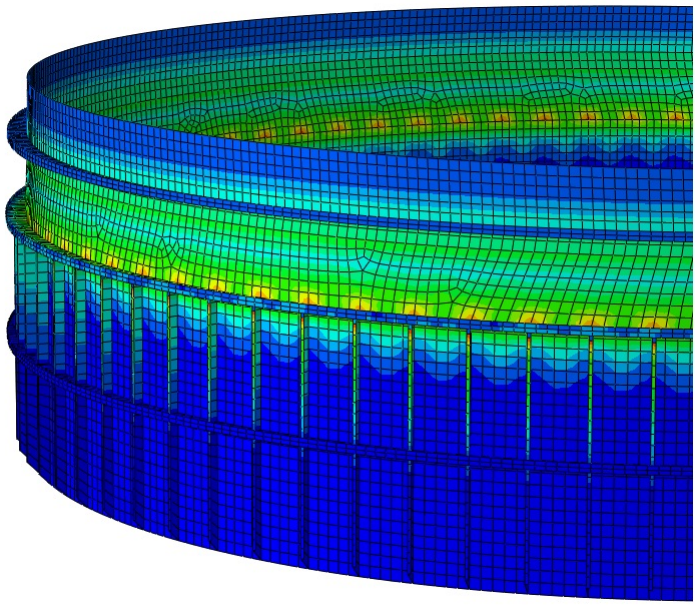

Figure 23: Stress Hot-Spots due to the Temperature-Displacement

6.5.2 Non-Linear Analysis of the Temperature-Displacement

In the non-linear analysis the temperature is increased over a number of increments linearly during a set time. The analysis then includes the non-linear effect of material and geometry which will slightly impact the deformation over the increments.

The number of increments used in this analysis was 111 to get a detailed comparison between the

linear analysis and the non-linear.

The results obtained from the non-linear analysis is very similar to the ones obtained in the linear analysis. This is the case both for the temperature-displacement and the stresses which can be seen in 5. The displacement difference between the linear and non-linear is $0.1mm$ for both cargoes which is small enough to be neglected. Its difference in the stresses observed as also quite small. It was found to be about $1MPa$ lower in the non-linear analysis for LH2 which is a change below 0.5%. A linear analysis will thus give quite similar results and the offset is higher values giving the linear analysis a conservative result. When further analysing the skirt structurally it may not be necessary to conduct a full non-linear temperature analysis of the skirt as it will save a lot of computing time and gives very similar results.

Cargo	Temperature Difference [℃]	Temperature - Displacement [mm]	Stresses [MPa]
LNG	203	97.2	158.5
LH2	293	140.3	228.4

Table 5: The temperature-displacement that occurs on the top of the support skirt and its resulting stresses, non-linear-analysis

The stress hot spots distribution which occurs from the temperature are the same in the non-linear analysis as shown in figure 23, but with the slightly lower values.

6.6 Heat Flow Through Thermal Break

This chapter will present the results of the heat flow through the thermal break for LNG and LH2.

Despite the low conductivity of the material in the thermal break and its insulating properties some heat flow will occur. Due to the low thermal conductivity of stainless steel the heat flow from the support skirt to the tank is reduced to a relatively low level. Stainless steel also has the suitable structural properties to withstand high stresses. The heat flow through the thermal break of the current model can be calculated analytically. It is dependent on the thermal conductivity of stainless steel, its area, and the length of the section. The analytical calculations for LNG and LH2 uses the same parameters except for their different temperature. Thus the heat flow due to temperature can be compared for the two cargoes and can be seen in table 6.

As the model is designed to carry LNG, loading the tank with H2 should result in higher heat flow through the thermal break with the same length.

	Cargo	Heat Flow [W/m^2]	Total Heat Flow [W]
Analytical	LNG	1486	8700
	LH2	2144	12553
Abaqus Analysis	LNG	1275	7465
	LH2	1844	10796

Table 6: Heat flow from skirt to tank through the thermal break

In table 6 the heat flow through the thermal break over a $1.913m$ length is presented. The interaction between the air and the steel section of the skirt gives the uninsulated section nearly constant air temperature. As the cargo has a lower temperature the heat flow will increase and over the same distance $LH2$ will have a higher heat flow than LNG.

The results obtained in the thermal analysis in Abaqus is lower than what was calculated analytically for both cargoes. This is likely due to the analytically calculations using the temperature difference between the two boundary conditions of the cargo and air. Thus not accounting for the reduction in temperature around the thermal break, mainly in the aluminium section. In figure 24 the heat flow distribution is shown for the support skirt with liquid hydrogen.

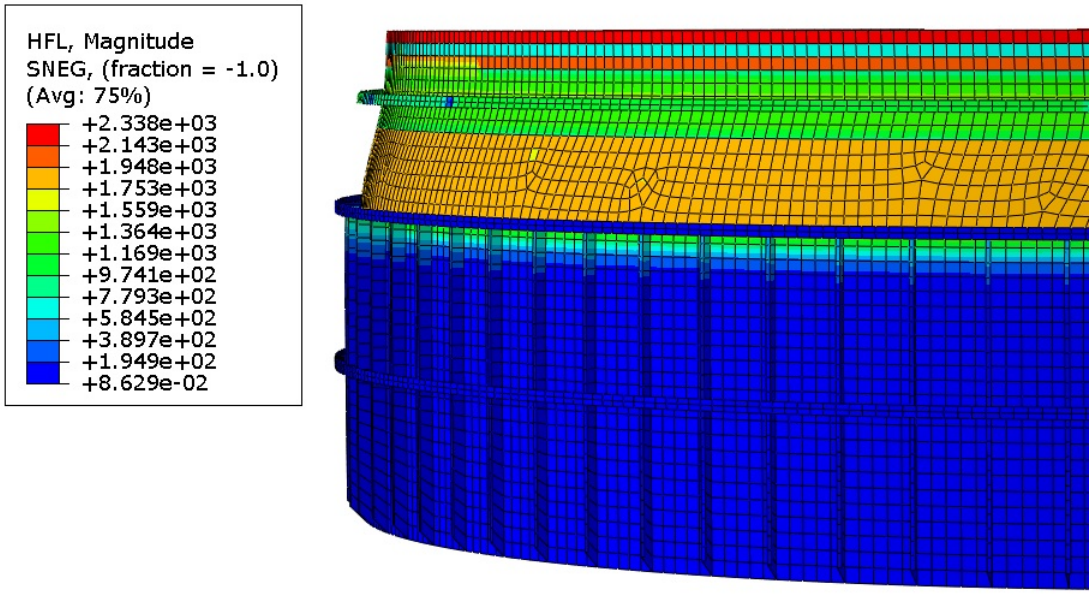

Figure 24: Heat flow through the support skirt $[W/m^2]$

The heat flow does not impact the structural properties of the support skirt directly, but rather due to the temperature-distribution in a steady state condition. The cooling required to keep the cargo liquefied is increased for LH2 due to the increased heat flow. As mentioned the length of the thermal break can be increased or its area reduced to use less power for cooling, but as this will impact the structural integrity of the support skirt a new structural analysis will have to be performed.

7 Buckling Analysis of Support Skirt

In this chapter the results of the buckling analysis of the skirt will be presented. A eigenvalue and non-linear analysis is performed in Abaqus to find the elastic-buckling strength and the plastic-yield of the structure. The results is compared with hand calculations found using DNV guideline DNV-RP-C202 [11].

To use a conservative estimate of the temperature of the skirts under constriction its reference point is set to 40℃. Such a temperature could occur in high temperature places on the earth where some of the yards is located. If the skirt is constricted under such conditions it will bring the total temperature difference of the skirt to 203℃ for LNG and 293℃ for liquid hydrogen.

The same temperature-displacement analysis was carried out with a second step to buckle the structure. In this analysis the additional temperature was applied, giving higher temperature-displacement for both skirts with exposed to LNG and H2 cargo temperatures. Assuming the no displacement reference point to be at 40 degrees, the analysis is carried out with a cargo load equal to the total temperature differences.

As expected both of the load cases had their critical buckling load reduced due to higher eccentricity of the axial load caused by the temperature-displacements. Both for elastic and elasto-plastic buckling strength was reduced, but with different magnitude.

7.1 Analytical Calculation of Critical Buckling Strength, DNV

The elastic buckling stress for the skirt is calculated using DNVGL-RP-C202 *Buckling Strength of Shells* [11]. It covers buckling of curved panels, unstiffened and stiffened cylindrical shells. Both is relevant for the support skirt as it has only the steel section is vertically stiffened and the aluminium and stainless sections is unstiffened. A separate elastic buckling analysis must be performed for all the sections, each using its respective length. The relevant theoretical background is presented in chapter 2.2.

The analytical calculations is calculated in two different ways. One which calculates the buckling for an ideal structure with perfect geometric and material properties and the other one accounts for the imperfections using a reduced knock-down factor ρ. A realistic structure will have imperfections both in its geometry and material and will thus have reduced buckling strength. In the guideline DNVGL-RP-C202 this is accounted for by introducing a reduced knock-down factor ρ which gives reduced buckling strength. For the ideal structures the knock-down factor is set to $\rho = 1$.

The buckling coefficient is calculated using the plate buckling coefficient ψ, the curved shell contribution η, and the knock-down factor ρ. These are presented in the DNVGL-RP-C202 and is found in table 1 for both vertically stiffened and unstiffened curved panels.

Chapter 4.6.3 shows the equations and factors used in calculation of the elastic buckling strengths and chapter 2.2.6 basis for the calculation of critical loads. A the relevant equations used are shown below.

Buckling coefficient with reduced knock-down factor is given by

$$C = \psi \sqrt{1 + \left(\frac{\rho \xi}{\psi}\right)^2} \tag{57}$$

Buckling strength of unstiffened cylinders:

$$\sigma_E = C \frac{\pi^2 E}{12(1-\nu^2)} \left(\frac{t}{l}\right)^2 \tag{58}$$

$$N_x = 2\pi r t \cdot \sigma_E \tag{59}$$

For the curved panels the buckling strength is given by

$$\sigma_E = C\frac{\pi^2 E}{12(1-\nu^2)}\left(\frac{t}{s}\right)^2 \tag{60}$$

$$N_E = 2\pi rt(1+\frac{A}{st})\cdot\sigma_E \tag{61}$$

Material	Stiffening	Shell thickness [mm]	σ_E [MPa]	N_E [MN]
Aluminium	Unstiffened Cylinder	62	343.6	2013.9
Thermal Break	Unstiffened Cylinder	45	275.9	1617.1
Steel Panels	Curved Panels	28	282.7	1159.6

Table 7: Analytical calculation of elastic buckling in the three different sections of the skirt with knock-down factor $\rho = 1$

The results form the analytical calculations of the elastic buckling force shows that the steel section has the lowest axial force required to buckle. Its the most slender section as its the longest and the thinnest. The elastic buckling strength is found to be below the yield strength of $350MPa$ even for a ideal structure with knock-down factor $\rho = 1$

To find the reduced buckling strengths the reduced knock-down factor has to be used. As the steel section clearly is the section which is most prone to buckling due to axial loads it will be further analysed for its reduced buckling strength. The reduced knock-down will effect both cylindrical shells and curved panels alike and is calculated with respect to their radius and thickness relation. A larger cylinder with high radius and lower thickness will have a significantly reduced knock-down factor and be vulnerable to imperfections.

Using the support skirts radius and the steel sections thickness given in table 2 the reduced knock-down factor was found to be $\rho = 0.2052$. The reduced buckling strength could thus be calculated to be $\sigma_E = 227.3MPa$, which is about 80% of the theoretical buckling strength.

ρ	Buckling Strength [MPa]	Axial Buckling Force [MN]	Reduction [-]
1	282.7	1160	-
0.2052	227.3	932	[0.804]

Table 8: Buckling strength of the steel panels between the stiffeners with and without imperfections

7.2 Buckling Strength of Support Skirt with Thermal Loads

To find the reduction in elastic buckling strength as a result of the temperature-displacement of the skirt, the displacements found in the linear analysis is used. These were found using the coupled temperature analysis in Abaqus and are listed in table 4.

The shrinking causes an eccentricity of the axial load on the skirt which again gives a moment around the top of the steel section. This section is already the weakest points for elastic buckling and will because of the thermal shrinking require less force to buckle due to the eccentricity of the load. Thus only the steel section is studied analytically with eccentricity analytical.

Simple hand calculations is conducted using the stress formula for axial force and bending. The calculations are rooted in basic force, moment, and stress formulas and is not directly related to reduction of elastic buckling strength. They are meant as a simple estimate and comparison of the reduction of the elastic buckling strength due to the eccentric load due to the temperature-displacement. With the assumption of constant elastic buckling strength in the steel section, as

bending is introduced from the eccentricity the reduced buckling load can be calculated using formula for stress.

$$\frac{N \cdot e}{I_z} y + \frac{N}{A_{cyl}(1 + \frac{A_{stiff}}{st})} = \sigma_E \tag{62}$$

This equation is based on the theory presented in chapter 2.2.6. The moment is $M = N \cdot e$, where$e$ is the eccentricity due to temperature-displacement.

Solved for axial force the buckling buckling loads are given in table 9.

$$N_{cr} = \frac{\sigma_E}{\frac{e \cdot y}{I_z} + \frac{1}{A(1+\frac{A}{st})}} \tag{63}$$

Cargo	Eccentricity (radial) [mm]	Buckling load [MN]	Devience [-]
No Cargo	0	1159.6 E6	-
LNG	97.25	1147.5 E6	98.9 %
LH2	140.4	1142.2 E6	98.5 %

Table 9: Calculation of Buckling Force due to Temperature Displacements

7.3 Linear Buckling Analysis

The linear buckling analysis of a skirt exposed to different temperatures is performed in Abaqus with separated into two different steps. Separating the temperature analysis and the buckling strength analysis is the most practical way to perform the analysis. The results from the temperature analysis is then used in the buckling strength analysis to calculate the reduction due to the temperature-displacements.

The first step of the analysis calculates displacement in the upper section of the skirt caused by the temperature. It uses the same analysis in Abaqus as was performed in chapter 6.5.1. At the upper part of the skirt the material is exposed to a constant temperature equal to that of the tanks temperature. No other constraint boundary conditions or loads are applied at this step. When this step is run, the result is a deformation where the upper section will retract in radial direction towards the center depending on the temperature applied from the tank.

Since the thermal expansion coefficient of aluminium is higher than that of stainless steel resulting in higher shrinking with lower temperatures for aluminium, thus the largest eccentricity at the top of the skirt.

After the first step in performed calculating the thermal displacements, the results are applied to the second step. In this step the linear eigenvalue analysis is conducted. The eigenvalue analysis uses a linear perturbation procedure to estimate the bifurcation point called the critical buckling load [22].

A load is place on the upper edge of the skirt to represent the load experienced from the tanks weight. The constraining boundary conditions are fixed both in the upper and lower ends, but allowed to translate in length direction to buckle. When the analysis is run the loads that causes the lowest buckling modes are returned based on the number of requested buckling modes. The first buckling mode is the mode which requires the least force to occur. When combining these two steps the buckling load for the skirt exposed to temperature shrinking is found in the eigenvalue analysis.

Table 10 show the material properties used in the support skirt for the three section used in the analysis.

	Aluminium	**Stainless Steel**	**Mild Steel**
Density [Kg/m^3]	2700	7800	7800
Elasticity [GPa]	70	210	210
Poisson ratio [-]	0.3	0.3	0.3
Conductivity [W/m K]	116	14	35
Yield Strength [GPa]	250	310	350
Ultimate Strength [GPa]	305	600	500
Expansion Coefficient [m / K]	2.2E-05	1.35E-05	1.2E-05

Table 10: Material Properties and Dimensions of the skirt used in the Analysis [5][7] [8]

The analysis was separately performed linearly for three different temperature load conditions. These where an empty tank with temperature equal to the surroundings of 40℃, a tank filled with liquid LNG of −163℃, and one with liquid hydrogen with a temperature of −253℃.

Table 11 shows the results from the linear buckling analysis performed for the three different temperature load conditions. As expected the buckling strength is reduced with lower temperatures as the top of the skirt shrinks causing eccentricity at when exposed to buckling load.

Cargo	Critical Buckling Load [MN]	Deviance [-]
No Cargo	1200.04	-
LNG	1191.60	99.29%
LH2	1165.90	97.15%

Table 11: Results from the linear eigenvalue analysis in Abaqus

The buckling strengths presented in table 11 is calculated using the critical line load returned from the eigenvalue analysis and the circumference of the skirt. Equation 7.3 shows the formula for calculating the critical buckling load.

$$N_{cr} = \text{Critical Line Load} \cdot \text{Circumference} = q_{cr} \cdot 2\pi r \tag{64}$$

Compared to the analytically results presented in table 9, the results from the eigenvalue analysis presented in 11 are slightly different. The reduction due to LNG are quite similar around 1%. For LH2 however the reduction was found to be almost 3% in the linear analysis compared to the analytical of 1.5%. The results in the linear overall calculated higher critical buckling loads than in analytical calculations. With no cargo and thus temperature-displacement the analysis shows a critical buckling load of $1200MN$ compared to $1160MN$ in the analytical. This is likely due to the analytical calculations being an estimate using the factors from the DNV guidelines and estimates for the effective lengths of the vertical stiffeners [11]. The analytical results estimates a more conservative buckling load.

The first eigenmode in steady state for the skirt with no temperature distribution is shown in figure 25. It can be seen that the buckling occurs locally in the curved steel panels between the stiffeners below the lowest ring stiffener.

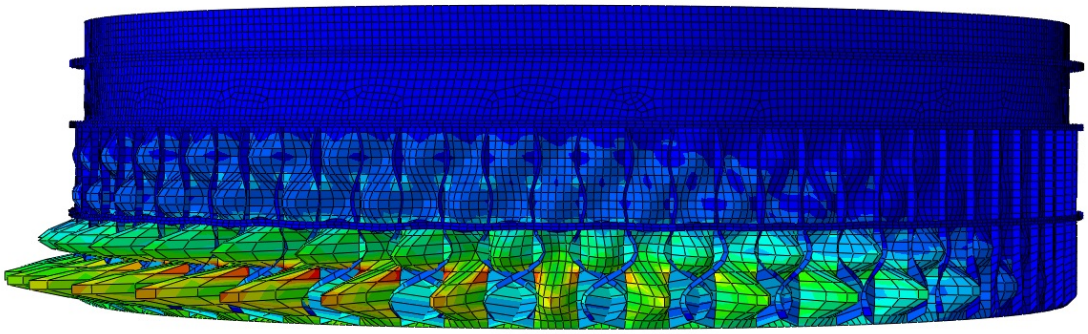

Figure 25: First Mode Air

Figure 26 shows the buckling mode that occurs when the skirt is loaded with and axial load and is affected with the temperature-displacement from LNG cargo. The buckling mode is now distributed over the length of the steel section, both over and under the ring stiffener. This is likely due to the bending which occurs due to the eccentricity of the axial load as the upper edge of the skirt retracts.

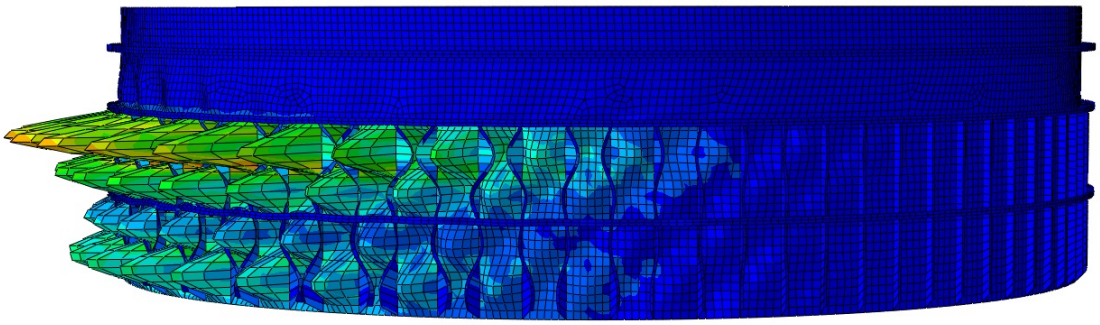

Figure 26: First Mode LNG

The mode changes even more with the temperature-displacement of LH2. In this mode the bending contributes sufficiently enough to cause the first buckling mode to occur over the steel ring stiffener as seen in figure 27. As discussed with the regards of the results presented in table 11 the buckling strength is reduced to around 97.15% as a result of this.

Even though the eccentricity is only $140.4mm$ (0.68% of the radius) it is enough to completely shift the first mode to occur in the upper steel section over the ring stiffener.

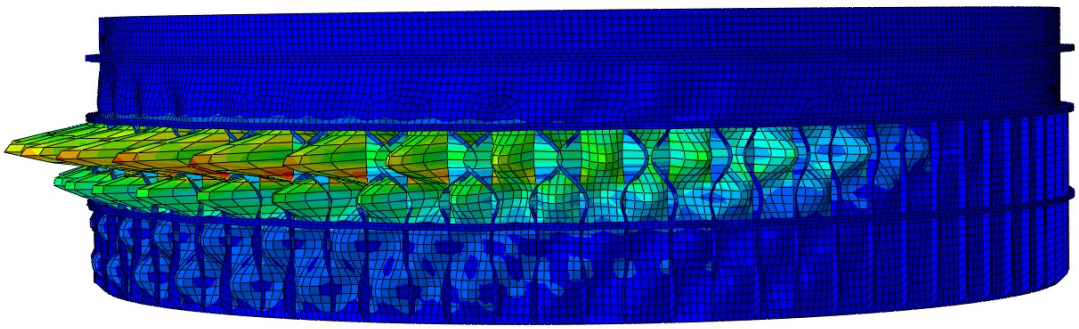

Figure 27: First Mode LH2

These first buckling modes of the linear eigenvalue analysis will be used in the non-linear analysis with introduced imperfections. As the first number of modes in each cargo category was quite identical only the first mode of each cargo is used. This is discussed further in chapter 9

7.4 Non Linear Analysis

In this analysis the skirt was forcefully displaced downwards to force plastic yield. Using a non-linear analysis with no imperfection the skirt was testes for yield for the three different cargo load cases. It show how the bending due to temperature-displacement amplifies and causes yield for lower axial loads due to the eccentricity.

The results from the non-linear plastic analysis showed a higher critical load for no temperature displacement than for the linear eigenvalue analysis. However with the temperature-displacement for LNG and LH2 cargoes the plastic yield occurs for lower loads. The bending due to eccentricity was sufficient to cause yield before elastic-buckling,

As the top of the skirt is displaced in z-direction compressing the cylindrical skirt the stresses increases and the reaction forces on the ends of the skirt. When a section reached the yield stress of its material plastic deformation occurred and the critical yield force was found. The critical loads for buckling stress is given in table 12.

In the non-linear analysis the force needed to cause yield in the skirt is lower than whats needed for buckling instability for LNG and LH2. With the bending for the temperature-displacement the yield occurred the thermal break rather than in the steel panels as it did not no cargo.

Cargo	Temperature displacement [mm]	Critical Load [MN]	Devience
No Cargo	0.0	1243.84	-
LNG	97.25	1078.49	86.71 %
LH2	140.4	975.63	78.44 %

Table 12: Critical Load for Plastic Yield of the Skirt

The critical buckling load for elasto-plastic buckling is reduced by 2.4% for the lowest temperature the skirt is exposed to by carrying liquid hydrogen, as seen in table 12. As the skirt buckles by plastic deformations instead of instability the critical buckling load is lower than for the linear analysis. The critical stress for LH2 elasto-plastic buckling is approximately 78% of the yield strength.

For the three different temperatures analysis the plastic yield occurs at different sections of the structure. When there is no displacement from temperature the yield occurs in the lower steel section close to the bottom boundary conditions.

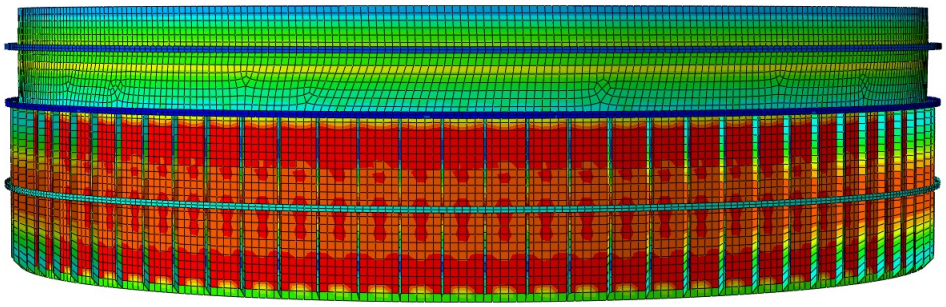

Figure 28: Yield in the steel panels with no temperature-displacement

When displacement is introduced in the top due to the colder temperature of LNG, the plastic yield shifts towards the top of the steel section. The top section of the steel experiences higher stresses due to the eccentricity of the load and which causes moment.

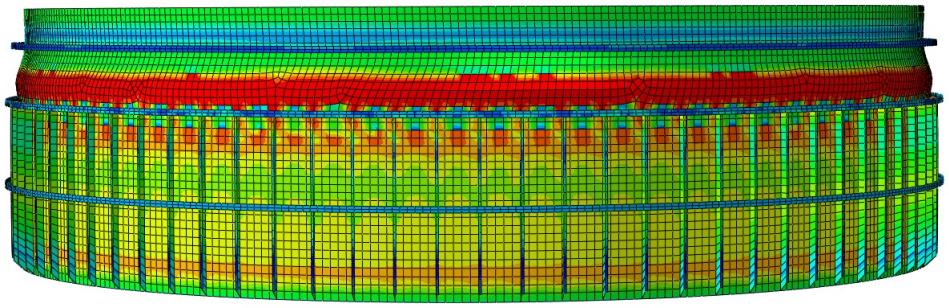

Figure 29: Yield in the thermal break with tank temperature of LNG $-163C^{\circ}$

When running the non linear analysis for liquid hydrogen the displacement caused by temperature retraction is at its highest. The elasto-plastic buckling is shifted further up and the yield occurs in the thermal break of stainless steel.

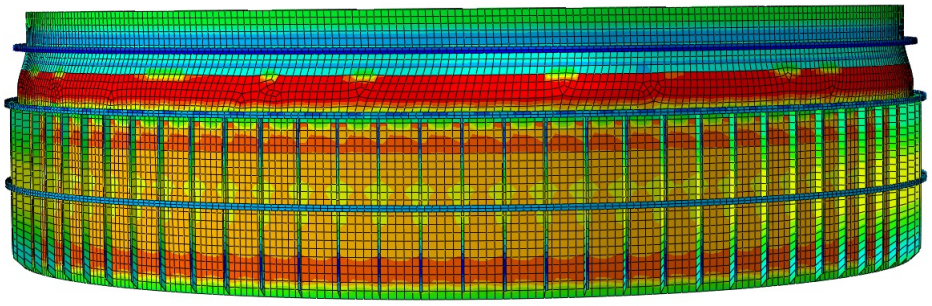

Figure 30: Yield in the thermal break with tank temperature of LNG $-253C^{\circ}$

For both cases with exposure to lower temperatures the displacement pattern of the upper end was similar, but the lowest temperature gave highest bending. As the displacement due to temperature first was applied it gave a retraction inwards towards the cylinder center. Then the upper end of the skirt was force displaced downwards from its current temperature displace position. When force displaced downwards a bending was caused between the steel section and the upper edge pushing the upper ring stiffener inwards. Its can be observed that the lower temperature applied the more bending in this section. For liquid hydrogen the additional bending also caused yield in

stainless steel section first. The critical axial force required to yield is reduced compared the other cases with less or no temperature displacement where yield occurs in the steel.

It was observed that the thermal stresses found in chapter 6.5.1 around the vertical stiffeners as a result of the temperature-displacement did not contribute significantly to earlier yield. As the skirt was incremental displaced down the stresses was relieved and the skirt yielded equally around the steel panels and the thermal break as discussed.

7.5 Comparison of Linear and Non-Linear Analysis

For the no cargo load condition the buckling occurred in the steel section for both elastic and elasoplastic buckling. This was not the case the LNG and LH2 cargoes. The non-linear analysis showed that the buckling would occur in the thermal break for both these cargoes. As the yield strength of the material is included in the non-linear buckling analysis, the stainless section experiences large stresses due to the additional bending caused by the eccentricity the temperature causes. This additional stress is large enough to cause yield in the transition between stainless steel and aluminium. The thermal break has a lower yield strength than the steel section, but is thicker. The results shows how the bending of the temperature-displacement reduces the buckling strength of the skirt notably and the yield occurs in the thermal break rather than the steel panels.

8 Non-Linear Imperfection Analysis

This chapter will present the results from the non-linear buckling analysis with implementation of imperfections to the structure. The buckling modes found in the linear eigenvalue analysis will be studied with imperfection amplitudes, compared and discussed.

All structures will in reality have some imperfections when manufactured. These can impact its structural properties depending on its severity. Typically there is a upper tolerance of the imperfection on a structure when manufactured given by guidelines and regulations. These will be discussed in this chapter through the DNV guidelines and its effect on the support skirt.

8.1 DNV Class Guidelines, DNVGL-CG-0134

The DNV class Guidelines outlines the tolerances for imperfections in the design and implementation LNG carriers. This is provided in the code DNVGL-CG-0134 in Appendix D, section 4.5 [12]. It presents the requirements in deviation of from the design shape used in calculations. The focus of this analysis will be the cylindrical support skirt of the LNG tank and not the tank. Thus a imperfection amplitude will only be applied to the support skirt.

In a symmetrical structure such as the support skirt with no obvious buckling mode it will be a imperfection that determine the buckling mode of the structure. The stresses would ideally be evenly distributed along the skirt when exposed to axial compression. In reality this will never be the case and when approaching yield strength it would be the weakest link in the structure where yield will occur first. This is called an imperfection. The deviation from its ideal shape is call the amplitude of this imperfection and will determine when the yield occurs. A smaller imperfection gives higher resistance to buckling.

An imperfection amplitude is the scale of the imperfection of the cylindrical shell will deviate from the geometrical perfect shell. This amplitude is in the class guidelines defined as δ_i. The imperfection amplitude for shell buckling of a cylindrical skirt in between the vertical stiffeners is given by

$$\delta_2 = \frac{0.01 g_2}{1 + \frac{g_2}{R}} \tag{65}$$

This imperfection amplitude is the upper tolerance and should not be exceeded. g_2 is the circular template length of the cylinder. It is a template to check for the circular out- of roundness of the shell and which is used to measure the imperfection amplitude relative to the curve.

$$g_2 = min[s, 1.15(l\sqrt{Rt})^{1/2}, \pi R/2] \tag{66}$$

For the cylindrical support skirt the buckling is expedited to happened either in the steel shell or the vertical stiffeners. The imperfection amplitude of the vertical stiffeners is based on their total length and the half-waves of the length.

$$\delta = 0.0015l \tag{67}$$

where l is the length of the vertical stiffeners.

The upper limit of the imperfection amplitude of the steel shell between the stiffeners was found to be equal to the stiffener distance of $s = 1628mm$ given in equation 8.1.

8.2 Imperfection Analysis with different Amplitudes

To find the eigenmodes that the support skirt buckles for a linear eigenvalue analysis was performed, finding first few buckling modes and their respective eigenvalues. The linear eigenvalue analysis find the weakest geometric points in the structure. To perform the non-linear buckling analysis of the skirt the imperfection will be applied to the same mode where the linear buckling occurred.

A analysis of the imperfections effects the buckling of the cylindrical skirt is performed using several amplitudes ranging no imperfection to equal of the thickness of the skirt. The effect of imperfection amplitude will be illustrated and compared to the DNV recommended amplitude for similar structures [12]. Then the effect of imperfections will be studied with the applied cargo temperatures how it will effect the buckling.

The material properties of the skirt analysed are the same used in table 10. Other parameters that was used for this analysis:

Radius of Cylindrical Skirt	20730mm
Total Length of Cylindrical Skirt	11548mm
Parameters of Steel Section	Length: 7305mm, Thickness: 28mm
Parameters of SUS Section	Length: 1913mm, Thickness: 45mm
Parameters of Aluminium Section	Length: 2330mm, Thickness: 62mm
Total length of Thermal Break	Length: 2530mm
Mesh size	0.3
Loads	Shell Edge Load (Axial Compression)

Table 13: Parameters of Cylindrical Skirt Analysed

In the linear analysis of the cylindrical skirt the elastic buckling force with no cargo was found to be $1200MN$, which is shown in table 11. Compared the analytical solution of $1164MN$ for the steel shell, using the DNV GL code RP-C202 shown in table 7. By applying a low imperfection amplitude in the non-linear imperfection analysis the skirt will buckle plastic and be comparable to the non-linear analysis in chapter 7.4.

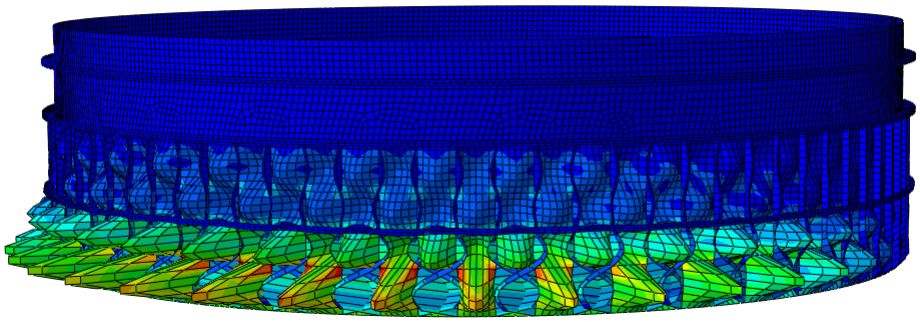

Figure 31: First Buckling Mode of the Linear Buckling Analysis of the support skirt.

The knock-down factor which is found using DNVGL-RP-C202 to account for the empirical reduction from imperfection is set to $\rho = 0.205$ for shells buckling of curved panels [11]. It's formula is given in table 1. Thus the analytical calculations will have a conservative relation to imperfections.

In the non-linear buckling analysis with applied imperfections the amplitudes would magnitude from smaller imperfections to include the full thickness of the shell. The effect of reduced buckling load due to imperfection on the steel section of the support skirt can then be illustrated as the imperfection is increased. A practical range of amplitudes to analyse would be an amplitude from $0mm$ to $28mm$.

To perform the non-linear buckling analysis the buckling modes from the linear buckling analysis shown in figure 31 was used and applied with the imperfection amplitude.

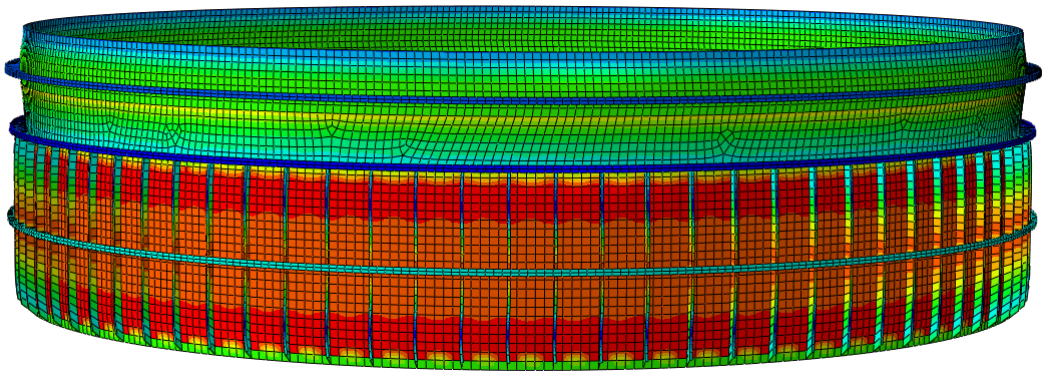

Figure 32: Non-Linear Buckling analysis with No Imperfection

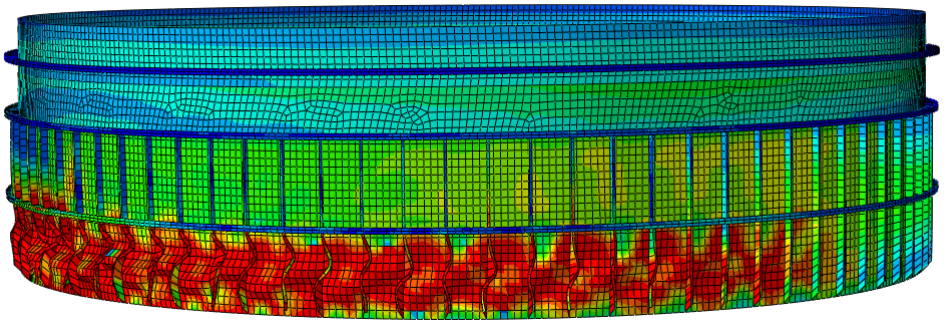

Figure 33: Non-Linear Buckling analysis with an 5mm Imperfection Amplitude

Imperfection Amplitude [mm]	Non-Linear Buckling Force [MN]	Knock-Down Factor
0	1241.98	1.000
1	1166.81	0.939
2.5	1111.57	0.895
5	1086.42	0.875
10	1054.41	0.849
15	1030.46	0.830
20	1015.65	0.818
25	1000.50	0.806
28	992.32	0.799

Table 14: Reduced buckling load with higher imperfection Amplitude

Described in chapter 8.1 the DNV guideline outlines a acceptable imperfection amplitude as production limit for the cylindrical shells. As there is only expected to be one halfway between the vertical stiffeners in the horizontal direction, as seen in the linear analysis it is reasonable to use the circular template length equal to the vertical stiffener distance which is found using equation 8.1. The circular template length for the skirt model then is $g_2 = 1628mm$ and thus upper limit for local shell imperfection recommended was found to be:

$$\delta_2 = 15.1mm \tag{68}$$

This value as an imperfection amplitude on the current support skirt is the upper production tolerance between each vertical stiffener around the skirt. It would result in a knock-down factor of 0.830 as seen in table 14

In chapter 7.1 the analytical calculations of the buckling strength with imperfections were performed. It was found that reduction in buckling strength due to accounting for imperfections using a DNV class knock-down parameter for curved panels was 80.4% of perfect shell, seen in table 8. This is comparable to the result non-linear analysis with a reduction of 83.0%. The non-linear analysis has less reduction in buckling strength, but on the other hand found a higher force required to cause axial buckling than the analytical results. The factors used in the analytical is an estimate of the buckling strength and is designed to be somewhat conservative.

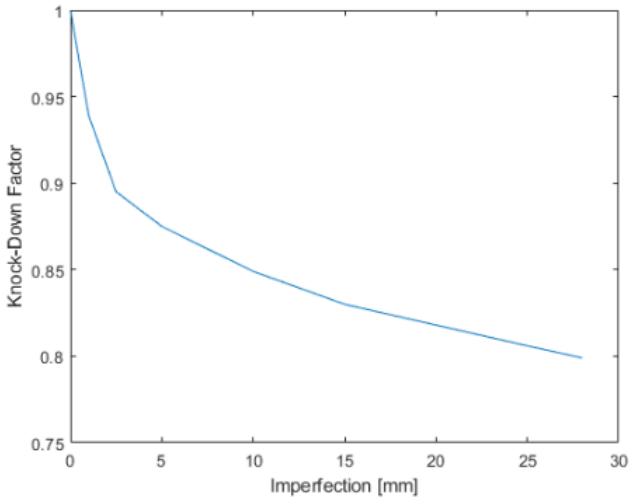

Figure 34: Knock-Down Factor sensitivity of Imperfection Amplitude

It can be observed that the knock-down factor change decreases as the imperfection increases. With an imperfection amplitude equal to the thickness the buckling force is reduced to about 80% of a perfect shell. This result is very similar to the analytical results presented in table 8 with a reduced knock-down factor. Due to the effect of the stiffeners around the skirt the imperfections can be limited to local buckling in the curved steel shell. As the buckling mode is in the curved steel panels the effect of imperfections is relatively low compared to what it would be in a cylindrical shell without stiffeners. This can be observed in chapter 9.2 of **Gjestvang P. 2020** thesis which studies the effect of imperfection on a unstiffened cylindrical shell extension on a non-spherical LNG tank [19]. This study found that the knock-down factor of a unstiffened cylindrical shell would be as low as 0.45 imperfection amplitude equal to the shell thickness and 0.6 for the recommended DNV amplitude for cylindrical shells. It should be noted that this study used an force of external pressure rather than axial force as in this case.

8.3 Effect of Imperfections with Temperature-Displacement

When studying the buckling modes in the linear eigenvalue analysis it was observed that the buckling modes changed as the upper section of the skirt when exposed to lower temperatures. With equal temperature along the the skirt the few first buckling modes would occur in the steel shell between the stiffeners and below the lower ring stiffener. As the skirt as exposed to the lower cargo temperatures of LNG and liquid hydrogen the buckling modes would shift towards the upper section of the skirt as seen in chapter 7.3. The modes changes up due the eccentricity of the axial loads, causing bending and thus weakest section of the shell. In table 14 the effect of imperfections on the buckling force of the skirt was presented. For the DNV production tolerance of 15mm the reduction of buckling force was found to have a knock-down factor of 0.83. Using this imperfection amplitude of $15mm$ the study was repeated with applied temperature displacements. The corresponding linear analysis with applied thermal loads which gave the shift in buckling modes where used in the non-linear analysis with the applied imperfection amplitude.

When performing the non-linear analysis with no imperfection the buckling loads was about the same for all three load cases. This is due to the analysis applying at the buckling modes found in the linear study when exposed to load and not applying the temperature-displacement in the non-linear analysis itself. If the temperature-displacements were applied the buckling load could be expected to be lower. Thus the results obtained with the imperfection amplitude recommended by DNV is the reduced buckling capacity due to the linear eigenvalue buckling mode.

Cargo	Buckling Force [MN]	Buckling Force Difference	Knock-Down Factor
No Cargo	1030.46	1.000	0.830
LNG	1022.12	0.992	0.823
LH2	999.87	0.970	0.805

Table 15: Effect of an imperfection amplitude of $15mm$ on the Buckling Force of a skirt exposed to temperature-displacement

In the results presented in table 15 shows the reduction in buckling strength due to the buckling mode shifting upwards in the skirt, caused by lower temperatures in the tank. The reduction due to having LNG cargo is relatively negligible at 99.2% of the buckling strength of no temperature-displacement. When the tank is filled with liquid hydrogen however the buckling strength is reduced disproportional more even tough it only has an additional temperature difference $90C$℃. This is likely due to the buckling mode being concentrated above the first ring stiffener rather than distributed over and under the ring stiffener. These changes in buckling modes due to temperature are illustrated in chapter 7.3.

As this design of the support skirt is designed for carrying LNG and its temperature its not as resistant to buckling when exposed to liquid hydrogen. Some changes might be favorable to resist the buckling modes caused by the liquid hydrogen.

9 Buckling Modes Analysis With Increased Thicknesses

In this chapter a deeper analysis of the buckling modes of the different support skirt sections will be described. It was observed in the results of the non-linear plastic analysis that the skirt would yield in the stainless section of the skirt when exposed to LNG and H2 cargo in chapter 7.4. The linear buckling modes for the thermal break and aluminium section will in this chapter be analysed.

The first series of buckling modes are located in the steel plates due to small geometric differences around the cylindrical skirt. To find the buckling modes and their corresponding buckling loads a linear eigenvalue analysis is performed with an increased thickness in the weaker section.

9.1 Buckling Modes in the Steel Panels

The most interesting buckling modes are usually the lowest ones. These are the modes which the skirt will buckle at first for a given load in steady state conditions. When performing a linear eigenvalue analysis on the support skirt in Abaqus and requesting the first 10 eigenvalues these gave quite similar values. This is due to the skirts symmetric geometry.

The linear eigenvalue analysis was performed requesting the first 10 buckling modes. Table 16 show the parameters used in this analysis which are the same used in chapter 7.3.

	Thickness
Mild Steel	28mm
Stainless steel (SUS)	45mm
Aluminium	62mm

Table 16: Shell thicknesses used in the eigenvalue analysis of the steel panels

The first and most critical buckling mode is shown i figure 35 with the buckling mode being concentrated on one side of the structure.

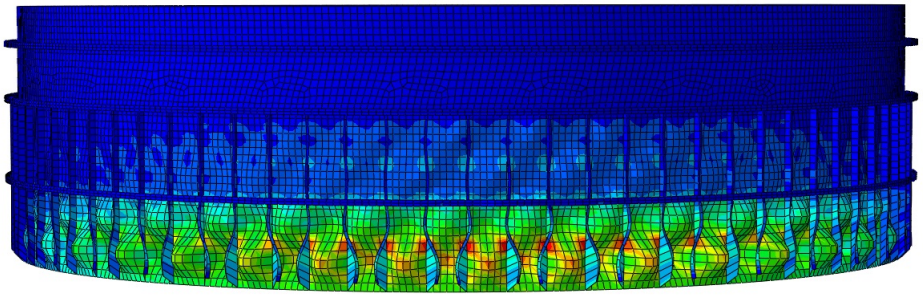

Figure 35: Buckling Mode 1 with panel thickness $28mm$

The first modes all occurs locally in the curved steel panels between the vertical stiffeners. The 5th and 10th modes shown in figure 35 and 36b

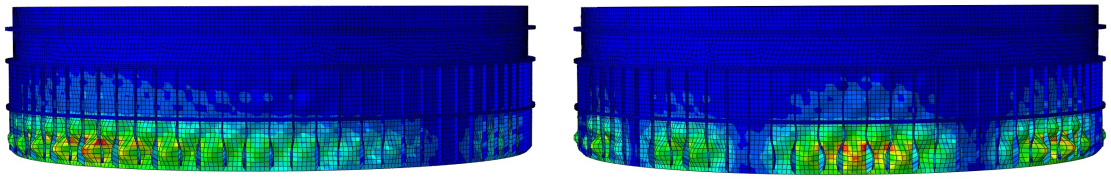

(a) Mode 5

(b) Mode 10

Figure 36: Buckling modes with panel thickness $28mm$

The difference in buckling force of the two mode is shown i table 17 and are relatively close. The modes between 1, 5 and 10 followed more or less linear pattern which will be discussed in chapter 9.4. With the small difference in buckling force between the modes quite a large amount of eigenmode had to be requested to force buckling in the other sections and in the vertical stiffeners.

	Mode 1	Mode 5	Mode 10
Linear Buckling Force [MN]	1200.04	1224.10	1243.14

Table 17: Buckling force with $28mm$ steel panels

9.2 Increased Thickness of the Steel Panels

By strengthening the steel panels gives them more resistance to buckling and other weaker points will be exposed. The thickness of the steel panels was increased to strengthen the section. In table 18 the thicknesses used for this eigenvalue analysis is given. This shifted the buckling modes from the steel plating to the thermal break. As this section is a cylindrical shell without vertically stiffeners, the buckling modes caused several waves around the cylinder.

Section	Thickness
Aluminium	62
Thermal Break	45
Steel	35

Table 18: Dimension with increased thickness in the steel panels

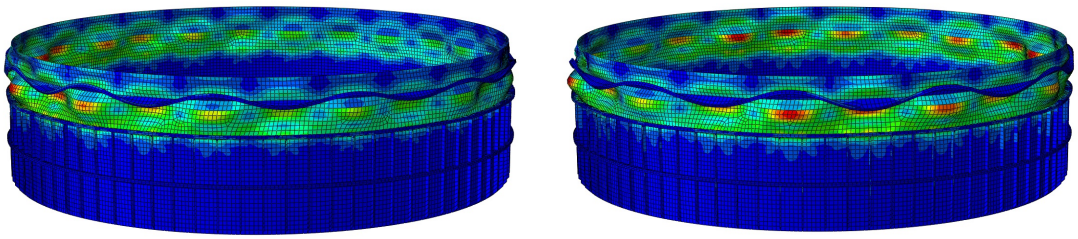

(a) Mode 1 (b) Mode 10

Figure 37: Buckling modes with panel thickness $28mm$

With the shift of buckling mode to the thermal break the required buckling load was increased compared to the buckling mode in the steel panels. The force difference between the buckling modes in the stainless steel however was even less.

As the stainless section is an unsiffened cylinder it allowed for half waves around the circumference. This causes less difference between the buckling modes as the next modes are the same mode just slightly shifted. It follows the patter where the half waves are distributed relative to the cylinders relation between the length of the section and the circumference. The number of half waves which occurs in the circumference direction in the cylinder is given as:

$$n = \frac{\pi \cdot 20730}{2530mm} = 26 \tag{69}$$

Equation 69 uses the length between the 2. and 3. ring stiffeners which includes the thermal break of $1913mm$ and part of the aluminium section of $617mm$. The dimensions are listen in table 13. The total number of waves are 52 as the two waves in the length direction of the cylinder.

In table 19 the required buckling force for the linear buckling modes in the thermal break is presented.

	Mode 1	Mode 5	Mode 10
Linear Buckling Force [MN]	1590.83	1594.55	1604.47

Table 19: Buckling force with $28mm$ steel panels

The force required to buckle in the thermal break is about 33% higher than for the steel panels. Thus in steady state conditions buckling in this section should not be expected. However for combined loads and forces of bending and axial forces the buckling strength of this section might be reduced.

The increased buckling force required to encounter a buckling mode outside of the steel panels show that the use of the first modes in the steel panels in the non-linear imperfection analysis is reasonable. If the required force to encounter the buckling mode in the thermal break was marginal to the steel panels, a thorough non-linear analysis should to be performed for the thermal break.

9.3 Buckling Modes in the Aluminium section

To check the buckling modes in the aluminium section the thickness of the steel panels and the thermal break was increased. This shifted the buckling modes above the thermal break. The aluminium section is also a unstiffened cylinder, but with a shorter length than the thermal break. Thus fewer half waves could be expected as well as a higher buckling strength. The thicknesses used in this eigenvalue analysis is given in table 20.

Section	Thickness
Aluminium	62
Thermal Break	62
Steel	35

Table 20: Dimensions with increased thicknesses in steel plated and thermal break

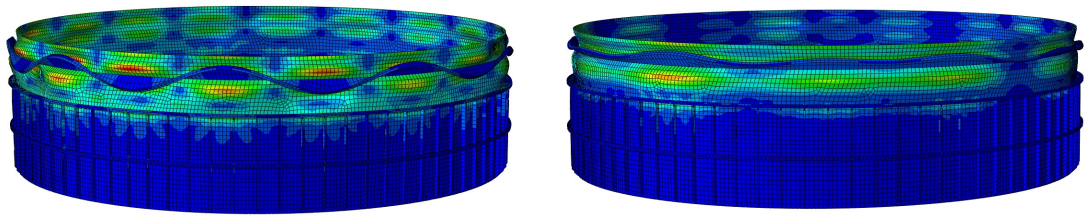

(a) Mode 1 (b) Mode 10

Figure 38: Buckling modes with increased thicknesses

With increased thicknesses in both the steel panels and the thermal break the buckling mode occurs in the aluminium section. The mode causes waves both in the aluminium section and the thermal break.

Mode 1 and 10 seen in figures 40a and 40b are quite different. The first mode follows the half waves patter around a unstiffened cylinder, but the half waves are alternating between the longer uneven waves round the circumference. Calculating the number of expected waves in both the aluminium and thermal break gave the following

$$n = \frac{\pi \cdot 20730mm}{1913mm + 2330mm} = 15.3 \tag{70}$$

Around 15 waves can be counted around the circumference of the first buckling mode, but the 10th buckling mode has longer waves concentrated at one side.

Table 21 show the buckling force for mode 1 to be about 24% higher when also increasing the thickness in the thermal break to cause buckling in the aluminium. Buckling in the aluminium might be caused for lower thickness adjustments as well, but in this case over both sections. Further increasing the thickness of the thermal break will cause the buckling to occur only in the aluminium section.

	Mode 1	Mode 5	Mode 10
Linear Buckling Force [MN]	1970.34	1975.45	1988.59

Table 21: Buckling force with $28mm$ steel panels

The difference in buckling load is quite low between the buckling modes. Similar to the relation between the modes of buckling in the thermal break in table 19. In the modes of the cylinders the buckling loads are quite alike, but make some jumps. Likely related to the buckling mode changing from a evenly distributed buckling waves to longer waves concentrated on one side.

9.4 Comparison of the Buckling Modes

All three section was analysed for buckling modes using linear eigenvalue analysis by increasing thickness of the weakest sections to force buckling in the other sections. It was observed that the

force for the thermal break to buckle was increased by 32.6% higher with an increase from $28mm$ to $35mm$ of the steel plates. When analysing the buckling modes in the unstiffened cylindrical shell at the thermal break it was observed that the buckling force difference between modes was noticeably lower compared to the stiffened plates. This is likely due to the increased possibilities of buckling modes that can occur by half waves patterns. For the vertically stiffened steel panels the buckling mode waves was concentrated one side of the skirt and not evenly distributed. This is due to the buckling occurring in the steel panels was local buckling between the stiffeners.

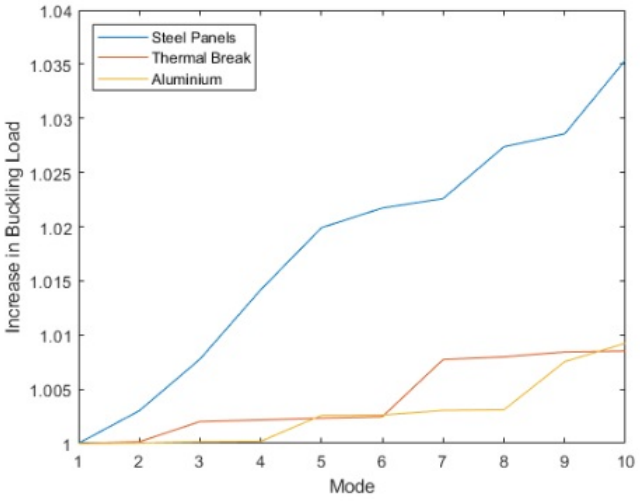

Figure 39: Increase in buckling force for the next buckling mode for the three sections

Figure 39 shows how the local buckling in the steel panels between the stiffeners has a larger force difference between the buckling modes than the unstiffened cylindrical shells has.

9.5 Temperature-Displacements effect on Buckling Modes

All three sections has been analysed for their buckling modes and buckling force. This was in a steady state condition and with no temperature-displacement. In this sub chapter the effect of the temperature-displacement on the reduction in buckling strength of the thermal break will be studied. As there is more bending introduced with the axial force on the displacements this should reduce the buckling strength. The steady state buckling modes of the skirt with cold cargoes was found to be in the middle and upper section of the steel section as seen in figure 37.

The linear eigenvalue analysis of the skirt was performed with increased thickness in steel panels to cause buckling in the thermal brake and also implementing the temperature-displacement from LH2 cargo. It was observed that the buckling mode was similar to the mode without cargo, but the buckling force required was lowered. The buckling force for the lowest buckling modes is given below in table 22

Tank temperature	Critical Buckling Load [MN]	Deviance
No Cargo	1590.83	[-]
LNG	1575.44	0.9903
H2	1567.89	0.9856

Table 22: Linear Buckling of Thermal break for the three cargos, steel panels $35mm$

The buckling force required to cause the thermal break to buckle was found have similar deviation

for LNG as found earlier in the linear analysis with buckling in the steel panels in chapter 11. For LH2 displacement however the the thermal break showed more resilience with 98.56% deviance compared to 97.15% in table 11.

The buckling modes in the thermal break are almost identical for no cargo and for LH2 cargo, compared to the steel panel buckling which changed buckling mode from the bottom of the section to the upper section above the ring stiffener seen in figures 25 and 27.

A non-linear analysis with an imperfection was performed for the skirt exposed to all three load cases using the buckling modes obtained linearly. The imperfection amplitude used is found in DNV-CG-0134 for cylinder, but using the total length between the two upper ring stiffeners which includes part of the aluminium section [12]. Using equation 46, it is found to be

$$\delta = \frac{0.01 g_1}{1 + g_1/R} = 19mm \tag{71}$$

where g_2 is the length between the ring stiffeners $g_2 = 2113mm$

The non-linear analysis was conducted with a imperfection amplitude of $19mm$. This amplitude is quite high relative to the thickness of $45mm$ and reduced the buckling strength substantially. A non-linear analysis with no imperfection was also performed in which the skirt yielded symmetrical. Figure 40 shows the imperfection amplitude applied with the non-linear buckling analysis.

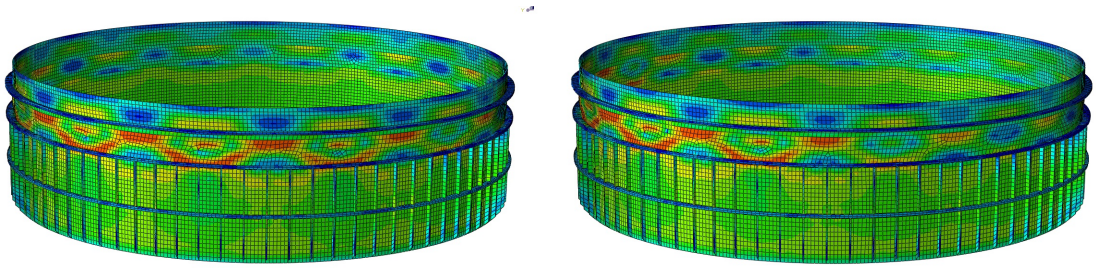

(a) No cargo

(b) LH2

Figure 40: Non-linear Buckling Analysis with Imperfection Amplitude $18mm$

As can be seen in table 23 the buckling mode in the thermal break actually showed more resilience against buckling for LH2 cargo with an imperfection of $19mm$ compared to no cargo. The difference is relatively small and might be due to smaller marginal factors in the plastic buckling of the section. Thus for LH2 the elastic buckling strength is lower relative to no cargo, but the opposite for non-linear elasto-plastic buckling. The mode which the skirt buckles for with LH2 cargo is concentrated more in one area of the skirt with fewer half waves on one side.

Tank Cargo	Critical Buckling Load [MN]	Deviance
No Cargo	949.08	[-]
LNG	948.00	0.9988
H2	954.94	1.0062

Table 23: Non-linear buckling analysis of thermal break with imperfection amplitude $19mm$

In the analysis of buckling in the thermal break with an increased thickness of the steel panels, it was observed that the temperature-displacement from the colder cargoes did not affect the thermal break more than it did the steel panels. Using the non-linear analysis showed that the lowest buckling mode for LH2 gave slightly more resistance to buckling compared to no temperature-displacement.

9.6 Comparison of the Skirt Sections

It was observed that the two upmost section of the thermal break and the aluminium section gave buckling modes with half waves around the circumference relative to the length between the ring stiffeners. In contrast to the steel section which the buckling occurred in the local steel panels concentrated to one half side of the skirt. For some later modes of the unstiffened cylindrical sections the waves were longer and concentrated at one side, such as for aluminium mode 10 in figure 40b.

As the thicknesses was increased to cause buckling in the upper sections rather than in the steel panels the critical buckling loads increased. The loads to cause buckling in these section agrees with and are in range of what was calculated analytically in table 7 in chapter 7.1.

In table 24 below the analytical and the analysis results with no temperature-displacement is presented.

Skirt Section	Analysis Buckling Load [MN]	Analytically Buckling Load [MN]
Aluminium	1970.3	2013.9
Thermal Break	1590.83	1617.1
Steel Panels	1200.04	1159.6

Table 24: Comparison of analytical results and the results obtained in the first mode of the eigenvalue analysis in Abaqus

The analytical results are somewhat conservative calculations compared the analysis results, but relatively similar. Only the steel panels are calculated to be higher in the analysis. This is likely due to some dimension margins in calculation of the stiffeners contributions to the buckling strength of the steel section.

For steady state elastic-buckling the results shows that the steel section is the weakest link in the skirt for axial load. The difference in load required for buckling is the other section is sufficiently higher that other contribution factors need to be in place for these sections to buckle elastically. However elasto-plastic buckling was shown in the non-linear analysis to occur earlier for both the thermal break and the steel panels.

10 Buckling Analysis of Skirt Model with Tank

In this chapter the skirt is analysed and described with the addition of the spherical tank connected to the skirt. The tank was in the earlier analysis left out to both reduce analysis computing time and reduce modeling effort. Analysis will be repeated for the Tank-Skirt model for linear eigenvalue analysis and plastic force-displacement for the same cargoes of LNG and LH2. The results obtained in the analysis of the Skirt-Tank model will be compared to the Skirt model analysed in the previous chapters. A brief description of the increased computing time caused by modeling the tank with the skirt will be given.

10.1 Model of Tank with Skirt

The skirt has been analysed separately from the tank and ship by using forced displacement, eigenvalue analysis and boundary conditions to represent the loads and constraints of the tank. Adding the tank to the skirt by mounting it on the top will potentially give a more accurate results of the real load conditions and constraints between the skirt and tank. The accuracy depends on the modelling of the tank, meshing, and the overall interactions between them.

Using DNV Genie the skirt model was expanded upon using adding a spherical tank on top of the skirt. The new model with the added tank will be referred to as the "Tank-Skirt" model

throughout the report.

Some simplifications were made in the Tank-Skirt model. The tank was applied as a fully spherical LNG tank with constant thickness used for the whole spherical tank. In reality the tank is composed of the different thicknesses through the shell which typically spans from $29 - 60mm$. The model is only constrained in the bottom of the skirt with a fixed condition as the upper end now is connected to the tank.

The crossover between the skirt and the tank is a thicker section which is used to properly transfer the stresses. This section increased the length of the skirt slightly as its placed on top of the skirt and connected to the tank. Figure 41 shows a connection between a skirt and tank.

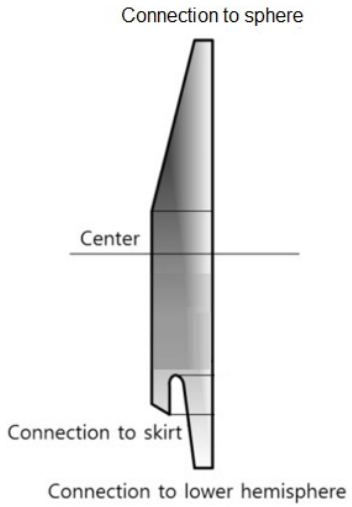

Figure 41: Connection between skirt and tank, [21]

Table 25 shows the dimensions used for the connection and the tank.

Module	Dimension [mm]
Tank Diameter	20730
Tank Thickness	50
Connection Length	570
Connection Thickness	167

Table 25: Dimensions used in the extension of the Skirt Model to the Tank-Skirt Model

The load capacity of the tank was assumed to be 80% of the tank total volume and using a typical LNG density the cargo weight is calculated. Based on the spherical shell volume the tank self weight is found using the density of aluminium used previously given i table 10. With a total weight of the cargo and tank the force exerted on the skirt due to gravity was found. This was applied as a total weight on the tank. The forces of the weight was the transferred through the transition in the equator line and the load case would be similar to the line load in the skirt analysis. Table 26 lists the weight and forces calculated of the spherical tank with cargo.

LNG density	$500kg/m^3$
Volume of Tank	$37315m^3$
Weight of Cargo	$18.66 \cdot 10^6 kg$
Weight of Tank	$0.72 \cdot 10^6 kg$
Total weight with cargo	$19.39 \cdot 10^6 kg$
Gravitational Force of total weight	$190.2 \cdot 10^6 N$

Table 26: Weight and forces calculated of the tank with cargo used in the analysis

10.2 Temperature-Displacement of Tank-Skirt model

In the temperature-displacement analysis in chapter 6.5.1 looking at the support skirt module, the cargo temperature was added as a boundary condition at the upper edge of the skirt. By analysing the total structure of both the support skirt and the spherical tank the total interaction is realised. The temperature-displacements due to the low cargo temperature of the support skirt are slightly different due to not being constrained to the tank and allowed to freely displace in radial direction. In reality when the support skirt is constrained by the tank it would be regulated by the tank displacements due to the temperature. When looking at only a spheres displacement due to temperature it would retract in radian direction towards the center in all directions.

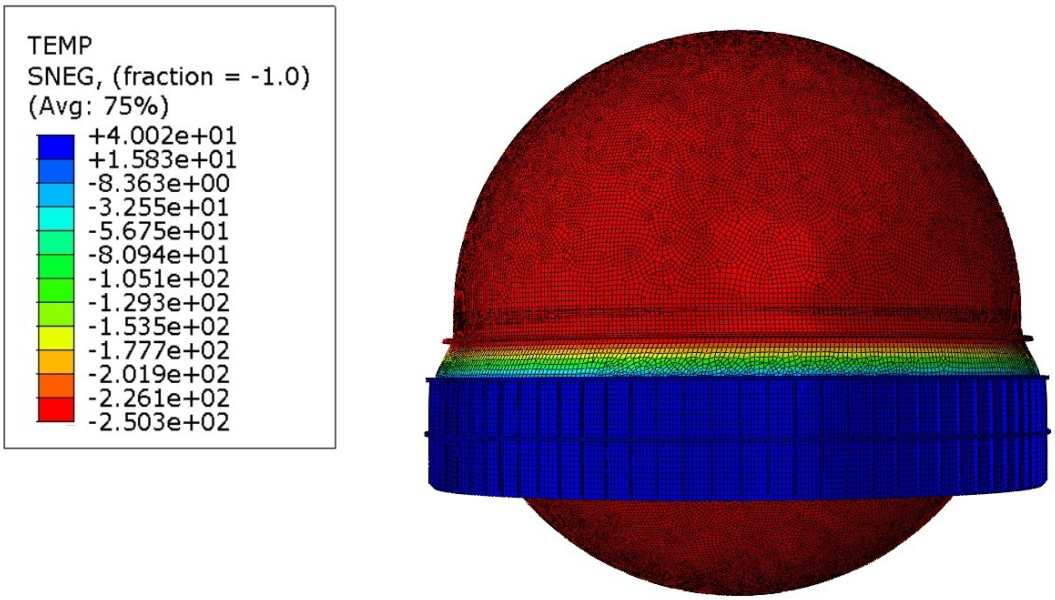

Figure 42: Temperature distribution of the Tank-Skirt model with LH2 cargo

The tank-skirt model was analysed linearly to find the temperature-displacements for the skirt connected with the tank. Instead of applying the upper edge of the skirt with a temperature boundary conditions its now applied to the tank surface. The heat from the air temperature is still an convection interaction around the steel section of the skirt. Figure 42 shows the temperature-distribution of the Tank-Skirt model with LH2 cargo. The distribution in the skirt is the same for the Tank-Skirt model and the model of only the skirt.

In the temperature-displacement analysis of the Tank-Skirt model it was observed that the temperature-displacements was slightly smaller than for the Skirt model analysed in chapter 6.5.1. The displacements for both models are shown i table 27.

Model	Displacement LNG [mm]	Displacement LH2 [mm]
Skirt	97.25	140.4
Tank-Skirt	92.78	133.9

Table 27: Temperature-Displacements for both models

Figures 43 shows the temperature-displacements of the Skirt-Tank model for the LNG and LH2 caroes. They are visualized using one direction displacement in x-direction.

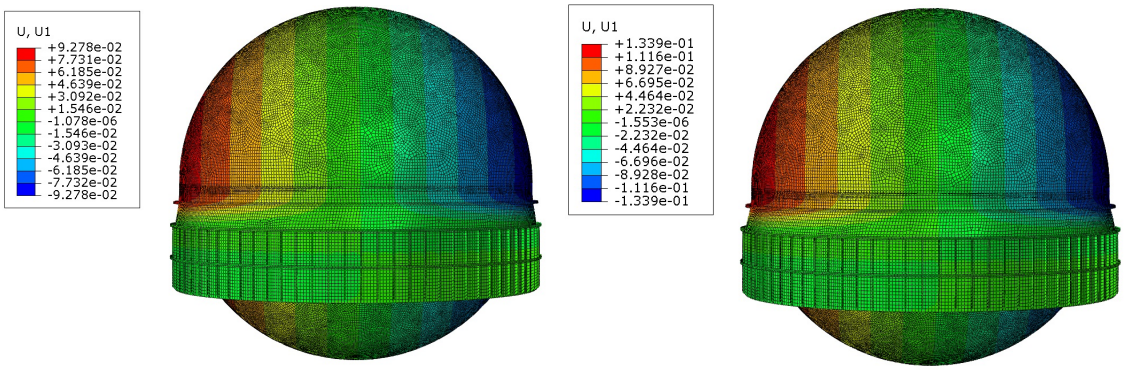

(a) Temperature-displacement with LNG cargo

(b) Temperature-displacement with LH2 cargo

Figure 43: Linear Temperature-displacement for Skirt-Tank Model

The difference in temperature-displacements is likely related to the difference in thicknesses or the extra mounting length of the skirt to the tank. With a reduced thickness of the tank the total retraction wont be as much at the support skirt. Thus the tank will resist the support skirt from its potential temperature-displacement, causing stress in transition between these two modules. The difference of the temperature-displacements is quite small compared to the total displacement that occurs due to the cargo temperature.

10.3 Linear Eigenvalue Analysis of Tank-Skirt Model

A eigenvalue analysis as performed with Skirt model in chapter 7.3 is performed with the Tank-Skirt model and applied the temperature-displacement caused by the cargo. The eigenvalue analysis is performed to find the linear elastic buckling modes for the structure. Loads are applied to the structure is the weight of the tank and cargo of $190.02MN$ found in the previous chapter. The eigenvalues returned are the steady state amplification of this load to cause elastic buckling. Table 28 shows the returned buckling loads from the eigenvalue analysis of the Tank-Skirt model.

Cargo	Eigenvalue	Critical Load	Critical Stress	Deviation
No Cargo	6.2334	1184.47	288.70	-
LNG	6.1771	1173.77	286.09	99.1%
LH2	6.0420	1148.10	279.84	96.9%

Table 28: Buckling Loads for the Skirt using a Model of the Tank and Skirt

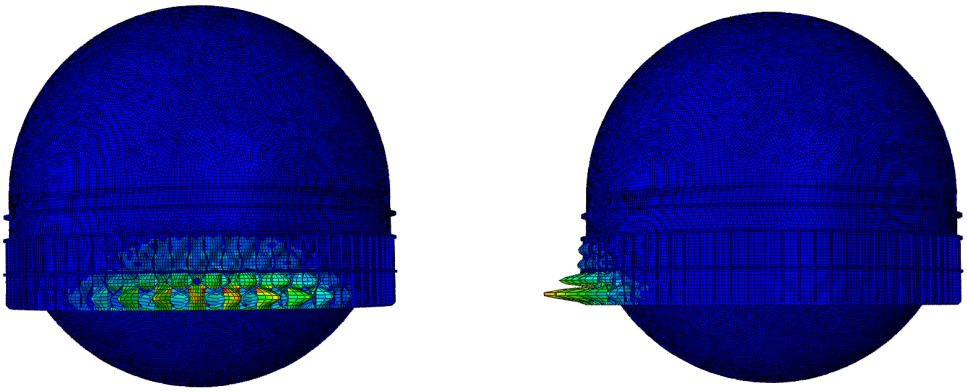

(a) Front view

(b) Side view

Figure 44: First Buckling Mode with no cargo

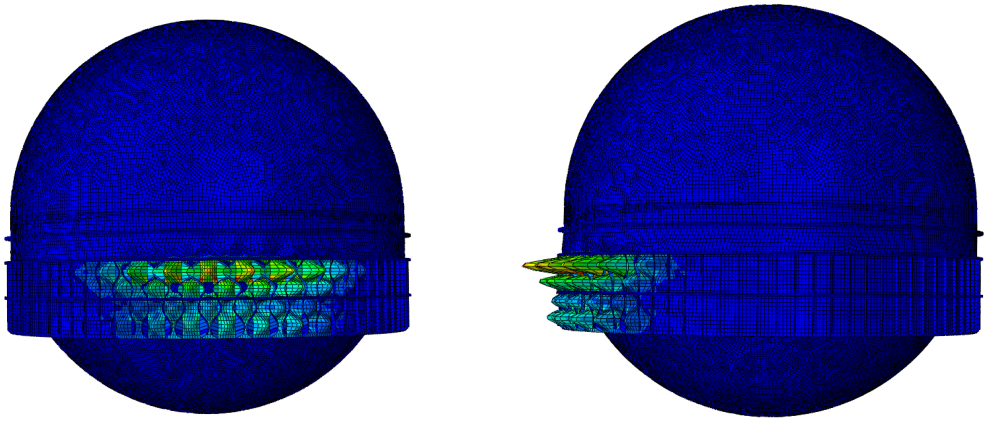

(a) Front view

(b) Side view

Figure 45: First Buckling Mode with LNG cargo

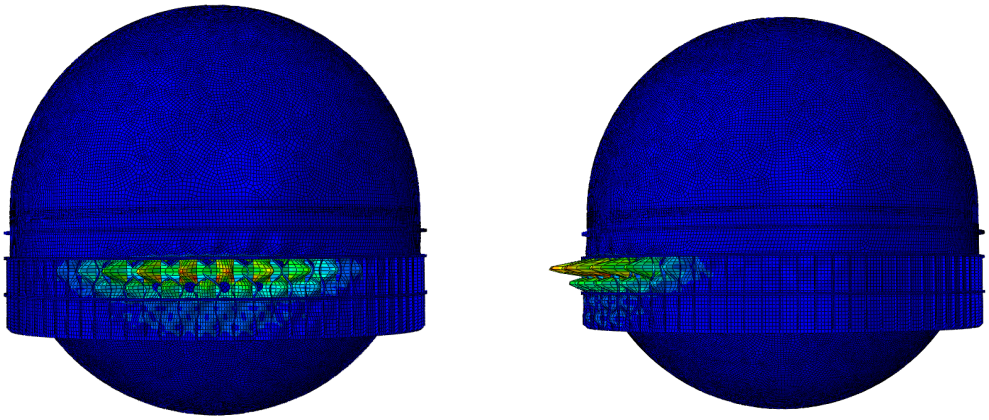

(a) Front view

(b) Side view

Figure 46: First Buckling Mode with LH2 cargo

Figures 44, 45, and 46 shows the first buckling modes for the skirt with the load applied through the tank and cargo weight. The buckling occurs in the steel panels. As the temperature-displacements occurs due to the temperature of the cargo the buckling mode shifts to the upper part of the steel section.

10.4 Non-Linear Elasto-plastic Analysis

A non-linear plastic analysis of the Tank-Skirt model performed where the skirt was analysed for yield due to axial load from the tank weight. The analysis was performed the same way as in chapter 7.4 for all three temperature-displacements. The load condition was implemented somewhat differently. To best represent the force from the tank and cargo it was based on the weight of a loaded tank and linearly increased until yield occurred. For the two analysis with cold cargo the temperature-displacements was first placed, then the force applied.

Table 29 shows the loads for which the skirt yielded in the analysis with the different load cases.

Cargo	Temperature displacement [mm]	Critical Load [MN]	Deviation
No Cargo	0	1193.13	-
LNG	92.78	1075.39	90.13
LH2	133.9	964.96	80.88

Table 29: Critical Loads for plastic yield in the skirt, using a mesh of $0.3m$

The results in this plastic analysis of the Tank-Skirt model was quite similar to the plastic analysis of the Skirt model in chapter 7.4. It can be seen that the reduction in critical load due to temperature-displacement was as significant in the Tank-Skirt model as in the skirt model. As the Tank-Skirt model has an extra length of $570mm$ due to the connection section it causes more eccentricity and more bending even though the temperature-displacements as slightly lower.

Yield occurred first in the steel section for no cargo or temperature-displacement as seen in figure 47. For both LNG and LH2 the yield occurred first in the thermal break due to the bending caused by the temperature-displacement. Figures 48 and 49 shows the yield in the skirt.

The yields found in this non-linear plastic analysis occur in the same places for both the Tank-Skirt model and the Skirt model. These similarities shows the critical contribution of the temperature-displacement on bending which causes the skirt to yield earlier. It should be noted that the temperature effect assumes warm weather conditions which makes the most extreme realistic cases. When the skirt is exposed to LH2's temperature, the displacements get height enough to cause a significant contribution of the critical load. The model used is designed to carry LNG is of course not designed for LH2. For use of LH2 this in such a model a the skirt should be designed to resist higher bindings due to temperature-displacements.

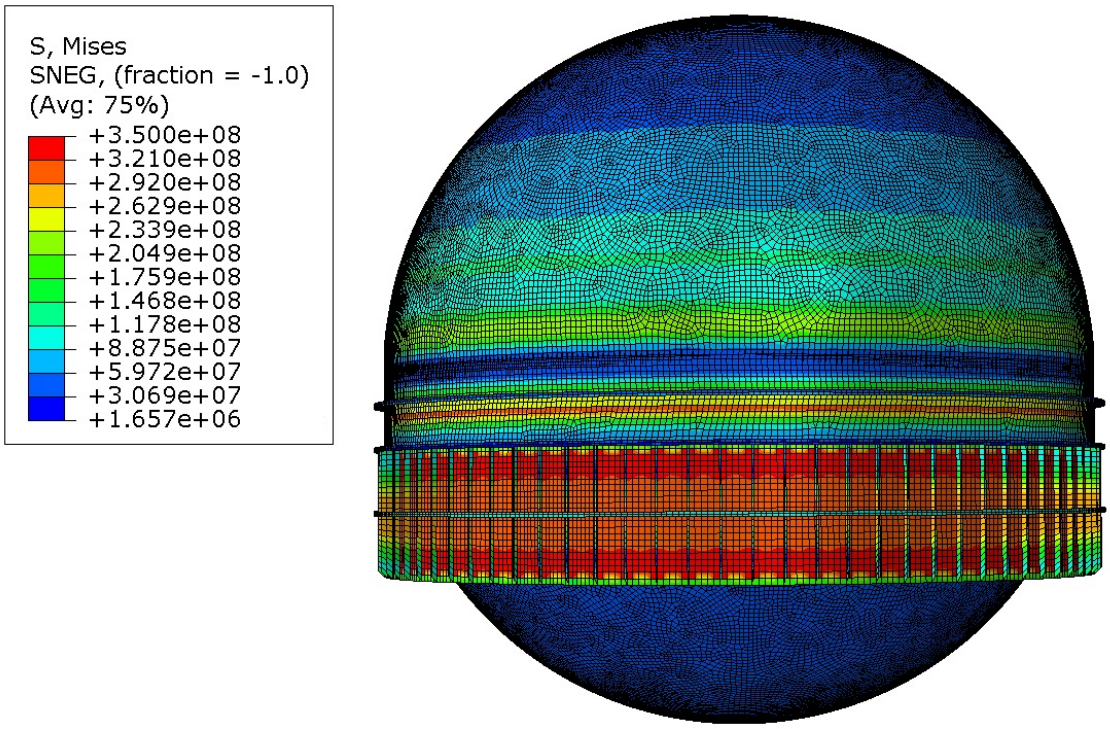

Figure 47: No Cargo, Yield in the Steel Panels, 350MPa

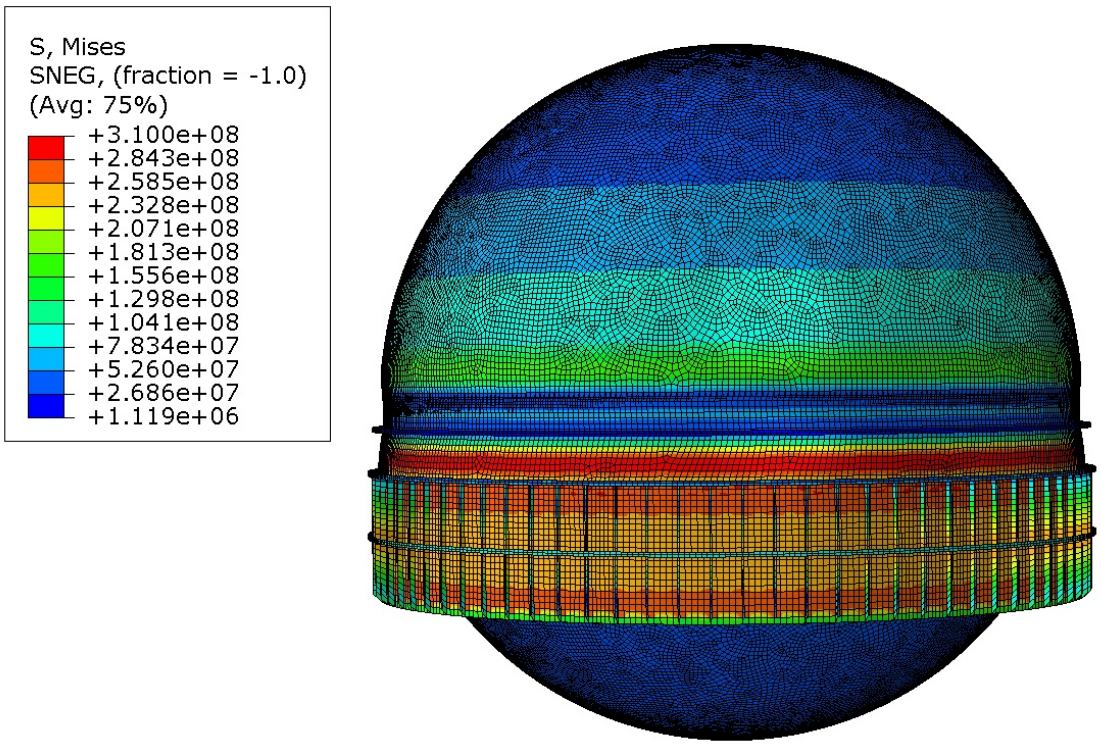

Figure 48: LNG Cargo, Yield in the Thermal Break, 310 MPa

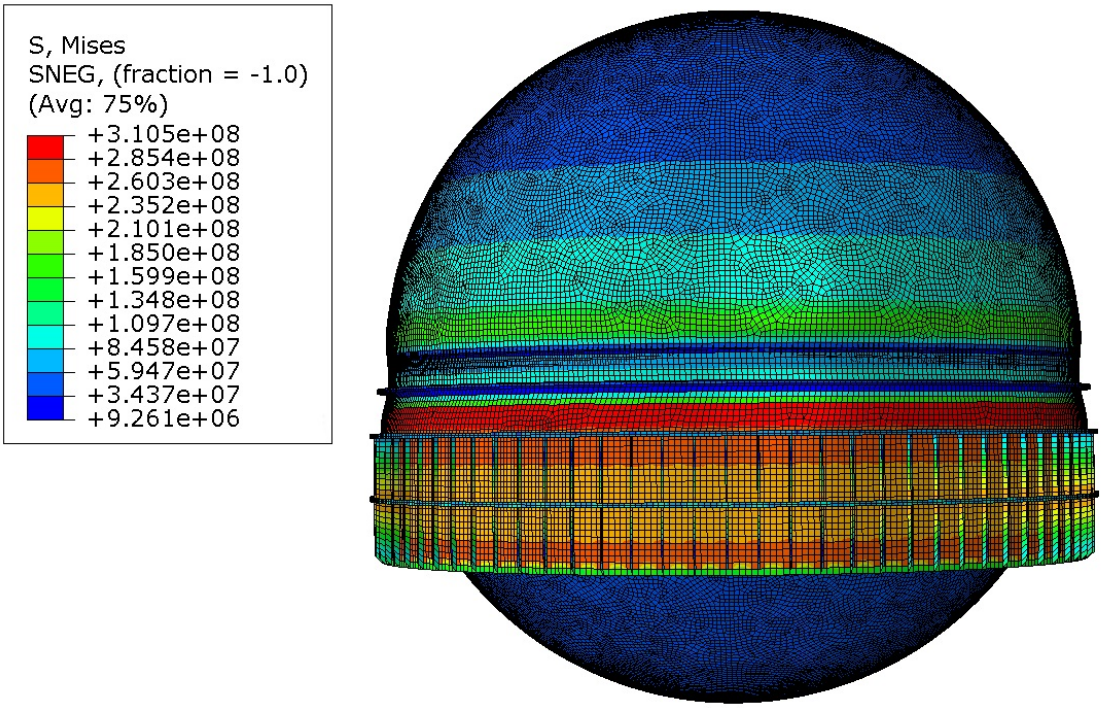

Figure 49: LH2 Cargo, Yield in the Thermal Break, 310 MPa

10.5 Comparison of the Models

It can be observed that the buckling pattern is the same for for both the support skirt model and the total tank and skirt model, seen in chapter 7.3 and 10.3. This illustrates that the load used on

the support skirt model was an accurate adaption of the real case. The main difference between the two modeled skirts is the extended section with larger thickness which mounts the tank to the skirt. When the load is transferred through the connection a slight eccentricity will occur which will slightly contribute to some bending rather than pure axial force.

When analysing the total structure of the model the eigenvalue of the first buckling was found to be slightly less than just for the support skirt analysis of about 1.32%. A comparison with hand calculations showed a result with the critical buckling load of 1.78%. The critical buckling of the tank with skirt was in between the analytical calculations and the analysis of the support skirt model.

10.6 Computing Time

By modeling the tank and the skirt the number of elements increases significantly. Depending on the mesh used in software analysis the elements will increase higher amount in the tank than in the skirt. For buckling studies with focus on the support skirt it would be advantageous to only have to model and analyse the skirt rather than the combined tank and skirt model. The issues by only modeling the skirt was the interaction between the tank and the skirt and their force transition as well as the temperature-displacement of the tank compared to the skirt.

In table 28 the results found in the linear eigenvalue analysis of the skirt showed very similar results to the analysis performed of only the skirt model. The results show slightly lower buckling loads, which is expected due to the slightly extended aluminium section to mount the tank. However the buckling modes was more or less identical for the three cargo load cases with temperature-displacements for the skirt model and the combines skirt-tank model.

All analysis in this study has used an element size of $0.3m$. Table 30 shows the number of element for used for both the Skirt and the Skirt-tank model.

Model	Element number
Skirt	25523
Tank-Skirt	97838

Table 30: Number of elements used for analysis for the models, mesh $0.3m$

The number of elements used to analyse the Tank-Skirt model is about four times higher than for the Skirt model. As discussed the results from the buckling analysis between the two models were similar enough to recommend only modelling the skirt for such analysis and applying the tank and cargo weight as a line load at the skirts upper edge.

11 Discussion

In this chapter the foundation, assumptions and simplifications, method, as well as the results in the study will be discussed. First the premises used when modelling using the right dimensions, loads and boundary conditions will be discussed. Then the method used and the software. Last the results will be discussed and how they compare to the DNV guidelines.

11.1 Procedures

In this sub chapter the geometry and model used for the skirt will be discussed as well as the assumptions and simplifications made. The extraction of results from the software and its accuracy will also be discussed.

11.1.1 Geometry of Model and Material

The model used in this report is based on drawing provided by Moss Maritime As for use and owned by Mitsubishi Heavy Industries. Some changes and simplifications were made of the drawing of the spherical LNG tanks before their implementations here. This was done both for some practical reasons in implementation and to respect the copy rights of the drawings.

Dimensions used for the support skirt are similar enough to reflect the structural integrity of the skirt. In the drawings the model was based on all three ring stiffeners use a different width. After a discussion with the supervisor it was agreed that all three ring stiffeners would be modeled with the same width of $570mm$. The impact of this simplifications was deemed to be minimal in terms of buckling on the skirt. In the drawing of the support skirt it is also outfitted with some spherical and oval holes in the steel section and the rings stiffeners. These are used to access the inside of the skirt and other areas of the structure. In the model these were neglected.

The skirt model in this report was limited in the upper end where the crossover section between the skirt and the tank started. In the drawing the connection section to the tank was used only for the Tank-Skirt model [41]. The exclusion of the connection section may have had a small impact on the potential buckling load. However not expected to be vital as the results from both Tank-Skirt and Skirt model are similar as discussed in chapter 10.5.

There were made some simplifications of the spherical tank in the Tank-Skirt. A spherical LNG tank in reality is composed of several sections with different thicknesses to withstand the local strength requirements, but in the analysis given a constant thickness. This simplification should not impact the results much as the connection section acts as a stiff shell between the tank and the skirt and constrains the skirt.

This study of the support skirt was limited to a cylindrical support skirt. It was discussed with the supervisor whether a horizontally stretched support skirt should be considered analysed, but it was concluded that the study should be limited to a cylindrical model in this report. For a non-spherical horizontally stretched tank the skirt would have to be stretched along the shape of tank with a cylindrical middle section and circular ends. This requires a thorough buckling analysis with considerations of axial buckling on such a shape. For the vertically stretched the support skirt would keep the cylindrical shape, but with consideration to the additional weight of the tank and cargo as well as increased center of gravity. A longer skirt would be required to connect it to its increased equator line, should it be mounted at the center of the stretched section of the tank.

11.1.2 Assumptions and Limitations

In addition to some simplifications regarding the skirt model there were also some assumption and simplifications made in the conditions applied to the analysis.

Some assumptions and foundations has to be outlined for the temperature effect on the structure. Warm weather was assumed when the tank was constructed and what it could encounter in operation. This would establish the temperature-displacement reference point at 40℃ and everything below would contribute to retraction. By assuming warm weather conditions the buckling reduction due to temperature-displacement would be a conservative calculation. It is stated "Warm weather conditions should be assumed" and is a requirement for calculations of thermal stresses in DNVGL-CG-0134 [12].

Application of the thermal loads was done in two different ways. A boundary condition on the upper edge of the skirt was set equal to the cargo temperature. Thus it will always have the same temperature as the cargo. This may not be precisely as in the real condition. As the content is kept cold inside the tank the change in temperature will start occurring already outside the tank. This temperature loss might be minimal and the tank insulated, but some heat loss will occur. The change of temperature and heat loss which has occurred in the intersection between the tank and skirt is thus assumed to be small enough to neglect.

The source of heat which warms the hull and the skirt is mainly the air temperature and the sun

warming the hull. For simplifications the skirt was assumed to be affected only by air temperature as high as 40℃. Sea temperatures can reach about $30-35$℃ in warm areas, but usually not higher than this. Thus it was reasonable to only apply a heat source to the skirt through air convection. Its heat contribution assumed as a constant interaction between air and the uninsulated steel section of the skirt with a reasonable film coefficient. The constant heat flow from air at 40℃ might not be realistic and the air between the skirt and the hull is separated from the air temperature outside of the ship, but gives a conservative estimate.

Heat transfer through radiation was neglected. After a quick calculation and study its effect on heating the skirt was deemed to be minimal and overshadowed by the convection effect. The load from the cargo and tank was considered evenly distributed and applied as a line load around the tank. This will thus only be the case for steady state situations with no accelerations or sea state. For the Tank-Skirt model the tank was given a body weight where the weight was evenly distributed. These conditions are very ideal and would have imperfections in reality. However the overall load situation would be quite close to the realistic one.

Boundary conditions at the bottom of the skirt was assumed fixed and analysed as such. In reality some rotations expected between the hull foundation and the skirt. The boundary conditions between the skirt and the tank was also set to fixed with the exception to translate in vertical direction to buckle. In reality the connection between the tank and skirt wouldn't behave as perfect fixed condition, but the relative thicknesses of the connection and cause rotations. The choice of boundary condition was found reasonable as an alternative to modeling of further components.

11.1.3 Abacus Calculations

The assumptions and conditions discussed above was used and implemented in Abaqus. Many of these was decided for their ability to be implemented in Abaqus, but had to be reasonable.

An important factor for the accuracy of the calculations is the choice of element mesh in Abaqus. This is usually a question between computing power, time, and the accuracy required for the results. A lot of time was spent in this study finding the right way to implement and run the analysis correct to get accurate. The mesh chosen for all the analysis was $0.3m$ per element. For the skirt model this gave 25523 elements and should give quite accurate calculations.

In abaqus the calculations was extract differently depending on the analysis. The most basic was the extraction of the temperature distribution and temperature-displacements. For these values the legend provided the correct values. The specific value for each node could also be checked by plotting and using Abaqus X-Y data function. These varied slightly but the highest value was most often chosen if it didn't deviate to much and seemed reasonable.

For the linear eigenvalue analysis the eigenvalues was presented with each requested eigenmode and extraction of the calculation should pose no threat to the accuracy on the results. Implementation, modelling, and meshing are the main sources for the accuracy in this calculations.

The calculation results from the non-linear plastic analysis was extracted using reaction forces in each node. As the plastic analysis was performed using forced displacement of the upper skirt edge, this caused reaction forces in all nodes in the top of the skirt. The sum of all these forces was expected to give the correct buckling load. It was found no practical way to extract and sum all of these and thus a mean value was estimated and multiplied with the number of nodes with reaction forces. This extraction method will give some error, but at the deviation between the nodal reaction forces was quite low the error not to large.

In the non-linear analysis with imperfections using the Arch-length "Riks" function, the results were extracted using a "Load Proportion Factor, LPF" which is a multiplier of the force exerted on the structure. The largest LPF multiplied with the force is then the calculated buckling load. It was one of the simpler calculated results to extract and should contain no error in extraction. An example of the extracted load using LPF is shown in figure 50

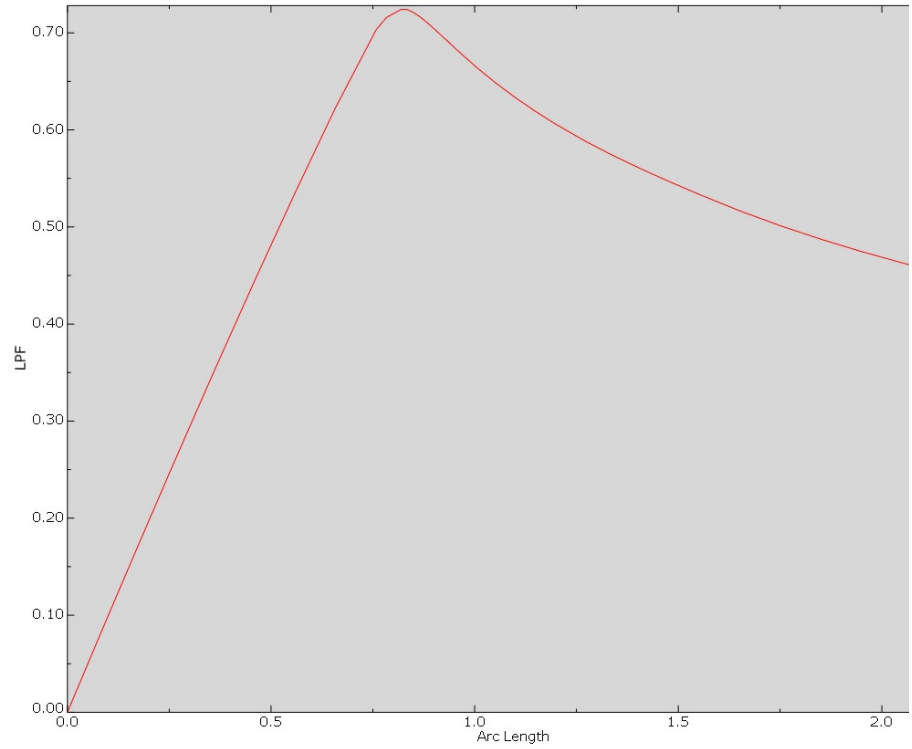

Figure 50: Example of LPF plot using Arch-length method with an imperfection amplitude of $15mm$

11.2 Brief Discussion of Results

The results obtained in the temperature analysis generally believed to be quite accurate and realistic. When compared to the expected distribution outlined by the DNV Guidelines the results obtained followed the same temperature-distribution [12]. Using a typical thermal expansion coefficient for the materials the temperature-displacements seem fair. When comparing the results from the Skirt-Model to the Tank-Skirt model, the results were quite similar.

The results from the eigenvalue analysis compared to the estimated linear buckling force calculated analytically was quite similar. When the temperature-displacement was applied for each cargo the effect on the elastic-buckling was quite small. Even for LH2 the reduction was found to be only 2.85% due to the temperature-displacement. As the buckling force estimation from DNV-RP-C202 and the results from Abaqus analysis are quite similar the analysis is believed to be quite accurate [11]. The estimation gave a somewhat more conservative estimation.

Two different non-linear analysis were performed. One using the linear eigenmodes obtained and applying an imperfection determined by the DNV guideline and analysing the buckling non-linearly. The Arc-Length method was used for the imperfection analysis non-linearly. One issue encountered was the application of the temperature-displacement with the Arc-length method, which was not applicable with imperfections. Thus the non-linear analysis was performed for the first eigenmodes of all three cargo's, but with no temperature-displacement in the Arc-length method. It would be of interest to be able to perform non-linear buckling analysis with imperfection along with the temperature-displacements to study the combined effect. As of the end of this study these effects have been analysed separately.

As the imperfection analysis not able to combine with the temperature-displacements a separate non-linear analysis was conducted. Using the Abaqus "Couples temperature displacement" function the temperature-displacements could be added and a force exerted on the structure. A force was applied in compression which increased linearly over a number of increments until yield occurred. A interesting find here was the shift form yield in from the steel panels with no

temperature-displacements to yield in the thermal break for both the LNG and LH2 cargoes. This is due to the bending caused by the displacements which is caused by the eccentricity. It was observed that the axial forces needed to cause yield was reduced to 86.71% for LNG and 78.44% for LH2 of the force needed with no displacements. Thus the temperature-displacements contributes significantly more towards plastic yield compared to elastic buckling.

These two analysis should ideally be combines to see the their combines effect. A non-linear buckling analysis which includes both imperfections and plastic yield due to axial load with temperature-displacements.

11.3 Changes to Skirt design for LH2

The design used in this study is a design for carrying LNG. With a lower temperature cargo such as LH2 which is 90℃ colder than LNG some changed is recommended. As the bending caused by temperature-displacement was quite high for LH2 cargo some changes might be suggested to prevent this. Another ring stiffener could be installed around the thermal break or adjust the positions of the existing ones.

With the lower temperature of LH2, one concern is the increased heat flow through the thermal break. A solution to this would be to increase the length of the thermal break, if reducing the area or changing to a lower conduction material isn't an option.

Concerning the temperature-displacement caused by the colder temperature of LH2, the bending will be higher with constant axial load. However it should be noted that LH2 has a density of about $0.070 Kg/m^3$ compared to $0.5 Kg/m^3$ LNG. Carrying a full tank of LH2 will thus be about 7 times lighter and the skirt is not likely to encounter the same axial force. The bending effect due to LH2's temperature-displacement should however be kept in mind when designing a skirt.

12 Conclusion

In this thesis the cargo temperatures effect on the buckling strength was studied. For elastic buckling it was found that the reduction in buckling strength was relatively low. The buckling modes found in the eigenvalue analysis changed from below the bottom ring stiffener to above it when the temperature changed, but still in the steel panels.

An non-linear buckling analysis with an introduced imperfection was performed for the skirt using several imperfection amplitudes. The reduction in buckling strength due to imperfections was found and the expected design reduction using DNV recommended imperfection amplitude. Using the DNV recommended imperfection amplitude the non-linear analysis was performed for all three load cases and found very similar reduction in buckling strength as the linear analysis.

In the non-linear plastic analysis the temperature-displacement was found to reduce the buckling capacity more drastically. The reduced buckling strength for LH2 was 78.44. Due to the lighter weight of LH2 the skirt still has quite a lot of capacity until buckling as the axial force is reduced. The bending caused by the temperature difference is still a concern in skirt design for LH2 tanks. A redesign to account for the temperature-displacements and the lighter cargo should be considered.

The elastic buckling strength was studied for the thermal break and the aluminium sections linearly by increasing the thickness of the other sections. Buckling in the thermal break required roughly 33% higher axial force and 64% for the aluminium section. The reduction in buckling strength in these cylindrical sections due to temperature-displacement was below 2% at the highest for LH2 in the thermal break.

A tank was modeled together with the skirt, analysed and compared with the isolated skirt model. The temperature-displacements was found to be slightly lower for the Tank-Skirt model. This was the case for the linear elastic buckling strength as well, but under 2% difference from the isolated skirt model. The buckling modes between these two models were the same for all three temperature load conditions. With these similar results the increased computing time by modeling the tank was described and found to be 4 times higher using a mesh with element size of $0.3m$.

12.1 Recommendations for Further Works

In this report, it has been studied at how the temperature affects the buckling strength of a cylindrical skirt for spherical LNG tanks. Further work might potentially look at how temperature will affect non-spherical LNG tanks. Below is listed some suggestions which might be looked further into.

- Buckling analysis of the skirt supporting a horizontally stretched LNG-tank with inclusion of thermal effects. Also to analyse the buckling strength of the skirt of a longitudinally stretched tank with its increased cargo weight.
- Buckling analysis of the skirt with non steady state conditions. Addition of forces and accelerations the a non-spherical tank will encounter while seagoing. A review if the regulations are sufficient with these conditions.
- Analysis of the skirt hull girder interaction. Model the ship structure with boundary conditions to the skirt. Perform calculations of the buckling/yield resistance for the hull girder due to the interaction with the skirt and tank.
- Work and suggestions to optimize the thermal break for LH2. Reduction of the bending caused by the temperature-displacements strengthening the structure, analysing and potential updates of guidelines.

Bibliography

[1] Khan Academy. *What is thermal conductivity?* URL: https://www.khanacademy.org/science/physics/thermodynamics/specific-heat-and-heat-transfer/a/what-is-thermal-conductivity (visited on 07/06/2022).

[2] Jørgen Amdahl. *TMR4205 Buckling and Ultimate Strength of Marine Structures ch.3.* MTS, 2005.

[3] Jørgen Amdahl. *TMR4205 Buckling and Ultimate Strength of Marine Structures ch.5.* MTS, 2010.

[4] Engineering Tool Box. *Engineering Tool Box , Air Convection.* URL: https://www.sciencedirect.com/topics/engineering/convection-heat-transfer-coefficient (visited on 07/06/2022).

[5] Engineering Tool Box. *Engineering Tool Box , Material Structural Properties.* URL: https://www.engineeringtoolbox.com/material-properties-t_24.html (visited on 07/06/2022).

[6] Engineering Tool Box. *Engineering Tool Box , Materials Conductivity.* URL: https://www.engineeringtoolbox.com/thermal-conductivity-d_429.html (visited on 07/06/2022).

[7] Engineering Tool Box. *Engineering Tool Box , Solid Material Conductivity.* URL: https://www.engineeringtoolbox.com/thermal-conductivity-metals-d_858.html (visited on 07/06/2022).

[8] Engineering Tool Box. *Engineering Tool Box , Thermal Expansion Coefficients.* URL: https://www.engineeringtoolbox.com/linear-expansion-coefficients-d_95.html (visited on 07/06/2022).

[9] DNV. 'DNV CN30-1, BUCKLING STRENGTH ANALYSIS OF BARS AND FRAMES, AND SPHERICAL SHELLS'. In: (2004).

[10] DNV. 'DNV CN30-2, STRENGTH ANALYSIS OF LNG CARRIERS WITH SPHERICAL TANKS'. In: (2009).

[11] DNV. 'DNV-RP-C202, Recommended practice, Buckling Strength of Shells'. In: (2013).

[12] DNV. 'Liquefied gas carriers with spherical tanks of type B'. In: (2018).

[13] Mitsubishi Heavy Industries. *Structural Design and Construction Method for "Apple-Shaped Liquefied Natural Gas Cargo Tank" for LNG Carriers.* URL: https://www.mhi.co.jp/technology/review/pdf/e532/e532011.pdf (visited on 07/06/2022).

[14] T Tsien HS von Karman. 'The Buckling of Thin Cylindrical Shells under Axial Compression. Journal'. In: (1941).

[15] Kawasaki. *Kawasaki Moss-type Tank.* URL: https://global.kawasaki.com/en/corp/newsroom/news/detail/?f=20170713_6041 (visited on 07/06/2022).

[16] Moss Maritime. 'PRELIMINARY SCANTLING OF SPHERICAL TANKS, 250.000 m^3 LNG-CARRIER'. In: (2005).

[17] Graham McGuire and Barry White. *Liquefied gas handling principles : on ships and in terminals, 3rd edition.* Witherby, 2000.

[18] Michael J. Moran. *Fundamentals of Engineering Thermodynamics, Eighth Edition.* Wiley, 2018.

[19] Gjestvang P. 'Gjestvang2020, Buckling of Non-spherical MOSS-LNG Tanks'. In: (2020).

[20] Andreas Sanne. 'Buckling of Non-spherical Moss-LNG tank'. In: (2019).

[21] Sciencedirect. *A study on forces generated on spherical type LNG tank with central cylindrical part under various static loading.* URL: https://www.sciencedirect.com/science/article/pii/S2092678216304976 (visited on 07/06/2022).

[22] Sciencedirect. *Eigenvalue Analysis Finite Element Method.* URL: https://www.sciencedirect.com/topics/engineering/eigenvalue (visited on 07/06/2022).

[23] Moan T. *Finite Element Modelling and Analysis of Marine Structures.* NTNU Dept. Marine Technology, 2003.

[24] (2020) The Norwegian Goverment. *The Norwegian Government's hydrogen strategy.* URL: https://www.regjeringen.no/contentassets/40026db2148e41eda8e3792d259efb6b/y-0127e.pdf (visited on 07/06/2022).

Appendix

A Excerpt of Skirt Drawing

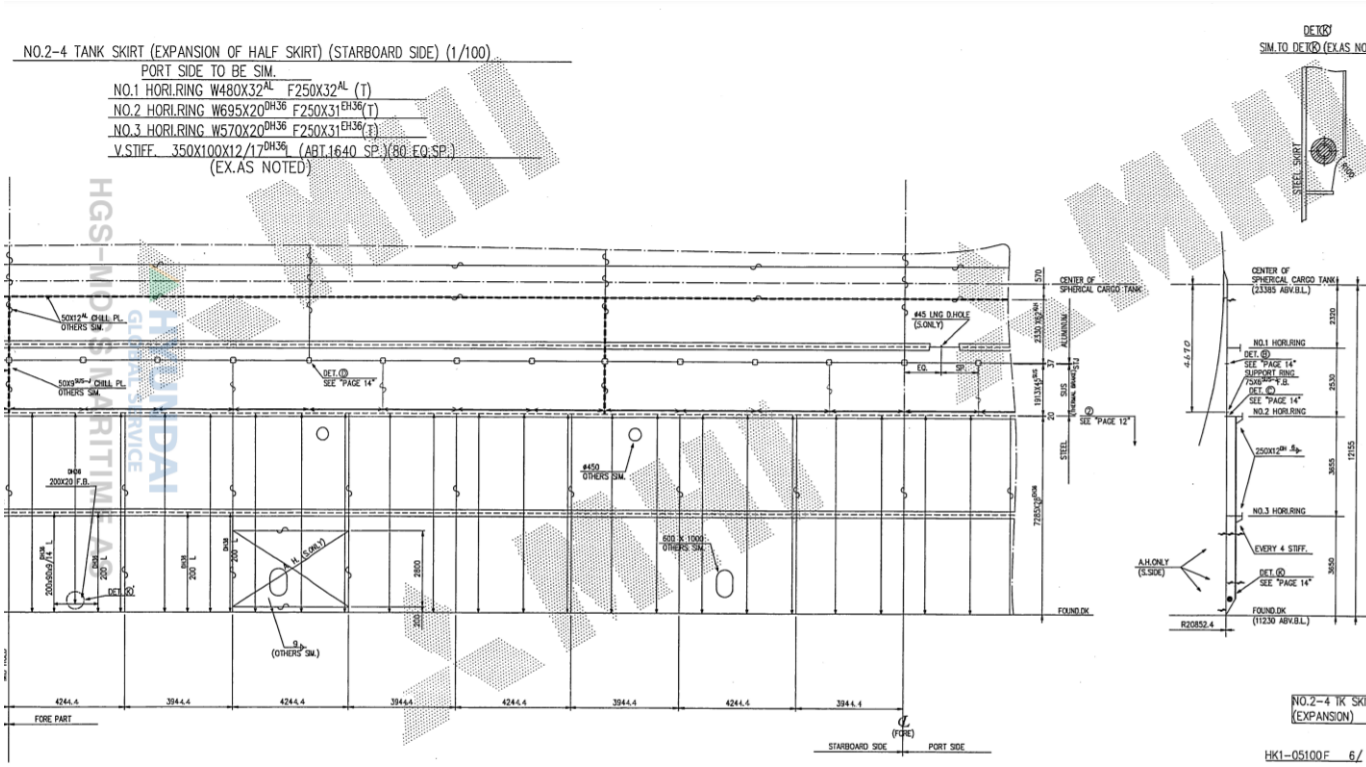

Figure 51: Excerpt of drawing used to modeling of the skirt

B LNG Results in Chapter 9.5

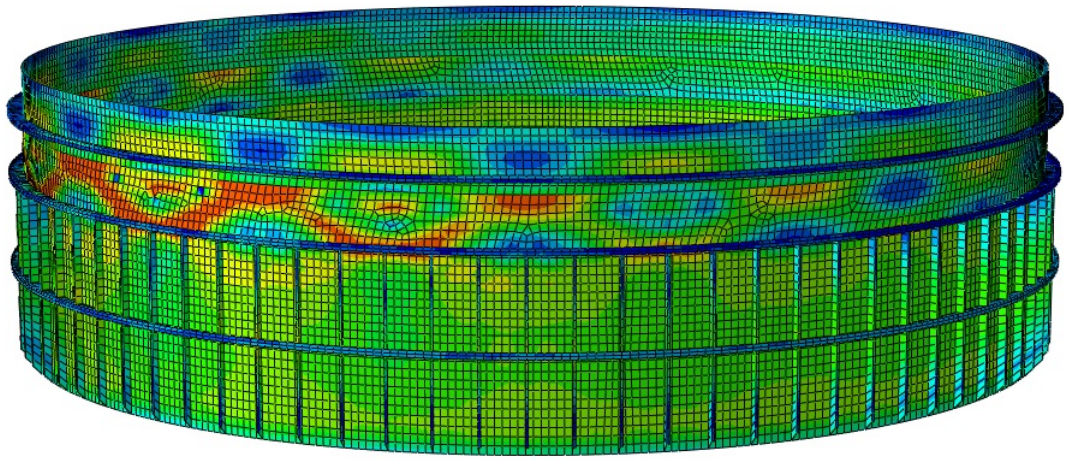

Figure 52: Non-linear Buckling Analysis with Imperfection Amplitude 18mm for LNG

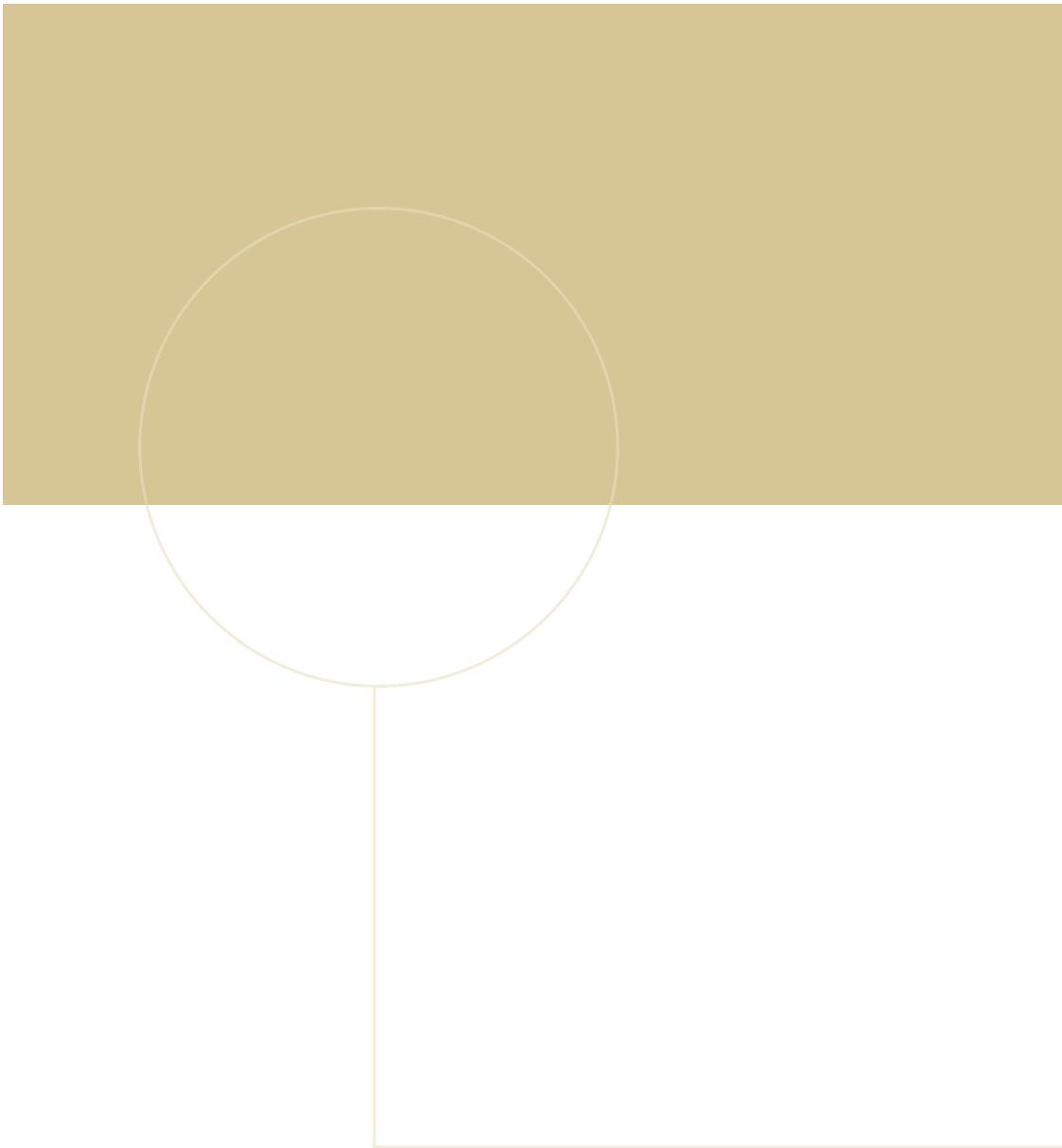

NTNU

Norwegian University of
Science and Technology